



MINISTÉRIO DA CIÊNCIA, TECNOLOGIA, INOVAÇÕES E COMUNICAÇÕES
INSTITUTO NACIONAL DE PESQUISAS ESPACIAIS

sid.inpe.br/mtc-m21c/2019/02.25.13.16-TDI

**EXTRATROPICAL TRANSITION OF SUBTROPICAL
CYCLONES OVER SOUTHWESTERN ATLANTIC
OCEAN**

Jessica Tatiane da Silva Oliveira

Doctorate Thesis of the Graduate
Course in Meteorology, guided by
Drs. Nelson Jesus Ferreira, and
Kevin Ivan Hodges, approved in
February 28, 2019.

URL of the original document:

<<http://urlib.net/8JMKD3MGP3W34R/3SQM9DS>>

INPE
São José dos Campos
2019

PUBLISHED BY:

Instituto Nacional de Pesquisas Espaciais - INPE
Gabinete do Diretor (GBDIR)
Serviço de Informação e Documentação (SESID)
CEP 12.227-010
São José dos Campos - SP - Brasil
Tel.:(012) 3208-6923/7348
E-mail: pubtc@inpe.br

**BOARD OF PUBLISHING AND PRESERVATION OF INPE
INTELLECTUAL PRODUCTION - CEPPII (PORTARIA Nº
176/2018/SEI-INPE):****Chairperson:**

Dr. Marley Cavalcante de Lima Moscati - Centro de Previsão de Tempo e Estudos
Climáticos (CGCPT)

Members:

Dra. Carina Barros Mello - Coordenação de Laboratórios Associados (COCTE)
Dr. Alisson Dal Lago - Coordenação-Geral de Ciências Espaciais e Atmosféricas
(CGCEA)
Dr. Evandro Albiach Branco - Centro de Ciência do Sistema Terrestre (COCST)
Dr. Evandro Marconi Rocco - Coordenação-Geral de Engenharia e Tecnologia
Espacial (CGETE)
Dr. Hermann Johann Heinrich Kux - Coordenação-Geral de Observação da Terra
(CGOBT)
Dra. Ieda Del Arco Sanches - Conselho de Pós-Graduação - (CPG)
Sílvia Castro Marcelino - Serviço de Informação e Documentação (SESID)

DIGITAL LIBRARY:

Dr. Gerald Jean Francis Banon
Clayton Martins Pereira - Serviço de Informação e Documentação (SESID)

DOCUMENT REVIEW:

Simone Angélica Del Ducca Barbedo - Serviço de Informação e Documentação
(SESID)
André Luis Dias Fernandes - Serviço de Informação e Documentação (SESID)

ELECTRONIC EDITING:

Ivone Martins - Serviço de Informação e Documentação (SESID)
Cauê Silva Fróes - Serviço de Informação e Documentação (SESID)



MINISTÉRIO DA CIÊNCIA, TECNOLOGIA, INOVAÇÕES E COMUNICAÇÕES
INSTITUTO NACIONAL DE PESQUISAS ESPACIAIS

sid.inpe.br/mtc-m21c/2019/02.25.13.16-TDI

EXTRATROPICAL TRANSITION OF SUBTROPICAL CYCLONES OVER SOUTHWESTERN ATLANTIC OCEAN

Jessica Tatiane da Silva Oliveira

Doctorate Thesis of the Graduate
Course in Meteorology, guided by
Drs. Nelson Jesus Ferreira, and
Kevin Ivan Hodges, approved in
February 28, 2019.

URL of the original document:

<<http://urlib.net/8JMKD3MGP3W34R/3SQM9DS>>

INPE
São José dos Campos
2019

Cataloging in Publication Data

Oliveira, Jessica Tatiane da Silva.

Ol4e Extratropical transition of subtropical cyclones over Southwestern Atlantic Ocean / Jessica Tatiane da Silva Oliveira. – São José dos Campos : INPE, 2019. xxvi + 130 p. ; (sid.inpe.br/mtc-m21c/2019/02.25.13.16-TDI)

Thesis (Doctorate in Meteorology) – Instituto Nacional de Pesquisas Espaciais, São José dos Campos, 2019.

Guiding : Drs. Nelson Jesus Ferreira, and Kevin Ivan Hodges.

1. Subtropical cyclone. 2. Extratropical transition. 3. Potential Vorticity Inversion. I.Title.

CDU 551.515.1



Esta obra foi licenciada sob uma Licença [Creative Commons Atribuição-NãoComercial 3.0 Não Adaptada](https://creativecommons.org/licenses/by-nc/3.0/).

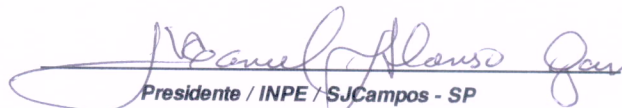
This work is licensed under a [Creative Commons Attribution-NonCommercial 3.0 Unported License](https://creativecommons.org/licenses/by-nc/3.0/).

Aluno (a): **Jessica Tatiane da Silva Oliveira**

Título: "EXTRATROPICAL TRANSITION OF SUBTROPICAL CYCLONES OVER SOUTHWESTERN ATLANTIC OCEAN"

Aprovado (a) pela Banca Examinadora em cumprimento ao requisito exigido para obtenção do Título de **Doutor(a)** em **Meteorologia**

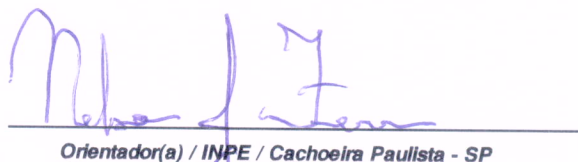
Dr. Manoel Alonso Gan


Presidente / INPE / SJC Campos - SP

Participação por Video - Conferência

Aprovado Reprovado

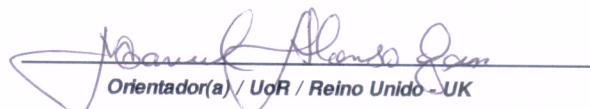
Dr. Nelson Jesus Ferreira


Orientador(a) / INPE / Cachoeira Paulista - SP

Participação por Video - Conferência

Aprovado Reprovado

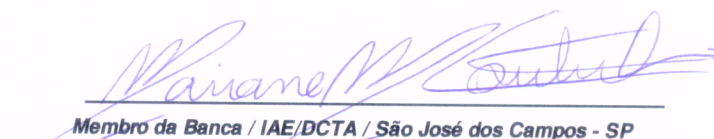
Dr. Kevin Ivan Hodges


Orientador(a) / UoR / Reino Unido - UK

Participação por Video - Conferência

Aprovado Reprovado

Dra. Mariane Mendes Coutinho


Membro da Banca / IAE/DCTA / São José dos Campos - SP

Participação por Video - Conferência

Aprovado Reprovado

Este trabalho foi aprovado por:

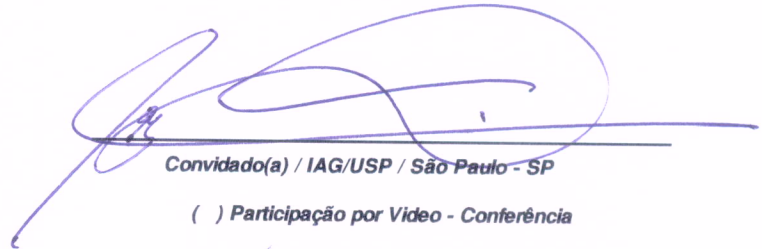
maioria simples

unanimidade

São José dos Campos, 28 de fevereiro de 2019

Aprovado (a) pela Banca Examinadora
em cumprimento ao requisito exigido para
obtenção do Título de **Doutor(a)** em
Meteorologia

Dr. Augusto José Pereira Filho

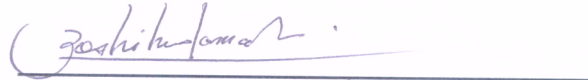


Convidado(a) / IAG/USP / São Paulo - SP

Participação por Video - Conferência

Aprovado Reprovado

Dr. Yoshihiro Yamazaki



Convidado(a) / UFPEL / Pelotas - RS

Participação por Video - Conferência

Aprovado Reprovado

Este trabalho foi aprovado por:

maioria simples

unanimidade

São José dos Campos, 28 de fevereiro de 2019

To my family.

ACKNOWLEDGEMENTS

I would like to express my sincere gratitude to my advisor Dr. Nelson Ferreira for the continuous support, motivation, encouragement and patient guidance. I would like to extend my deepest gratitude to Dr. Kevin Ivan Hodges for his external guidance and support with the TRACK software, for the helpful contribution, practical suggestions, insightful comments and corrections to improve the English writing.

Special thanks to Dr. Christopher Davis for the support with the Potential Vorticity Inversion code.

I am extremely grateful to my friend Aline Bilhalva for many conversations, support and for being an example of resilience, bravery and faith.

Thank you to my friend Theomar Neves for the opportunity to contribute in his course of Synoptic Meteorology at UFOPA and for making this experience so smoothly.

I would like to thank the National Institute for Space Research (INPE) for providing infrastructure for the development of this thesis.

I would like to thank the Brazilian federal government for the financial support through the Coordination for the Improvement of Higher Education Personnel (CAPES) and the National Council for Scientific and Technological Development (CNPq) for my scholarship.

Last but not least, I am deeply grateful to my family for their love, support, generous care and encouragement. And most of all, I am thankful for my loving husband Fernando for always being there when I really needed.

ABSTRACT

Subtropical cyclones that often develop over the southern coast of Brazil can significantly impact agriculture, transport and the day-to-day lives of the population. However, there is a lack of studies regarding these weather systems that is of scientific and operational interest. The goal of the current study is to improve the knowledge of the dynamical processes related to subtropical cyclones undergoing extratropical transition (SCET) and to identify the main associated mechanisms for this process. To achieve this purpose, a climatological analysis of the SCET over the Southwestern Atlantic Ocean was developed. 47 SCET were identified during the austral summer (November-March) in the 1985-2015 period. An annual mean of 1.6 SCET per year with standard deviation of 1.3 was found. The monthly distribution of these systems showed that the months with higher SCET frequency were January, February and December, respectively. The main features of the structure of SCET are investigated using composite analysis of meteorological fields. The results indicate that SCET are associated with the intrusion of upper level Potential Vorticity (PV) and the propagation of cyclonic systems at the rear of the SCET. Also, the low level temperature advection plays a key role in the extratropical transition (ET) of these systems. A case study is presented to illustrate SCET pattern and investigate the impacts of PV anomalies in its life cycle. A case study was analyzed using as reference the cyclone Anita, which developed near the southeastern coast of Brazil in March 2010. The potentially significant anomalies of PV during the ET are identified through the PV inversion method. The results confirm the intrusion of an upper tropospheric PV anomaly during the pre-transitioning stage of Anita. However, the lower level PV anomalies are also found to be of great importance at the ET time. Numerical experiments with the regional model WRF (Weather Research and Forecasting) indicate that the lower level PV anomalies were fundamental to the ET of Anita. On the other hand, although the upper tropospheric PV anomaly impacts significantly the propagation and intensity of Anita, its absence did not prevent the ET occurrence. Sensitivity test suggests that the interaction of Anita with a shallow extratropical cyclone prior to the ET was not the primary mechanism to the transitioning process, but impact the time and position of its occurrence, contributing to prevent the re-intensification of Anita.

Keywords: Subtropical Cyclone. Extratropical transition.
Potential Vorticity Inversion.

TRANSIÇÃO EXTRATROPICAL DE CICLONES SUBTROPICAIS SOBRE O OCEANO ATLÂNTICO SUDOESTE.

RESUMO

Os ciclones subtropicais que tipicamente ocorrem nas proximidades da costa sul do Brasil impactam significativamente os meios de transporte, agricultura e o dia a dia da população. Apesar disso, existem poucos estudos abordando essa temática de grande interesse científico e operacional. Este estudo visa aprimorar o conhecimento da dinâmica dos ciclones subtropicais que passam por transição extratropical (CSTE) e identificar os mecanismos fundamentais para ocorrência desse processo. Para tal, uma análise da climatologia dos CSTE sobre o Oceano Atlântico Sudoeste foi elaborada. 47 CSTE foram identificados durante o verão austral (Novembro-Março) durante o período de 1985-2015. Desse modo, foi encontrada uma média de 1,6 CSTE por ano, com desvio padrão de 1,3. A distribuição mensal desses sistemas mostrou que os meses com maior frequência de CSTE foram Janeiro, Fevereiro e Dezembro, respectivamente. A estrutura dos CSTE foi investigada através da análise de composições. Os resultados indicam que os CSTE estão associados com a intrusão de anomalia de Vorticidade Potencial (VP) de altos níveis e com a propagação de um sistema ciclônico na retaguarda do CSTE. Além disso, a advecção de temperatura na troposfera inferior desempenha um papel importante no processo de transição extratropical (TE) desses sistemas. Um estudo de caso é apresentado para ilustrar os CSTE e para investigar os impactos das anomalias de VP durante o ciclo de vida desses sistemas. O ciclone escolhido para esse estudo de caso foi o Anita, que se desenvolveu próximo a costa sudeste do Brasil em Março de 2010. As anomalias de VP potencialmente significantes para a TE foram identificadas através do método da Inversão da Vorticidade Potencial. Os resultados confirmaram a intrusão de uma anomalia de VP na alta troposfera durante o estágio pré-transição do Anita. No entanto, as anomalias de VP de baixos níveis desempenham um papel importante durante a TE. Experimentos numéricos com o modelo WRF (WeatherResearchandForecasting, sigla em inglês) indicaram que a anomalia de VP de baixos níveis é fundamental para a TE do Anita. Por outro lado, embora as anomalias de VP na alta troposfera influenciem significativamente a propagação e intensidade do Anita, a ausência delas não impediu a ocorrência de TE. Testes de sensibilidade sugerem que a interação do Anita com um ciclone extratropical fraco no período que antecede a TE, não foi o principal mecanismo para o processo de transição, mas impactou o tempo e a posição em que a transição ocorreu, contribuindo para que a não re-intensificação do Anita.

Palavras-chave: Ciclones Subtropicais. Transição extratropical. Inversão da Vorticidade Potencial.

LIST OF FIGURES

	<u>Pág.</u>
Figure 2.1 – Conceptual model of geopotential height at 300 hPa of subtropical cyclogenesis patterns in NEAO: (a) cut-off-low, (b) bifurcation, and (c) prolongation.	7
Figure 2.2 – Subtropical cyclogenesis and cyclolysis density over SAO.	9
Figure 2.3 – Hurricane Catarina as seen on Visible high resolution image for 1355 UTC 27 th March 2004, obtained from Moderate Resolution Imaging Spectroradiometer (MODIS)/Terra Satellite.	10
Figure 2.4 – Trajectory of the six named SC based on 925 hPa relative vorticity.	12
Figure 3.1 – SC tracking area used in the current study.	19
Figure 3.2 – Schematic of the three steps to the compositing.	23
Figure 3.3 – Domain used for numerical simulations of cyclone Anita.	27
Figure 3.4 – Diagram for SCET analysis.	30
Figure 4.1 – (a) Trajectories (red lines) and (b) trajectories density of SCET in the SAO, obtained through the method of tracking cyclones, for the 1985-2015 period. Unit of density is number per season per unit area.	33
Figure 4.2 – Density of (a) density, (b) extratropical transition and (c) lysis of SCET in the SAO for the 1985-2015 period. Unit of density is number per season per unit area.	34
Figure 4.3 – Cyclonic vorticity in the genesis (light gray) and extratropical transition (dark gray) of SCET in the SAO for the 1985-2015 period.	36
Figure 4.4 – Composite mean SCET for the 1985-2015 period. (a) -VTL vs B and (b) -VTL vs -VTU.	38
Figure 4.5 – Life cycle composites of SCET for the 1985-2015 period.	40
Figure 4.6 – Mean frequency of thermal wind parameter in the lower troposphere (-VTL) for the period (a) Prior and (b) Post extratropical transition of the SCET for the 1985-2015 period.	42
Figure 4.7 – Mean frequency of thermal symmetry (B) for the period (a) Prior and (b) Post extratropical transition of the SCET for the 1985-2015 period.	43
Figure 4.8- Monthly frequency of SCET (dark gray) and SC (light gray) in the SAO during the 1985-2015 period, based on CFSR reanalysis. .	45
Figure 4.9 - Annual frequency of subtropical cyclones (dark gray line) and SCET (light gray line) in the SAO during the 1985-2015 period, based on CFSR reanalysis.	46

Figure 4.10 – Decadal frequency of SCET in the SAO during 1985-2015 period.	46
Figure 4.11 – Lifetime of SCET (a) total and (b) before (dark gray) and after (light gray) extratropical transition during the 1985-2015 period.	47
Figure 4.12 – Composites of SLP (contour) and Potential Vorticity at 250 hPa (shaded) of SCET in a) t = -72h, b) t = -48h, c) t = -24h, d) t = 0, e) t = +24h, f) t = +48h e g) t = +72h. Units of PV and SLP are PVU and hPa, respectively.....	51
Figure 4.13 – Composites of geopotential height anomaly at 500 hPa (shaded) and horizontal wind at 250 hPa (streamlines) of SCET in a) t = -72h, b) t = -48h, c) t = -24h, d) t = 0, e) t = +24h, f) t = +48h e g) t = +72h. Units of geopotential height are gpm.....	54
Figure 4.14 – Composites of total heat flux (shaded – latent heat flux + sensible heat flux) and sea surface temperature (contours every 2 °C) to SCET in a) t = -72 h, b) t = -48 h, c) t = -24 h, d) t = 0, e) t = +24 h, f) t = +48 h e g) t = +72 h. Units of SST and total fluxes are °C and Wm ² , respectively.	58
Figure 4.15–Composites of temperature advection (shaded) and velocity potential (contour) at 850 hPa of SCET in a) t = -72h, b) t = -48h, c) t = -24h, d) t = 0, e) t = +24h, f) t = +48h e g) t = +72h. Units of temperature advection is 10 ⁻⁵ Ks ⁻¹	61
Figure 5.1 - Anita tracking based on relative vorticity at 925 hPa from CFSR reanalysis.	65
Figure 5.2 – Phase space diagram for cyclone Anita from 00 UTC on 5 March to 18 UTC on 13 March 2010: (left) B versus -VTL (right) -VTU versus -VTL.....	66
Figure 5.3 – 925 hPa Relative vorticity (shaded), SLP (blue contour each 4 hPa) and 500 hPa geopotential height (red dashed contour each 100 gpm) for cyclone Anita from CFSR reanalysis for the 09-13 March 2010 period: (a) 09 – 18 UTC, (b) 10 – 12 UTC, (c) 11 – 18 UTC, (d) 12 – 18 UTC and (e) 13 – 18 UTC.....	69
Figure 5.4 – Wind vectors and PV at 250 hPa (shaded) for cyclone Anita from CFSR reanalysis for the 08-13 March 2010 period: (a) 09 – 18 UTC, (b) 10 – 12 UTC, (c) 11 – 18 UTC, (d) 12 – 18 UTC and (e) 13 – 18 UTC.	70
Figure 5.5 – (left) Geopotential height and wind from CFSR reanalysis and (right) geopotential and non-divergent wind from PV inversion at 250 hPa on 09 - 12th of March 2010 period at 18 UTC.....	72
Figure 5.6 – (left) Geopotential height and wind from CFSR reanalysis and (right) geopotential and non-divergent wind from PV inversion at 850 hPa on 09- 12th March 2010 period at 18 UTC.....	73

Figure 5.7 – Difference between the total CFSR wind and the non-divergent wind (vectors), divergence (shaded) at (left) 250 hPa and (right) 850 hPa and vertical velocity at 500 hPa (contour) at 18 UTC on the 09th, 11th and 12th of March.	75
Figure 5.8 – Geopotential height anomaly at 500 hPa from (left) CFSR reanalysis and (right) balanced field from PV inversion at 18 UTC on the 09th, 11th and 12th of March.	76
Figure 5.9– Vertical cross section of relative vorticity associated with PV anomalies at (left) high levels: 400 – 100 hPa, (center) low levels: 975 – 700 hPa (blue/red lines) and potential temperature at inferior boundary (1000 hPa – green lines) and (right) total (1000 – 100 hPa), for 18 UTC on 09th of March (top) and on 10th of March (bottom).	80
Figure 5.10– Vertical cross section of relative vorticity associated with PV anomalies at (left) high levels: 400 – 100 hPa, (center) low levels: 975 – 700 hPa (orange lines) and potential temperature at inferior boundary (1000 hPa – green lines) and (right) total (1000 – 100 hPa), for 18 UTC on 12 of March (top) and 06 UTC on 13 of March (bottom).	81
Figure 5.11 – Phase space diagram for cyclone Anita from CTL on 06 UTC on 9 March to 00 UTC on 14 March 2010: (left) B versus -VTL (right) -VTU versus -VTL. Shaded circles are 925 hPa relative vorticity intensity. A indicates the beginning of Anita life cycle while Z indicates the end. Relative Vorticity units are 10^{-5} s^{-1}	83
Figure 5.12–(right) 925 hPa Relative vorticity (shaded), SLP (blue contour each 4 hPa) and 500 hPa geopotential height (red dashed contour each 100 gpm) (left) wind vectors and PV at 250 hPa (shaded) for cyclone Anita from CTL for the 09-11 March 2010 period.	84
Figure 5.13 - (right) 925 hPa Relative vorticity (shaded), SLP (blue contour each 4 hPa) and 500 hPa geopotential height (red dashed contour each 100 gpm) (left) wind vectors and PV at 250 hPa (shaded) for cyclone Anita from CFSR reanalysis for the 12-13 March 2010 period.	85
Figure 5.14- (left) Total surface heat fluxes (sensible heat + latent heat) and (right) temperature advection at 850 hPa for cyclone Anita from CTL for the 09-11 March 2010 period.	87
Figure 5.15 - (left) Total surface heat fluxes (sensible heat + latent heat) and (right) temperature advection at 850 hPa for cyclone Anita from CTL for the 12-13 March 2010 period.	88
Figure 5.16- (left) ThetaE (K) and wind vectors at 925 hPa (right) vertical cross-section of PV (dashed lines, PVU) and relative humidity	

	(shaded, %) for cyclone Anita from CTL for the 09-11 March 2010 period.	91
Figure 5.17	- (left) ThetaE (K) and wind vectors at 925 hPa (right) vertical cross-section of PV (dashed lines, PVU) and relative humidity (shaded, %) for cyclone Anita from CTL for the 12-13 March 2010 period.	92
Figure 5.18	- Phase space diagram for cyclone Anita from (top) CYC2, (middle) UPV and (bottom) BTPV. (left) B versus -VTL (right) -VTU versus -VTL.....	94
Figure 5.19	- Time evolution of thermal symmetry (B) of cyclone Anita from CFSR (black), CTL (red), CYC2 (green), UPV (blue) and BTPV (orange).....	96
Figure 5.20	- Trajectory of Anita cyclonic core from CFSR (black), CTL (red), CYC2 (green), UPV (blue) and BTPV (orange).....	97
Figure 5.21	- Wind vectors and PV at 250 hPa (shaded) for cyclone Anita from (top) CYC2, (middle) UPV and (bottom) BTPV for days 09 and 11 March 2010 at 18 UTC. PV units are PVU.	99
Figure 5.22	- Wind vectors and PV at 250 hPa (shaded) for cyclone Anita from (top) CYC2, (middle) UPV and (bottom) BTPV for days 12 and 13 March 2010 at 18 UTC. PV units are PVU.	100
Figure 5.23	- 925 hPa Relative vorticity (shaded), SLP (blue contour each 4hPa) and 500 hPa geopotential height (red dashed contour each 100 gpm) for cyclone Anita from (top) CYC2, (middle) UPV and (bottom) BTPV for days 09 and 11 March 2010 at 18 UTC. Relative Vorticity units are 10^{-5} s^{-1}	102
Figure 5.24	- 925 hPa Relative vorticity (shaded), SLP (blue contour each 4hPa) and 500 hPa geopotential height (red dashed contour each 100 gpm) for cyclone Anita from (top) CYC2, (middle) UPV and (bottom) BTPV for days 12 and 13 March 2010 at 18 UTC. Relative Vorticity units are 10^{-5} s^{-1}	103
Figure 5.25	- Temperature advection at 850 hPa for cyclone Anita from (top) CYC2, (middle) UPV and (bottom) BTPV for days 9 and 11 March 2010 at 18 UTC. Temperature advection units are 10^{-5} K s^{-1}	106
Figure 5.26	- Temperature advection at 850 hPa for cyclone Anita from (top) CYC2, (middle) UPV and (bottom) BTPV for days 12 and 13 March 2010 at 18 UTC. Temperature advection units are 10^{-5} K s^{-1}	107
Figure 5.27	- Equivalent potential temperature and wind vector at 925 hPa for cyclone Anita from (top) CYC2, (middle) UPV and (bottom) BTPV for days 9 and 11 March 2010 at 18 UTC. ThetaE units are K.....	109

Figure 5.28– Equivalent potential temperature and wind vector at 925 hPa for cyclone Anita from (top) CYC2, (middle) UPV and (bottom) BTPV for days 12 and 13 March 2010 at 18 UTC. ThetaE units are K.....	110
Figure 5.29 - Vertical cross-section of PV (dashed lines) and relative humidity (shaded) for cyclone Anita hPa for cyclone Anita from (top) CYC2, (middle) UPV and (bottom) BTPV for days 9 and 11 March 2010 at 18 UTC. RH units are % and PV units are PVU.	112
Figure 5.30-Vertical cross-section of PV (dashed lines) and relative humidity (shaded) for cyclone Anita hPa for cyclone Anita from (top) CYC2, (middle) UPV and (bottom) BTPV for days 12 and 13 March 2010 at 18 UTC. RH units are % and PV units are PVU.	113
Figure 5.31 - Total surface heat fluxes (sensible heat + latent heat) for cyclone Anita from (a) CTL, (b) UPV, (c) CYC2 and (d) BTPV at 00 UTC on 12th of March.	115
Figure 5.32 – Time evolution of the mean of vertical wind shear magnitude (200 hPa – 925 hPa) from CTL (red), UPV (blue), CYC2 (green) and BTPV (orange).	117

LIST OF TABLES

	<u>Pág.</u>
Table 3.1 – Summary of WRF configuration.....	27
Table 3.2 – Summary of sensitivity tests.	28
Table 3.3 – WRF Physics parameterizations.....	29
Table 4.1 – Mean cyclonic vorticity at the SCET in the SAO.....	35
Table 4.2 – Mean features for the selected periods for SCET evolution. Values in parentheses are standard deviation.	39
Table 4.3 – Criteria for SC identification used in previous studies.....	44

LIST OF ABBREVIATIONS

ATOVS	Advanced TIROS Operational Vertical Sounder
BTPV	Experiment with the lower tropospheric PV anomalies removed
CFSR	Climate Forecast System Reanalysis
CPS	Cyclone Phase Space
CYC2	Experiment with the ECY removed
ECY	Cyclone over Northern Argentina which interacts with Anita
ECMWF	European Centre For Medium-Range Weather Forecasts
ET	Extratropical Transition
GFDL	Geophysical Fluid Dynamical Laboratory
GS1	Gridpoint Statistical Interpolation
IEC	Intense Extratropical Cyclone
INPE	Instituto Nacional De Pesquisas Espaciais
LSM	Land Surface Model
MODIS	Moderate Resolution Imaging Spectroradiometer
MOM	Modular Ocean Model
NCAR	National Center for Atmospheric Research
NCEP	National Centers For Environmental Prediction
NEAO	Northeastern Atlantic Ocean
NHC	National Hurricane Center
NOA	North Atlantic Ocean
NOAA	National Oceanic And Atmospheric Administration
PV	Potential Vorticity
PVI	Potential Vorticity Inversion
SASA	South Atlantic Subtropical Anticyclone
SAO	Southern Atlantic Ocean
SC	Subtropical Cyclones
SCET	Subtropical Cyclones Undergoing Extratropical Transition
SID	Serviço De Informação E Documentação
SLP	Sea Level Pressure
SPG	Serviço De Pós-Graduação
SST	Sea Surface Temperature
SCT	Subtropical Cyclone
TC	Tropical Cyclone
TDI	Teses E Dissertações Internas
TIROS	Television And Infrared Observation Satellite
TOVS	TIROS Operational Vertical Sounder

TT	Tropical Transition
UPV	Experiment with the upper tropospheric PV anomalies removed
WEC	Weak Extratropical Cyclone
WISHE	Wind Induced Heat Exchange
WRF	Weather Research And Forecasting

SYMBOLS LIST

W	West
E	East
S	South
N	North
-VTL	Thermal wind at low levels
-VTU	Thermal wind at upper levels
B	Thermal symmetry
t	Time
PVu	Upper tropospheric Potential vorticity anomaly (400-100 hPa)
PVI	Lower tropospheric Potential vorticity anomaly (975-750 hPa)
TTb	Potential Temperature anomaly at lower boundary (1000 hPa)
PVt	Total Potential Vorticity anomaly (1000-100 hPa)

SUMMARY

	<u>Pag.</u>
1 INTRODUCTION	1
1.1. Objectives	4
2 BACKGROUND	5
2.1. Subtropical cyclones	5
2.2. Subtropical cyclones over SAO	8
2.3. Transition processes of cyclones	12
2.4. Potential Vorticity Inversion.....	14
3 DATA AND METHODOLOGY	17
3.1 Data	17
3.2 Tracking and Identification of SCTE	18
3.3 Numerical study of cyclone Anita	23
3.3.1 PVI	24
3.3.2 The WRF.....	26
4 CLIMATOLOGY AND COMPOSITES OF SUBTROPICAL CYCLONES UNDERGOING EXTRATROPICAL TRANSITION IN THE SOUTHWEST ATLANTIC OCEAN	31
4.1 Climatology of subtropical cyclones in SAO.....	31
4.2 Composite analysis.....	48
5 CASE STUDY: CYCLONE ANITA.....	64
5.1 Synoptic analysis and control simulation of cyclone Anita.	64
5.2 Potential Vorticity Inversion analysis.....	71
5.3 Numerical experiments: cyclone Anita	82
5.3.1 Control simulation.....	82
5.3.2 Sensitivity tests	93
6 SUMMARY AND CONCLUSIONS	119
6.1 Future work.....	122
REFERENCES.....	123

1 INTRODUCTION

In the last decades cyclones activity in the Southern Atlantic Ocean (SAO) have drawn considerable attention due to their impact in the regional weather, flooding, damage to infrastructure and loss of lives in Southeast Brazil. From the meteorological point of view these systems have an important role in the general atmospheric circulation because they are associated with the transport of energy, water vapor and momentum (GAN; RAO, 1991). Regarding their characteristics, extratropical cyclones most frequently occur over the SAO and the environs, but subtropical cyclones also occur in this region. On the other hand, the occurrence of tropical cyclones are rare because the SAO region is dominated by high values of vertical wind shear and relatively low sea surface temperatures, which are detrimental environmental conditions for the development of this type of system (EVANS; BRAUN, 2012).

The life cycles of tropical and extratropical cyclones have been studied for decades (SUGI et al., 2002; HART et al., 2006; RAMSAY et al., 2012; GAN; RAO, 1991; SIMMONDS; KEAY, 2000; REBOITA et al., 2010). Initially it was believed that tropical and extratropical cyclones had very different structures and life cycles. Later, it was acknowledged that transition processes between these cyclone types allow the existence of a hybrid type between them. These hybrid cyclones have characteristics of both tropical and extratropical types and are called Subtropical Cyclones (SC) (HART, 2003). SC are non-frontal low pressure systems which originate over oceanic areas in tropical and extratropical regions. They can develop as a pure subtropical cyclone or as a transition from one type of cyclone to another one. These systems present a low level warm core and high level cold core, whereas tropical cyclones have an upper level warm core and extra-tropical cyclones an upper level cold core. SC have a closed circulation at the surface and often stronger winds away from their center. A considerable fraction of SC energy is provided by baroclinic processes (WMO, 2012). Furthermore, these cyclones have potential to undergo extratropical and tropical transition. The transition process occurs

when one type of cyclone evolve into cyclone of a different type, representing a deviation from the typical development of that type of cyclone (HART; EVANS, 2001). Extratropical transition (ET) represents the transition of a subtropical/tropical cyclone to an extratropical one. On the other hand, tropical transition (TT) is the transition of an extratropical/subtropical cyclone into a tropical one.

In both hemispheres, cyclone characteristics have been studied through distinct methods, such as synoptic and composite analysis, objective tracking, cyclone phase space, potential vorticity inversion. These methods allow the evaluation of the environment in which a cyclone is embedded as well as its main features, identify and track cyclones during its entire life cycle, provide information about the cyclone structural evolution enabling a classification of the cyclone phase and contribute to the interpretation of the its dynamics, respectively. Cyclone tracking has previously been used to analyze the storm tracks in the Southern/Northern Hemisphere (HOSKINS; HODGES, 2002, 2005), the changes in extratropical cyclones in a warming climate (BENGTSSON; ROECKNER, 2006; CATTO et al., 2011), the seasonal variability of upper-level cut-of-lows in Southern Hemisphere (KOUSKY; GAN, 1981; KEABLE et al., 2002; REBOITA et al., 2010; PINHEIRO et al., 2017). The Cyclone Phase Space (CPS - HART, 2003) is a method to classify cyclones through their thermal vertical structure and has been used to evaluate the extratropical transition of Atlantic tropical cyclones (HART; EVANS, 2001; HART et al., 2006), tropical cyclones life cycles (SCHENKEL; HART, 2012), and SC climatologies (EVANS; GUSHARD, 2009; EVANS; BRAUN, 2012; GOZZO et al., 2014). Also, the transition processes of cyclones have been studied using Potential Vorticity Inversion (MCTAGGART-COWAN et al., 2001; AGUSTÍ-PANADERA, et al., 2005).

As an example of an extreme weather situation in the SAO region the occurrence of hurricane (Catarina) in March 2004 was an unusual event. This system developed as a subtropical cyclone but with characteristics typical of a tropical storm as well as of an extratropical cyclone (SILVA DIAS et al., 2004).

Hurricane Catarina had a severe impact on the southern coast of Brazil including loss of human lives, flooding and damage to property. After this rare weather event for the region, more attention has been given to subtropical cyclones and tropical transitions systems in the SAO region. In March 2010 another subtropical cyclone in the SAO region drew attention, when a cyclone called Anita developed as a subtropical cyclone and presented the potential for tropical transition. However, the transition never took place because of the prevailing reduced oceanic heat content and the interaction with an extratropical disturbance, resulting in an extratropical transition (DIAS PINTO et al., 2013).

Recently Evans and Braun (2012) presented a climatology of subtropical cyclones in the SAO. They identified several synoptic characteristics and development mechanisms of 63 subtropical cyclones that occurred in the 1957 – 2007 period. Gozzo et al. (2014) observed that the subtropical cyclones are more frequent in the austral summer and that cyclone genesis occurs mainly on the southeastern coast of Brazil. They also found an annual mean of 7 subtropical cyclones in the 1979 - 2011 period. In addition, they observed that in the SAO region subtropical cyclones travel smaller distances and more slowly than extratropical cyclones, which allow them to interact strongly with the environment, supporting convective activity and causing adverse weather conditions, and frequently undergo extratropical transition reaching maxima intensity in the subtropical phase (GOZZO et al., 2014).

Although subtropical cyclones are not as frequent as extratropical cyclones, the understanding and forecast of these systems are very important since the development of subtropical cyclones in the SAO region can be associated with several adverse weather conditions in the important industrial region of southeastern Brazil. Nevertheless, there are few studies of subtropical cyclones in the South American region and most are case studies. Subtropical cyclones typically reach the southeastern coast of Brazil, having associated strong winds, extreme rainfall and strong sea waves.

Many studies have been dedicated to the extratropical transition of tropical cyclones (HART; EVANS, 2001; MCTAGGART-COWAN et al., 2003; HART et

al., 2006, STUDHOLME et al., 2015). On the other hand, there are few studies regarding the extratropical transition of subtropical cyclones. Despite that, Gozzo et al. (2014) indicated that many SC undergo ET during the summer, the most cyclogenetic season of SC in the SAO.

Previous studies showed that subtropical cyclones undergoing extratropical transition (SCET) are relatively frequent during the austral summer in the SAO. Although, it has been established that SC in this region can be associated with adverse weather, there is a lack of studies evaluating the meteorological conditions associated with SCET and their impact in the weather over the South America. Understanding the environment associated with SCET and the main mechanisms leading to ET may improve the forecast of these transitioning cyclones. Also, it can provide more information for potential TT cases. In this context, it is important to improve the knowledge of SCET in the SAO to evaluate the dynamical features associated with these systems and investigate the synoptic environment associated with the transition process.

1.1. Objectives

The main objectives of this study are to investigate the leading dynamical features of subtropical cyclones undergoing extratropical transition in the SAO. Specifically the science questions are:

- a) What is the climatology of SCET in the SAO?
- b) What are the main mechanisms associated with extratropical transition in the SAO?
- c) What are the impacts of Potential vorticity anomalies on the life cycle of SCET?

2 BACKGROUND

2.1. Subtropical cyclones

SC are non-frontal low pressure systems which originate over the ocean in tropical and extratropical regions. Because these systems have characteristics of tropical and extratropical cyclones (low level warm core and high level cold core) they are also called hybrid cyclones. Similar to tropical cyclones, SC have a closed circulation in the surface wind field. However, SC often have stronger winds away from their center and less symmetry in their winds and convection. Furthermore, a considerable fraction of their energy is provided by baroclinic processes (WMO, 2012). SC are defined as subtropical storms if they attain wind speed greater than 17 ms^{-1} . These cyclones may be associated with adverse weather conditions, such as strong winds, extreme rainfall and flooding. Moreover, SC have potential to undergo extratropical and tropical transition.

Simpson (1952) presented the first climatological analysis of SC structure and evolution. In that study, Kona storms, which occur on the Eastern Pacific Ocean during winter season, were referred as SC. Initially, Kona cyclones have a cold core low in the mid to upper troposphere. Subsequently, these systems can develop warm core features similar to tropical storms, causing intense winds and extreme rainfall over Hawaii. The evolution of these SC is associated with the development of a stationary occluded cyclone or with the propagation of upper level trough/cut-of-low towards the equator (SIMPSON, 1952; MORRISON; BUSINGER,2001; OTKIN; MARTIN,2004).

SC are also observed along the eastern coast of Australia, mainly in winter. Holland et al. (1987) identified three types of cyclones developing in this region. Types 1 and 3 are small and short lived systems. On the other hand, type 2 represents meso-scale cyclones that cause strong winds and heavy precipitation for several days. Over the Tasmanian Sea, SC genesis is associated with the presence of a trough or cut-of-low in the mid troposphere in

a strongly baroclinic region. Braun (2009) inferred that SC in South Atlantic Ocean develop over an environment similar to the observed for east coast Australia cyclones. Both regions have Mountains near the coast and warm oceanic current transporting warm water towards higher latitudes.

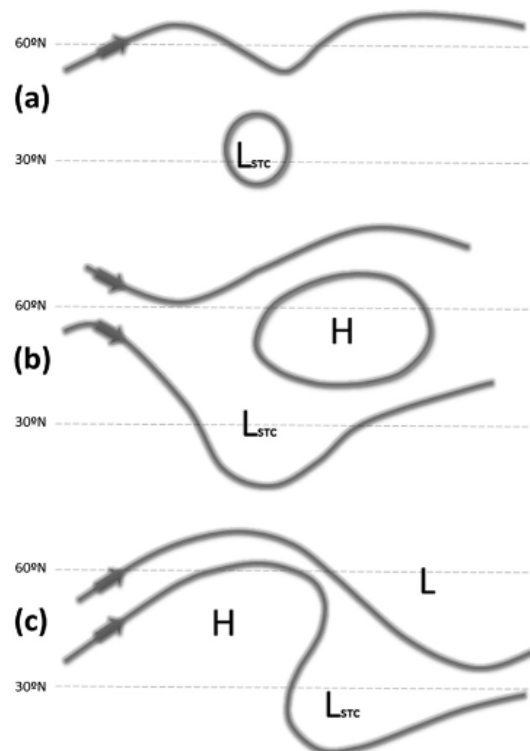
Evans and Guishard (2009) used the cyclone phase-space (HART, 2003) to elaborate the first conceptual model of the genesis of SC in the North Atlantic Ocean. They observed that a high level trough intrusion in a region of high Sea Surface Temperature (SST) and weak static stability is the main mechanism for the genesis of SC. Evans and Guishard (2009) proposed four categories of subtropical cyclogenesis with respect to SST's and wind shear: 1) tropical environment – SST greater than 25°C and wind shear lower than 10 ms⁻¹; 2) subtropical environment – SST greater than 25°C and wind shear greater than 10 ms⁻¹; 3) extratropical environment 1 – SST less than 25°C and wind shear greater than 10 ms⁻¹ and 4) extratropical environment 2 – SST less than 25°C and wind shear less than 10ms⁻¹.

High SSTs contribute to the genesis of SC as it does for tropical cyclones. However, in the case of SC development, the SST required is lower ($T > 25^{\circ}\text{C}$). As SC do not have a deep warm core, it is improbable that these systems could fully develop and sustain their circulation with only surface fluxes without interacting with a high level trough or cut-of-low. These negative vorticity anomaly systems generate deep ascending motion resulting in cyclonic development by Wind Induced Surface Heat Exchange (WISHE) (GUISHARD et al., 2009). It is worth mentioning that if there is sufficient convection so the SC's warm core deepens up to higher levels, dissipating the upper level cold core, then this system can become auto-sufficient and the tropical transition can occur (GUISHARD et al., 2009).

González-Alemán et al. (2015) performed a classification and synoptic analysis of SC that occur over the Northeastern Atlantic Ocean (NEAO). They evaluated 15 SC occurring in the 1979 – 2011 period. Synoptic analysis showed that subtropical depressions act as a precursor when isolated from the westerly flow. Three conceptual models of subtropical cyclogenesis based on geopotential

height at 300 hPa were presented: cut-off-low, flow bifurcation and prolongation (Figure 2.1). Furthermore, it was observed that most of these systems occur in an environment with strong wind shear and low SSTs (<25°C). González-Alemán et al. (2015) indicate that SC over NEAO have features more similar to extratropical cyclones, while the ones over the Western Atlantic Ocean have features resembling tropical cyclones. On the other hand, SC over NEAO resemble the ones found in the SAO due to the similarities between the environments in which they develop.

Figure 2.1 – Conceptual model of geopotential height at 300 hPa of subtropical cyclogenesis patterns in NEAO: (a) cut-off-low, (b) bifurcation, and (c) prolongation.



The arrows indicate the approximately sense of the flow at 300 hPa; L denotes low pressure region, H high pressure region and STC denotes subtropical cyclone.

Source: Adapted from González-Alemán et al. (2015).

2.2. Subtropical cyclones over SAO

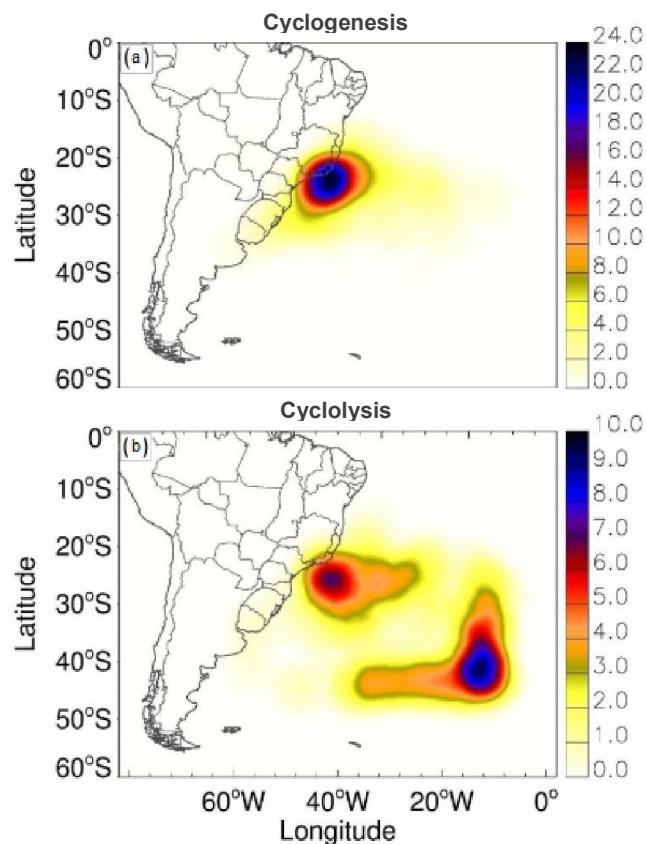
The first climatology of SC over the SAO was obtained by Evans and Braun (2012). Employing the 40-yr European Centre for Medium-Range Weather Forecasts (ECMWF) reanalysis, they identified 63 SC from 50 years (1957-2007) and found that the preferential area of genesis was located between 20°S-40°S/60°W-30°W. Gozzo et al. (2014) used the Interim ECMWF reanalysis and the NCEP/NCAR reanalysis to elaborate a climatology of SC and observed an annual mean frequency of approximately 7 SC per year in the 1979-2011 period. This value is higher than the one found by Evans and Braun (2012) due the inclusion of shallow and weak SC, i.e., cyclones that did not deepen in to mid troposphere and with wind magnitudes lower than 17 ms^{-1} , which suggests that this type of SC is actually very frequent in the SAO. The previously mentioned studies also differ on the seasonal variability of SC. While the first identified the cold seasons as the season with the higher cyclogenesis, the later found that SC are more frequent in the austral summer. This discrepancy is due to the summer environment favors the development of shallow hybrid cyclones, which were only included in the climatology presented by Gozzo et al. (2014).

The main subtropical cyclogenesis region near South America is located on the southeast coast of Brazil (Figure 2.2), between 20°S – 40°S and 60°W – 10°W. More than half of these SC develop over the Brazil Current region due to the convection favored by local surface fluxes or warm air advection. Areas of cyclolysis are centered in 25°S/40°W and 40°S/10°W with the first being very close to the genesis region (Figure 2.2b). This occurs because SC propagate smaller distances and are slower than extratropical cyclones in the South Atlantic basin. Thus, these systems can interact strongly with the environment, favoring convective activity and causing adverse weather over the SAO region (EVANS; BRAUN, 2012; GOZZO et al., 2014).

The main mechanism of SC development over the Brazilian southeast coast is associated with the establishment of a cyclonic circulation northward of an anticyclonic one at upper levels. This configuration is known as Rex blocking

pattern which often decreases wind shear and prevents the propagation of cyclones. The cyclonic circulation at upper levels, associated with negative anomalies of Potential Vorticity (PV) westward of the surface cyclone, and the presence of a cut-of-low in the mid troposphere act to deepen the cyclones. At mid and upper levels, the structure of SC over the SAO resembles the ones that develop in extratropical 1 and extratropical 2 environments described by Evans and Guishard (2009), specifically during the austral summer and autumn (GOZZO et al., 2014).

Figure 2.2 – Subtropical cyclogenesis and cyclolysis density over SAO.

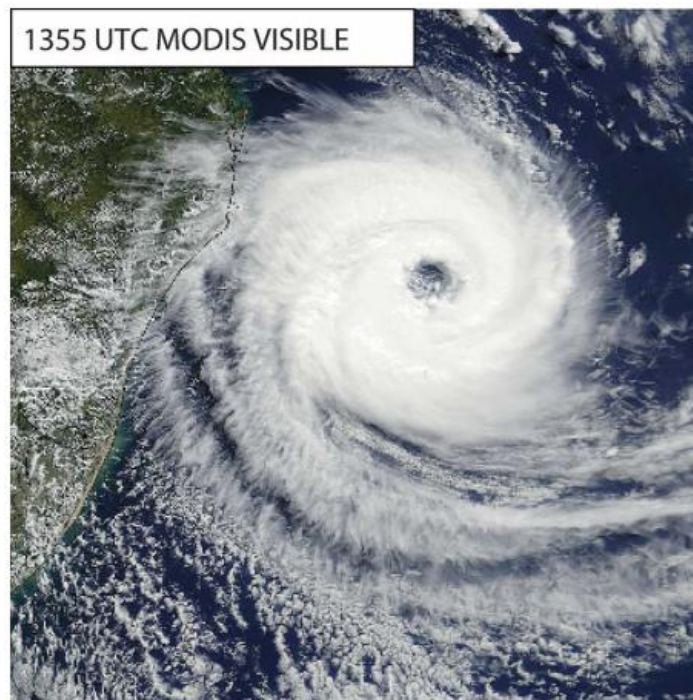


Source: Adapted from Gozzo et al. (2014).

Hurricane Catarina, which occurred in March 2004 over the SAO, was the first of its category registered in this region (

Figure 2.3). Several studies showed that this system initially developed as an extratropical cyclones propagating toward the southeast coast of Brazil (MCTAGGART-COWAN et al., 2006; VEIGA et al., 2008, PEZZA et al., 2009). The presence of an intense dipole-type blocking, made this extratropical cyclone reverse its trajectory, propagating toward the continent. This environment favored the development of a hybrid cyclone and subsequently its tropical transition. The tropical transition occurred over relatively cool SSTs (near 25°C) and with weak vertical wind shear (MCTAGGART-COWAN et al., 2006; PEZZA et al., 2009).

Figure 2.3 – Hurricane Catarina as seen on Visible high resolution image for 1355 UTC 27th March 2004, obtained from Moderate Resolution Imaging Spectroradiometer (MODIS)/Terra Satellite.

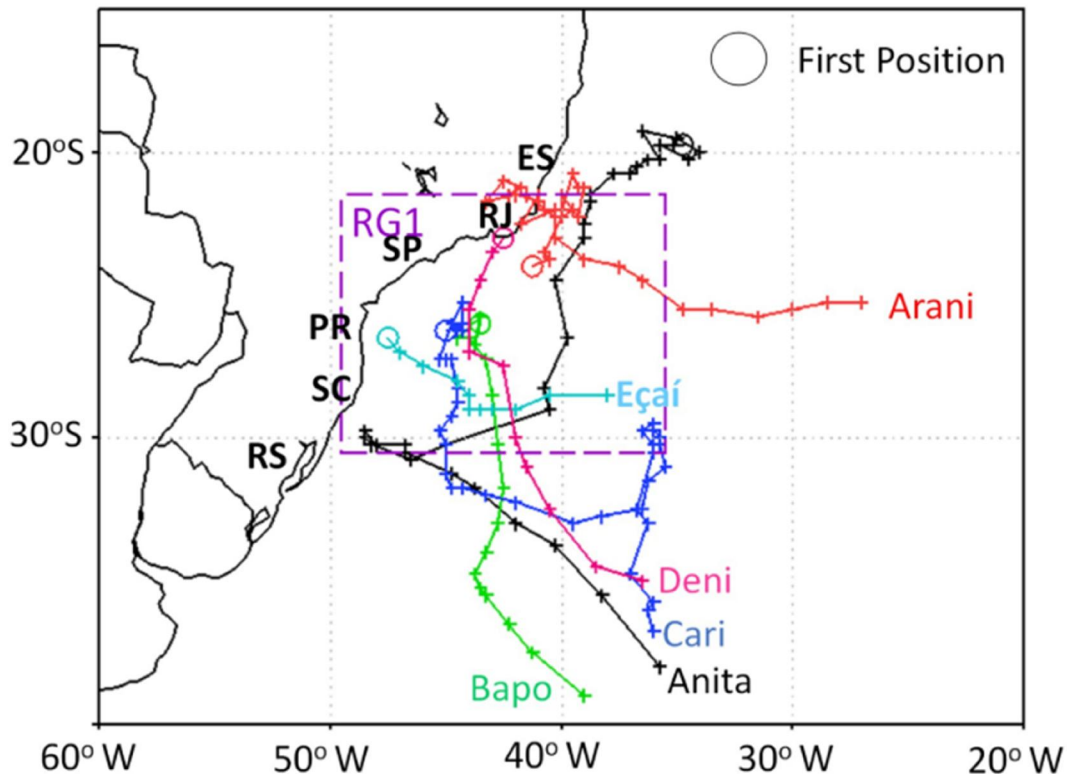


Source: Adapted from McTaggart-Cowan et al. (2006).

In March 2010, SC Anita, developed over the southeast coast of Brazil. Dias Pinto et al. (2013) highlighted that this system developed as a pure subtropical cyclone and had the potential to undergo tropical transition during its life cycle. However, this transition did not happen due to the decrease of turbulent heat fluxes and the interaction of cyclone Anita with an extratropical disturbance in that region, leading to an increase of vertical wind shear causing the system to undergo extratropical transition. Thus, Anita propagated westward toward cooler waters decreasing the turbulent heat fluxes (DIAS PINTO et al., 2013).

Six named SC that occurred in the last decade over the SAO, near the Brazilian coast were studied by Reboita et al. (2019). The genesis of these systems was found to be associated with a cut-off low (or mid-level trough), weak vertical wind shear and moisture flux convergence. The trajectories of each SC are shown in Figure 2.4. All of these cyclones, excepted Anita, developed on the main subtropical cyclogenetic region over the SAO (GOZZO et al., 2014). Reboita et al. (2019) verified that these SC were associated with extreme weather events, such as strong winds and large amount of precipitation, with the most intense events being associated with rainfall higher than the monthly climatology of the affected region. Analyzing the structure of these cyclones, Reboita et al. (2019) observed that 5 of them underwent extratropical transition. It should be mentioned that in this studied the extratropical transition was characterized as the time when the cyclone became a cold core system.

Figure 2.4 – Trajectory of the six named SC based on 925 hPa relative vorticity.



The circles indicate the first position of each system. The purple box defines the southeastern coast of Brazil called RG1. RS, SC, PR, SP, RJ and ES indicate the Brazilian states: Rio Grande do Sul, Santa Catarina, Paraná, São Paulo, Rio de Janeiro and Espírito Santo, respectively.

Source: Adapted from Reboita et al. (2019).

2.3. Transition processes of cyclones

Tropical and extratropical cyclones have been studied separately for decades until close inspection of modern satellites images allowed the observation that one type of cyclone can evolve into another one. For tropical cyclones, this transition usually occurs when the cyclone propagates toward higher latitudes, over colder waters with stronger wind shear. This process is called extratropical transition (HART; EVANS, 2001). Hart and Evans (2001) presented an

extensive analysis of tropical cyclones over the North Atlantic Ocean (NAO) in the 1950-1996 period using the National Hurricane Center (NHC) best-track dataset. They observed that 46% of the identified tropical cyclones underwent extratropical transition. Also, they pointed out that the northeast coast of United States, Western Europe and Canadian Maritime region are the preferred regions for the extratropical transition of these systems. This process is more frequent between 30°N - 35°N (40°N – 50°N) at the beginning and end (peak) of the hurricane season.

Hart et al. (2006) found that the extratropical transition of tropical cyclones for the NAO is conducted by angular momentum changes associated with a trough. The PV forcing generates adiabatic upward motion and cooling in its core and under the forcing, in order to restore the thermal balance. Also, the heat flux is significant only after the extratropical transition takes place. The structure and intensity of the post-transition cyclones are very ambiguous, being mainly associated with the tropical cyclone-trough interaction. On the other hand, SST plays a role key up until the transition phase (HART et al., 2006).

Kitabatake (2008) investigated the extratropical transition occurring in the Northwestern Pacific Ocean in terms of frontal evolution. It was observed that 44% of the identified tropical cyclones underwent extratropical transition. These systems were classified into three categories based on the equivalent potential temperature and features of tropical cyclones and their environment: 1) temporary warm seclusion in the tropical phase and occlusion in the post-transition phase and occurs downstream of a strong trough at upper levels; 2) cold advection type where the tropical cyclones (TC) apparently were absorbed into preexisting fronts associated with midlatitude cyclones; and 3) cyclones associated with baroclinic zones at mid latitudes.

TT occurs when an extratropical baroclinic cyclone evolves into a warm core tropical cyclone. According to NOAA's Tropical Prediction Center, almost half of tropical cyclones in the NAO, in the 2000-2003 period, developed from an extratropical cyclone (DAVIS; BOSART, 2004). Davis and Bosart (2004)

identified two different categories of tropical transition, one occurring from an intense extratropical cyclone (IEC) and another from a weak one (WEC). In the IEC cases, a frontal cyclone develops with sufficient strength to trigger off WISHE. Also, the upper level flow and the redistribution of diabatic potential vorticity decrease the vertical wind shear. On the other hand for the WEC, act to organize convection, which in its turn generates a disturbance capable of self intensification (DAVIS; BOSART, 2004).

Garde et al. (2010) analyzed a tropical transition case related to cyclone Duck over southeastern Australia. This weather event developed over the Tasmanian Sea in March 2001 with hybrid cyclone characteristics. The atmospheric environment in which Duck took place presented a blocking pattern over the Tasmanian Sea. This blocking caused bifurcation and a northward displacement of the subtropical jet, allowing the weakening of the wind shear in that region. The constant intrusion of potential vorticity anomalies from high latitudes reinforced the associated environment. The SST's anomalies were negative near the Australian coast but with values above 26.5°C. All these features favored tropical transition (GARDE et al., 2010). Furthermore, Garde et al. (2010) suggested that the atmospheric conditions associated with Duck were similar to that observed for Hurricane Catarina in March 2004.

2.4. Potential Vorticity Inversion

Potential Vorticity Inversion (PVI), developed by Davis and Emanuel (1991), allows the dynamical effects of surface cyclogenesis associated with PV anomalies in the lower and upper troposphere to be evaluated due to the invertibility and conservative properties of PV. The conservative principle allows the identification of the friction and diabatic processes associated with of the cyclone's development (DAVIS; EMANUEL, 1991).

Besides the evaluation of the dynamical contributions of PV to cyclogenesis, this method also can be applied to improve the initial conditions for Numerical Weather Forecast Models. Through PVI, Huo et al. (1998) calculated the balanced temperature field associated with a storm that took place in the

Mexican Gulf in 1993. The balanced temperature was used as initial conditions for forecasting this storm. It was observed that a significant improvement in the simulation of the storm's intensity and trajectory occurred due to the improved treatment of errors associated with the near surface temperature.

Funatsu (1999) analyzed the influence of PV anomalies on the development of an extratropical cyclone in South America. The extratropical cyclone developed due the propagation of an upper level cyclonic vortex which extended to the surface. After crossing the Andes Mountains, this vortex interacted with a stationary wave (induced by the Andes), generating a baroclinic structure which provided energy to the developing extratropical cyclone. Most apparent were the contributions of three distinct PV anomalies: surface potential temperature, upper level PV and low level PV (FUNATSU, 1999).

Applying the PVI method, McTaggart-Cowan et al. (2001) evaluated the role of PV anomalies in the re-intensification of Hurricane Earl that occurred on the eastern coast of the United States in 1998. It was observed that the upstream trough was essential for the storm regeneration. On the other hand, the circulation at low levels associated with the cyclone decay played a secondary role.

Iwabe (2012) analyzed the impact of PV anomalies on different types of secondary cyclones in the SAO (Type 1 and type 2). Type 1 cyclones developed over the warm front region of the primary cyclone and type 2 formed over the low level cold advection region. The study found that secondary cyclones were significantly impacted when the PV anomalies were removed from the initial conditions. Type 1 secondary cyclones developed later and weaker. Subsequent analysis showed that the interaction between the PV anomaly and surface fluxes was actually the main mechanism to the intensification of this system. On the other hand, type 2 secondary cyclones did not developed in the absence of PV anomalies.

3 DATA AND METHODOLOGY

3.1 Data

The data used for this study is derived from the National Centers for Environmental Prediction (NCEP) - Climate Forecast System Reanalysis (CFSR). This data set was produced from a global, ocean-atmosphere-land coupled system, considering ice and sea surface. The CFSR uses a global atmospheric spectral model with a spatial resolution of approximately 38 km (T382) with 64 hybrid vertical levels. The ocean model used is the Modular Ocean Model (MOM). This model has 40 vertical levels and a meridional resolution of 0.25° between 10°S and 10°N latitudes, increasing gradually toward higher latitudes up to 0.5° in 30°N and 30°S. The surface model has four soil layers while the sea ice model has three. The Land Surface Model (LSM) used is the Noah LSM and the sea ice model is from the Geophysical Fluid Dynamical Laboratory (GFDL) Sea Ice Simulator. The NCEP-CFSR uses the atmospheric GSI (Gridpoint Statistical Interpolation) data assimilation system. A fixed set of conventional observations is assimilated along with temperature retrieved from TIROS (Television and Infrared Observation Satellite) Operational Vertical Sounder (TOVS) and Advanced TOVS (ATOVS). An ocean analysis for SST is performed through optimal interpolation.

The dataset used in the present study has 27 levels, a horizontal resolution of 0.5° x 0.5° (latitude x longitude), a time resolution of 6h (00, 06, 12, 18 UTC) and covers the period 1985 – 2015. The 925 hPa relative vorticity was used for tracking the cyclones over the SAO. The geopotential height fields at 300, 600 and 900 hPa were used to compute the thermal wind and thermal asymmetry. For the composites the PV, Sea level Pressure (SLP), SST, temperature, geopotential height, wind components and sensible/latent heat fluxes fields were used. The data used to compute the Potential vorticity inversion was similar to the above, but has 26 pressure levels and horizontal resolution of 2.5°

x 2.5° due to the software used requiring lower resolution data. The fields used were geopotential height, wind components and temperature.

3.2 Tracking and identification of SCTE

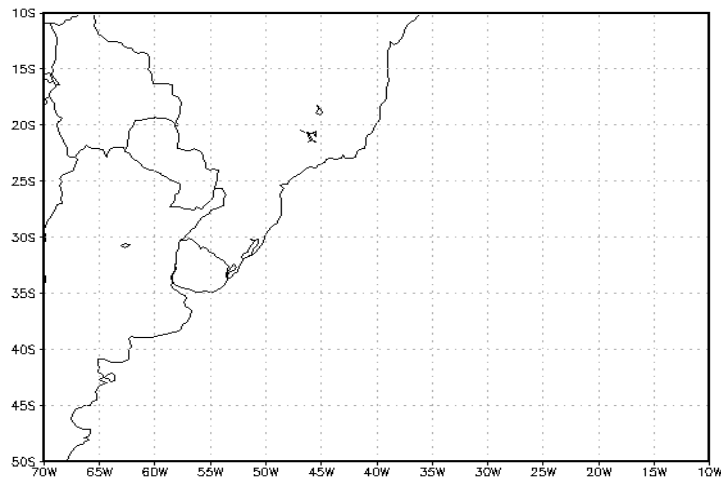
The identification and tracking of the cyclones was performed using the TRACK algorithm (HODGES, 1994, 1995). The TRACK method consists of the identification of objects such as extremes points in meteorological fields. The vorticity is spectrally filtered using a spherical harmonic expansion based on the fast spectral transform. The filter truncates to T63 resolution and tapers the coefficients to reduce Gibbs noise, the planetary scales are also removed by setting total wave numbers $n \leq 5$ to zero. This has the effect of smoothing the noisy high resolution vorticity data. Vorticity minima are identified on the T63 grid that are below $-0.5 \times 10^{-5} \text{ s}^{-1}$ (feature points), which are then used to identify the off-grid points using B-splines and minimization, this has the benefit of producing smoother tracks. The feature points are initialized into tracks based on the nearest neighbor method. These tracks are refined using an optimization method that minimizes a cost function for the track smoothness, measured in terms of changes in direction and speed, subject to adaptive constraints on the displacement distance in a time step and the local track smoothness. This function is build from the trajectories deviation, calculated using the positions of feature points in three consecutive frames. For each trajectory the deviation can be computed from direction, speed or acceleration individually or combined in any way. After the tracking has completed the tracks are filtered to retain only those that last longer than 1.5 days. The tracking was applied to the November-March months.

Initially, all cyclonic systems that occurred between 50°S-10°S and 70°W-10°W were selected (Figure 3.1). The thresholds used for identification of these systems through TRACK algorithm are: 925 hPa relative vorticity less or equal $-1.5 \times 10^{-5} \text{ s}^{-1}$ and lifetime of at least 24 hours. These systems may or not present closed isobars in the SLP field, i.e., the presence of a closed isobar is not a necessary condition for the system to be considered a cyclone, since its occurrence depends on the flow intensity (SINCLAIR, 1994). Dates and hours, positions and intensities of the cyclones are used to calculated the parameters in the phase-space diagram from which the identification of subtropical cyclones

are done according to the criteria presented by Gozzo et al. (2014). These parameters are obtained from the geopotential height field. The data is sampled into a 5 degree radial grid orientated in the direction of propagation of the cyclones. Then the CPS parameters are added to the tracks.

The systems that occurred during the November-March of 1985-2015 period were selected. This period was chosen since these are the months with highest occurrence of SC in the SAO (GOZZO et al., 2014). Evans and Braun (2012) found that SC are more frequent during the austral autumn and winter. However, Gozzo et al. (2014) found that the highest occurrence of these cyclones in the SAO region occurs along the austral summer and autumn. Evans and Braun (2012) used a more rigorous criteria for SC selection, such as the presence of a cut-of-low at 500 hPa and minimum wind of 17 ms^{-1} . Thus, shallow cyclones with weaker wind intensities were excluded. In the present study, the criteria of minimum wind and presence of mid level cut-of-low were not used in order to simplify the identification of shallow subtropical cyclones.

Figure 3.1– SC tracking area used in the current study.



Source: Author's Production.

The Cyclone Phase Space (HART, 2003) diagram describes the life cycle of cyclones allowing them to be classified according to their cyclone structure. This

diagram defines the structure of the cyclones using three parameters that are calculated through the geopotential height field: the lower tropospheric thermal symmetry (B) and the lower – and – upper tropospheric thermal wind parameters (-VTL and -VTU, respectively). Large positive (near-zero) values of B indicate an asymmetric (symmetric) cyclone. Positive values of -VTL or -VTU indicate a warm core structure of the cyclone. On the other hand, negative values of these variables are related to a cold core structure. A subtropical cyclone is characterized by small values of B, positive -VTL and negative -VTU, indicating that these systems are almost symmetric (non-frontal) and present a low (upper) level warm (cold) core. Thus, a tropical cyclone is characterized by positive -VTL and -VTU, with -VTL presenting higher magnitude. Differently, an extratropical cyclone has negative values of these parameters, with -VTU presenting higher magnitude. Hybrid cyclones, warm seclusion and transitioning ones can have opposite signs for the thermal wind parameters.

The thermal wind parameters are defined as the variation of thickness between two pressure levels, at low and high levels, and are calculated as:

$$-|V_T^U| = \frac{\partial(Z_{max} - Z_{min})}{\partial \ln p} \Big|_{600}^{300} = \frac{(Z_{max} - Z_{min})|_{300} - (Z_{max} - Z_{min})|_{600}}{\ln 300 - \ln 900}$$

$$-|V_T^L| = \frac{\partial(Z_{max} - Z_{min})}{\partial \ln p} \Big|_{900}^{600} = \frac{(Z_{max} - Z_{min})|_{600} - (Z_{max} - Z_{min})|_{900}}{\ln 600 - \ln 900}$$

where Z is the isobaric height evaluated in a 500 km radius around the cyclone Center. This radius is necessary for adequately solve the vertical cross-section of zonal height gradient by the vertical tilt associated with extratropical cyclones.

Similarly as the thermal wind, the thermal asymmetry considers the thickness variations in two semicircles of 500 km radius around the cyclone center. This parameter is defined as:

$$B = h(\overline{Z_{600} - Z_{900}}|_D - \overline{Z_{600} - Z_{900}}|_E)$$

where D represents the right semicircle related to the cyclone Center, E is the left semicircle and h is equal -1 (1) in South Hemisphere (Northern Hemisphere). Positive values of B represent mature or developing extratropical cyclones. On the other hand, near zero values indicate tropical or occluded extratropical cyclones.

The criteria for SC identification are as follow:

- a) Cyclones must develop between 20°S-40°S. This criteria was employed to avoid the inclusion of meso-scale vortices and polar lows at high latitudes that also have a warm core due latent heat release.
- b) To be characterized as a hybrid thermal structure, with upper level cold core and low level warm core, persisting for at least 36 hours. The thermal wind parameters must be $-V_T^U \leq -10$ e $-V_T^L \geq -50$.
- c) The thermal asymmetry parameter (B) must be less than 25 m for at least 36 consecutive hours.
- d) To above mentioned parameters values ($-V_T^U, -V_T^L$ e B) must be attained within the first 24 hours of the cyclones' life cycle. This criteria ensures that only pure subtropical cyclones are identified, i.e., the cyclones which developed with hybrid structure and maintained this feature for at least 24 hours.

After tracking the SC, only the systems that underwent extratropical transition were selected. The identification criteria for the transitioning cyclones are defined as the time when the lower tropospheric thermal wind indicates a cold core and intensification in the asymmetry of the cyclone. This means that $-VTL < -50$ and $B > 25$ m. To avoid the selection of short lived SCET this features should remain for at least 24 hours. This understanding of extratropical

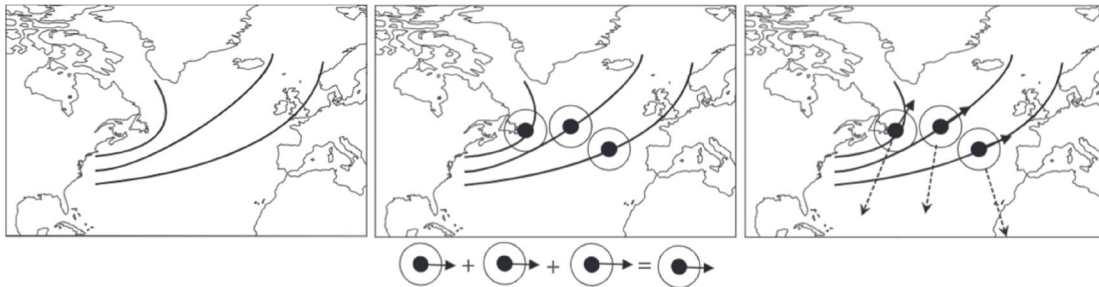
transition for subtropical cyclones is similar to the one for tropical cyclones which consider that transition is completed when the cyclone turn into a cold core system and loses its symmetry (ARNOTT et al., 2004; STUDHOLME et al., 2015).

The statistics of the trajectories, the track, cyclogenesis and cyclolysis densities and the density of extratropical transition location were computed from track data using the spherical nonparametric estimators (HODGES, 1996). This technique uses adaptive spherical kernel functions to provide smoothing to the statistical diagnostic fields.

Subsequently, composites of meteorological fields were computed to evaluate the mean structure and synoptic features associated to these cyclones. The method used by Bengtsson et al. (2007) allows the evaluation of the typical structure of cyclones by sampling a field onto a cyclone centered spherical cap radial grid which obviates the kind of biases that can be introduced if using a projection. The radial grid is defined centered on the north pole and then is rotated to be centered on the cyclone center.

The basic steps to compute the composites of SCET are described by the following steps. The first one evolves the identification of the SCET trajectories. The second one finds the point in which the ET threshold is reached at each trajectory. A radial coordinate system centered on the pole is created for a spherical cap of a chosen radius. In the third step, this spherical cap is positioned over the selected track point and then is rotated to the propagation direction of the cyclone. Then, the region under this spherical cap is extracted on to the radial grid. Finally, the average over all selected cyclones is taken. A detailed description of this procedure is found in Catto et al. (2010).

Figure 3.2 – Schematic of the three steps to the compositing.



Source: Adapted from Catto et al. (2010).

Composites have been performed for different fields, such as SLP, PV at 250 hPa, 500 hPa geopotential height, surface heat fluxes, wind at 250 hPa. For each field, the 20° spherical cap is extracted using the feature point at 925 hPa relative vorticity as the reference. Time $t = 0$ was considered as the time step of extratropical transition occurrence. The fields of 72 h, 48 h and 24 h before ($t = -72$ h, $t = -48$ h, $t = -24$ h, respectively) and after ($t = +72$ h, $t = +48$ h, $t = +24$ h, respectively) the transition time were also analyzed. Next a case study of a SCET is used to illustrate the main meteorological features of these weather systems. The selected SCET case was related to the cyclone Anita, because it presented a condition favorable to tropical transition before it becomes an extratropical cyclone. Different meteorological fields are analyzed along Anita's life cycle to give insight of its dynamical structure and synoptic features. Also, the impact of PV anomalies to the extratropical transition was evaluated.

3.3 Numerical study of cyclone Anita

To investigate the impact of potential vorticity anomalies in the development and transition processes of subtropical cyclones in the SAO region the potential vorticity inversion method and the WRF (Weather Research and Forecasting) model were used. First, the PV inversion is applied to identify potentially significant PV perturbations in the life cycle of the subtropical cyclone. Therefore, each PV anomaly was analyzed separately by removing it from the mean state and using the PVI to obtain the pertinent balanced fields. These

new fields, without the respective PV anomaly, are then used as initial conditions for WRF in order to obtain a prognosis of the impact of each one of these in the SCET life cycle.

From the PVI, geopotential height and stream function associated with the PV anomalies were recovered, which allowed the non-divergent wind fields to be obtained. Also, the temperature field was calculated from the following hypsometric equation:

$$\Phi_2 - \Phi_1 = \frac{R\bar{T}}{g} \ln\left(\frac{p_1}{p_2}\right) \quad (3.1)$$

where Φ is the geopotential height, R is the specific gas constant of dry air, T is temperature, g is gravitational acceleration and p is pressure.

Thus, the balanced fields (without the PV anomaly) of geopotential height, temperature and wind were adapted to use as initial conditions for the WRF model. A control simulation was used to corroborate an analysis of the influence of the forcing mechanisms.

3.3.1 PVI analysis

The PV inversion method allows the balanced dynamical fields to be recovered using the invertibility principle. This is possible because PV is a conserved quantity in the absence of frictional and diabatic processes, allowing one to identify developments that are influenced by these processes. Also, the invertibility principle can be used to quantify such effects (DAVIS; EMANUEL, 1991). The balanced fields obtained from the PV inversion are the geopotential height and the stream function. From these fields, variables like temperature, pressure and wind can be obtained.

The PV inversion method (DAVIS; EMANUEL, 1991) is derived from the Charney balance equation (CHARNEY, 1955). This equation is obtained by taking the horizontal divergence of the horizontal momentum equations and

decomposing the wind field into a rotational non-divergent and an irrotational divergent part through the Helmholtz Theorem. Applying scale analysis (HALTINER; WILLIAMS, 1980) and assuming the irrotational divergent winds are much smaller than the rotational non-divergent winds, the terms associated with the former can be neglected. The resulting equation in spherical coordinates is:

$$\nabla^2 \phi = \nabla(f \nabla \psi) + \frac{2}{a^4 \cos^2 \phi} \frac{\partial(\frac{\partial \psi}{\partial \lambda} \frac{\partial \psi}{\partial \phi})}{\partial(\lambda, \phi)} \quad (3.2)$$

Where ϕ is the geopotential, f the Coriolis parameter, ψ the non-divergent stream function, λ longitude, ϕ latitude and a represents the earth's radius. Equation 3.2 reduces to geostrophic balance if f is constant and the Jacobian term is neglected. In order to close the system and obtain ϕ and ψ , the Ertel's Potential Vorticity equation is used:

$$PV = \rho^{-1} \zeta_a \nabla \theta \quad (3.3)$$

where ρ is the air density, ζ_a the absolute vorticity vector and θ the potential temperature. Considering the vertical component of the Equation 3.3 in vertical coordinates of pressure and then changing it to the Exner function π , the following equation is obtained:

$$PV = -g \frac{k\pi}{p} \left[(f + \zeta) \frac{\partial v}{\partial \theta} - \frac{\partial v}{\partial \pi} \frac{\partial \theta}{a \cos \phi \partial \lambda} + \frac{\partial u \partial \theta}{\partial \pi a \partial \phi} \right] \quad (3.4)$$

where ζ is the relative vorticity. Applying the Helmholtz theorem to Equation 3.5, assuming that the irrotational divergent component is smaller than the rotational non-divergent component and considering the flow in hydrostatic balance, equation (3.5) can be written as:

$$PV = g \frac{k\pi}{p} \left[(f + \nabla^2 \psi) \frac{\partial^2 \Phi}{\partial \pi^2} - \frac{1}{a^2 \cos^2 \phi} \frac{\partial^2 \psi}{\partial \lambda \partial \pi} \frac{\partial^2 \Phi}{\partial \lambda \partial \pi} - \frac{1}{a^2} \frac{\partial^2 \psi}{\partial \phi \partial \pi} \frac{\partial^2 \Phi}{\partial \phi \partial \pi} \right] \quad (3.5)$$

The equations 3.2 and 3.5 form a closed system for the unknown variables Φ and ψ , given PV . The solution for this system is obtained through the Successive Overrelaxation method (DAVIS; EMANUEL, 1991).

3.3.2 The WRF model

The WRF model is a non-hydrostatic model developed by the National Center for Atmospheric Research (NCAR), the National Centers for Environmental Prediction/National Oceanic and Atmospheric Administration (NCEP/NOAA) and others centers (SKAMAROCK et al. 2008). This model was developed with the aim of improving the understanding and prediction of meteorological mesoscale systems as it allows the user to generate atmospheric simulations based on real data or idealized conditions. The model has two dynamical cores the Advanced Research WRF (ARW) and the Nonhydrostatic Mesoscale Model (NMM). The two cores differ concerning the formulation of the equations, the temporal integration method, the prognostic variables and other aspects. In the current study the ARW core was used. The physics parameterizations used in the simulations follows Gozzo (2014) and are listed in Table 3.3.

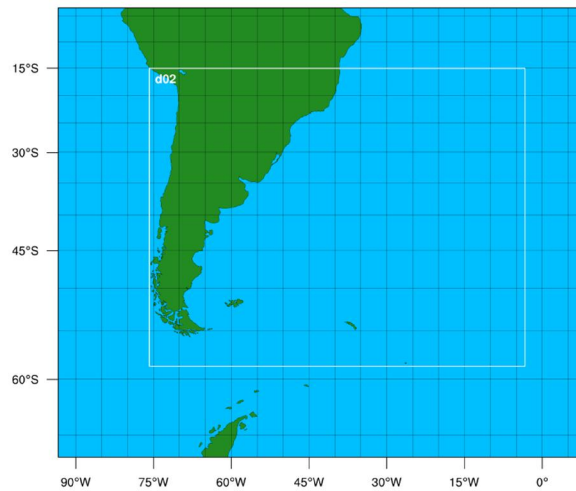
The initial and boundary conditions for the numerical simulations come from the NCEP-CFSR reanalysis as described in section 3.1. The simulations were initialized three days before the extratropical transition to evaluate the associated physical process. A summary of the configuration used in the model is presented in Table 3.1. The simulations used:

- External domain (d01) : -90°W to 10°E and -75°S to -10°S (Figure 3.3);
- Internal domain (d02): -75°W to 0° and -60°S to -20°S (Figure 3.3);
- Vertical levels: 27 levels in pressure coordinate for initial condition.

Table 3.1 – Summary of WRF configuration.

Domain	Number of grid points	Horizontal Resolution	Spin-up
<i>d01</i>	140 x 120	60 km	6h
<i>d02</i>	298 x 238	20 km	

Figure 3.3 – Domain used for numerical simulations of cyclone Anita.



Source: Author's Production.

Dias Pinto et al. (2013) observed that during its subtropical phase, cyclone Anita presented potential for tropical transition. They inferred that this transition was prevented by the interaction of Anita with an extratropical cyclone which developed over northern Argentina, which in turn allowed Anita to undergo extratropical transition. This interaction was also noted by Dutra et al. (2017). In order to investigate the role played by the previously mentioned cyclone in the ET process, the first experiment CYC2 was conducted. This experiment consists in the removal of the extratropical cyclones over Argentina (ECY) from the initial conditions. This was done subtracting the PV anomaly associated with

ECY from the PV fields and then applying PVI to recover the balanced fields that was used as initial conditions in WRF model. The PV anomalies associated with ECY were removed from all pressure levels.

From the PVI analysis, there were observed three distinct PV concentrations over the center of cyclone Anita during its life cycle. One at the upper troposphere (400-100 hPa), other at the lower troposphere (975 - 700 hPa) and the last one is a surface anomaly of potential temperature. The experiment UPV was done to evaluate the contribution of the upper tropospheric PV anomalies. This was done by isolating the PV anomalies at upper levels (400-100 hPa), using the PVI to obtain the associated balanced fields and subtracting the balanced fields from the initial and boundary conditions. Experiment BTPV was constructed similarly to UPV, but the lower tropospheric PV and the surface potential temperature anomaly were removed. Figure 3.4 represents the diagram of the above mentioned procedures for the SCET analysis in SAO.

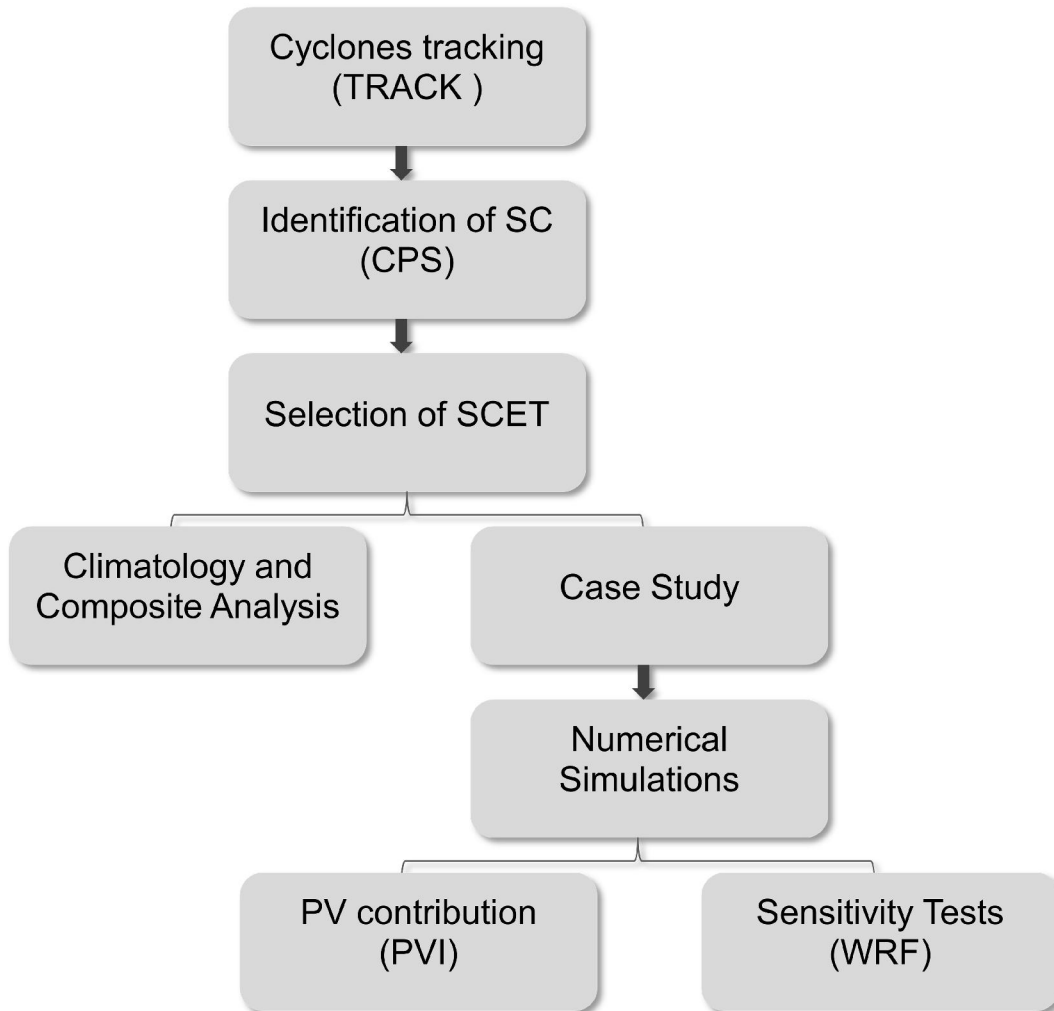
Table 3.2 – Summary of sensitivity tests.

Experiment	Description
CYC2	ECY removed
UPV	Upper tropospheric PV anomalies removed (400 -100 hPa) from 35°S to 65°S.
BTPV	Lower tropospheric PV anomalies removed (1000-700 hPa) from 35°S to 65°S.

Table3.3 – WRF Physics parameterizations.

	Parameterization	Description
Microphysics	<i>Goddard scheme</i>	A scheme based on Lin et al. (1983) with new techniques for saturation, microphysics treatment that do not involve phase changes.
Cumulus	<i>Grell-Devenyi Ensemble scheme</i>	This scheme uses large ensemble of assumptions and data assimilation techniques to determine the optimal value for feedback to three-dimensional models. Based on Grell (1993).
Long Wave Radiation	<i>RRTM (RapidRadiativeTransferModel)</i>	It is based on Mlawer et al. (1997) and accounts for multiple bands, trace gases, and microphysics species.
Short Wave Radiation	<i>Dudhia</i>	Based on Dudhia (1989). Simple downward integration allowing efficiently for clouds and clear-sky absorption and scattering.
Surface Layer	<i>SimilarityTheory: Monin-Obukhov</i>	Computes surface exchange coefficients for heat, moisture, and momentum.
Land-Surface	<i>Noah Land Surface</i>	Scheme with soil temperature and moisture in four layers, fractional snow cover and frozen soil physics.
Boundary Layer	<i>Yonsei University</i>	Non-local-K scheme with explicit entrainment layer and parabolic K profile in unstable mixed layer.

Figure 3.4 – Diagram for SCET analysis.



Source: Author's Production.

4 CLIMATOLOGY AND COMPOSITES OF SUBTROPICAL CYCLONES UNDERGOING EXTRATROPICAL TRANSITION IN THE SOUTHWEST ATLANTIC OCEAN

In this section the mean features of subtropical cyclones that undergo extratropical transition near the southeast Brazil coast are analyzed during the period of the austral summer of 1985-2015. The study was done using NCEP-CFSR reanalysis and the TRACK program. The tracks of the SCET cyclones and their genesis, extratropical transition and lysis are analyzed. The evolution of these cyclones was analyzed through the cyclone phase space diagram. Also, presented is the monthly and annual frequency of SCET and SC as well as their lifetime variability. Finally, the role of the mean lifetime and intensity on the SCET lifecycles in the SAO is presented.

4.1 Climatology of subtropical cyclones in SAO

The spatial statistics of the SC that undergo ET are shown in Figure 4.1. The SCET trajectories show a cyclogenesis area near the Southeast Brazilian Coast and show a narrow spatial distribution (Figure 4.1). Only two cyclones have a significantly different trajectory propagating along the coast of the South American continent. The majority of the systems do not travel great distances; however, there was one single system that almost goes around the South Pole. The distribution of the trajectories of SCET resembles those of extratropical cyclones which develop in the cyclogenesis region of south and southeast coast of Brazil during the austral summer and fall observed by Guia (2011).

The SCET has one main region of genesis centered in 25°S/45°W, over the coast of São Paulo and Rio de Janeiro states (Figure 4.2a). Although this region of intense cyclogenesis activity of SCET agrees with the subtropical cyclogenesis area observed by Gozzo et al. (2014), it is also important to highlight that this has also been identified as the third cyclogenetic region of extratropical cyclones of the South American continent (SINCLAIR, 1995;

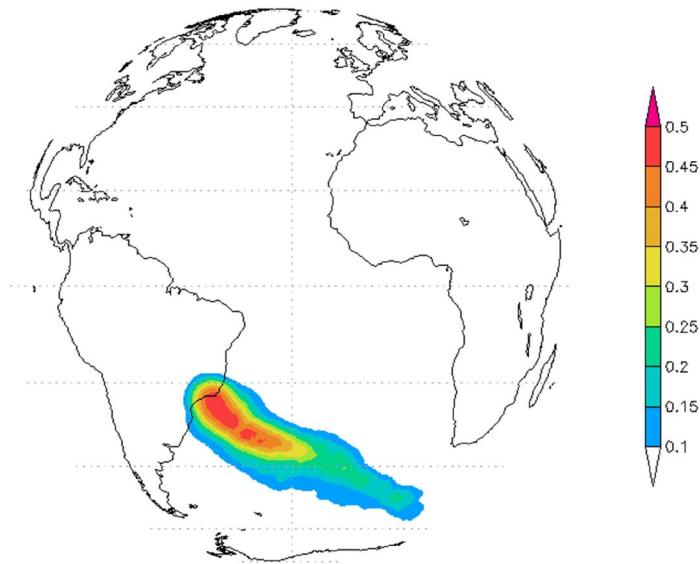
HOSKINS; HODGES, 2005; REBOITA et al., 2010). The main genesis areas for extratropical cyclones in South America are located a) south/southeast Brazil, b) Uruguay and c) over the Gulf of San Matias, in the south of Argentina (GAN; RAO, 1994; HOSKINS; HODGES, 2005; REBOITA, 2008). The last two of the cited regions are associated with the propagation of troughs at upper levels propagating from the Pacific Ocean towards the Atlantic Ocean (REBOITA, 2008). Furthermore, these studies demonstrate the important role of the continental topography for the genesis of the cyclones in the aforementioned regions. On the other hand, the systems that have genesis over the south/southeast Brazil are mainly associated with heat and humidity transport by the low level jet at east of the Andes Mountains (HOSKINS; HODGES, 2005; REBOITA, 2008). Due to the cyclogenesis features of the extratropical cyclones on the southeast coast of Brazil, Gozzo et al. (2014) suggest most of the cyclones developing in this area are actually subtropical ones. In their study they documented that 34% of the identified cyclones in summer, the season with greater cyclogenesis activity, are subtropical.

Figure 4.2b shows the SCET track density, therefore, the preferential region for occurrence of extratropical transition of subtropical cyclones in the Southwestern Atlantic Ocean. This process occurs between 20° - 50° W and 25° - 45° S over the ocean, with the highest density around 30° - 35° S e 30° - 40° W. Regions of lysis are found significantly far away from the genesis areas (Figure 4.2c). Higher lysis density of SCET is positioned between 35° - 20° W e 40° - 35° S, being near the center of the extratropical transition. This suggests that most SCET do not propagate great distances after the transition. A second area of lysis is observed approximately 34° S/ 12° W and a third region that is actually the further one, is located in extratropical latitudes centered in 48° S/ 13° E.

Figure 4.1 – (a) Trajectories (red lines) and (b) trajectories density of SCET in the SAO, obtained through the method of tracking cyclones, for the 1985-2015 period. Unit of density is number per season per unit area.



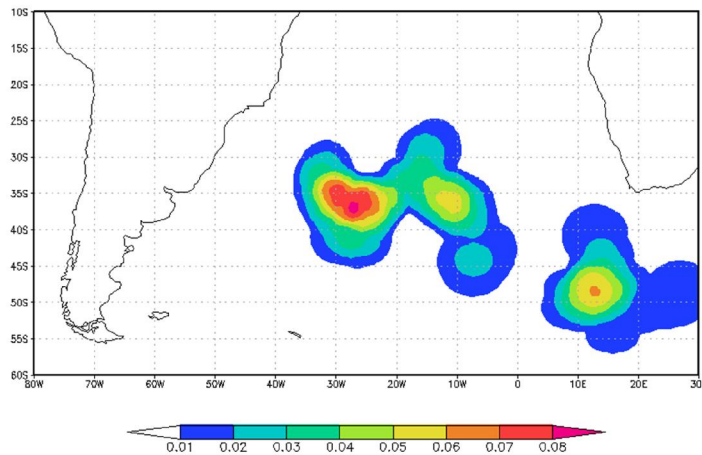
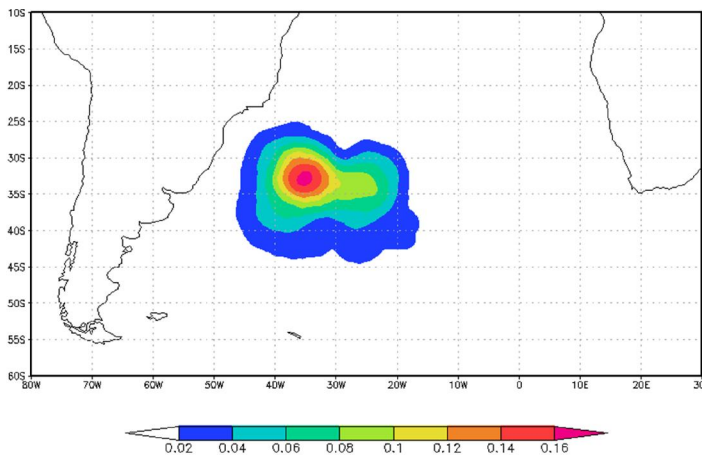
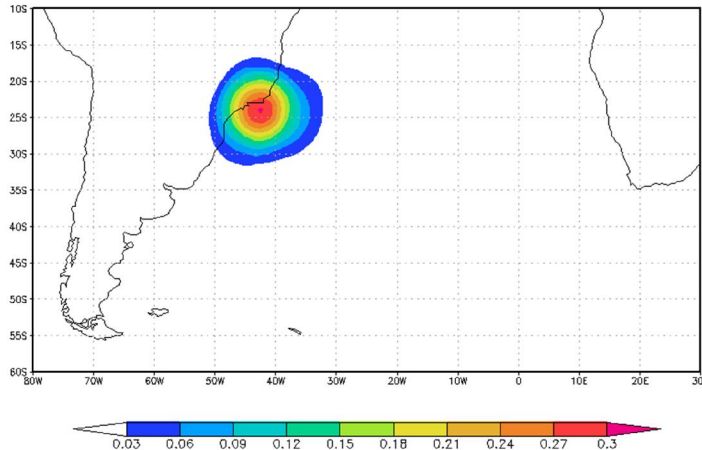
(a)



(b)

Source: Author's production.

Figure 4.2 – Density of (a) density, (b) extratropical transition and (c) lysis of SCET in the SAO for the 1985-2015 period. Unit of density is number per season per unit area.



Source: Author's production.

Regarding the dynamical features, the cyclonic vorticity at the cyclone centers during genesis and at the moment of the extratropical transition shows that these cyclones are more intense at the time of transition (Figure 4.3). More than 70% of the SCET develop with magnitude between -1 and $-3 \times 10^{-5} \text{ s}^{-1}$. On the other hand, the magnitude of these systems at the transition time is more scattered, with a peak cyclonic vorticity around -4 to $-5 \times 10^{-5} \text{ s}^{-1}$. It is worth noting that nearly 35% of SCET attain more extreme values and can reach negative vorticity up to $-9 \times 10^{-5} \text{ s}^{-1}$. The mean cyclonic vorticity during the subtropical phase, therefore, in the period prior to the extratropical transition, is smaller than that during the extratropical phase (post transition period). The mean intensity along the life cycle of the SCET is $-4.53 \times 10^{-5} \text{ s}^{-1}$ (Table 4.1). These results differ from Gozzo et al. (2014) who documented that SCET intensity is higher during the subtropical phase. Although, it should be mentioned that Gozzo et al. (2014) used the minimum cyclonic vorticity and the strongest low level winds as a measure of SC intensity.

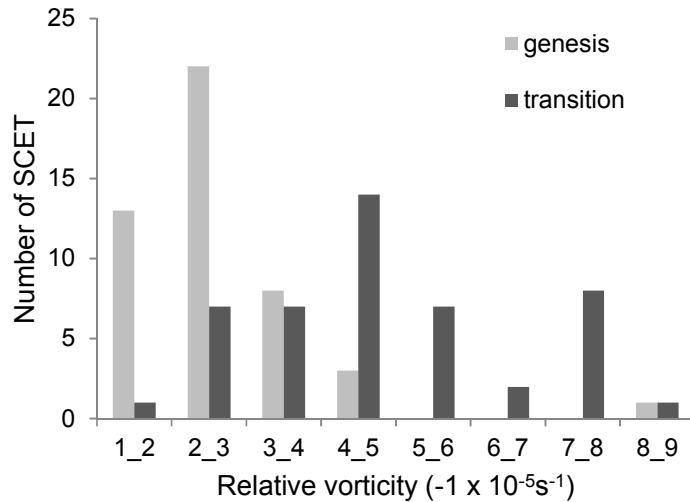
Table 4.1 – Mean cyclonic vorticity at the SCET in the SAO.

Mean cyclonic vorticity			
	Total	Before ET	After ET
Vorticity (10^{-5} s^{-1})	-4,53	-3,77	-5,49

Figure 4.4 depicts the SCET mean cyclone phase space evolution which is based on the parameters: lower tropospheric thermal wind (-VTL), upper tropospheric thermal wind (-VTU) and storm relative motion thermal asymmetry (B). It should be noted the importance of these parameters to describe and distinguish the structure of tropical, extratropical and subtropical cyclones and also to diagnose the transition process that occurs during the life cycles of these weather systems. In this context, the life cycle of the cyclones is shown from 72 hours prior to ET to 72 hours after it. Thus it is possible to identify the evolution

of the SCET from a mature subtropical cyclone to an asymmetric cold-core cyclone.

Figure 4.3 – Cyclonic vorticity in the genesis (light gray) and extratropical transition (dark gray) of SCET in the SAO for the 1985-2015 period.

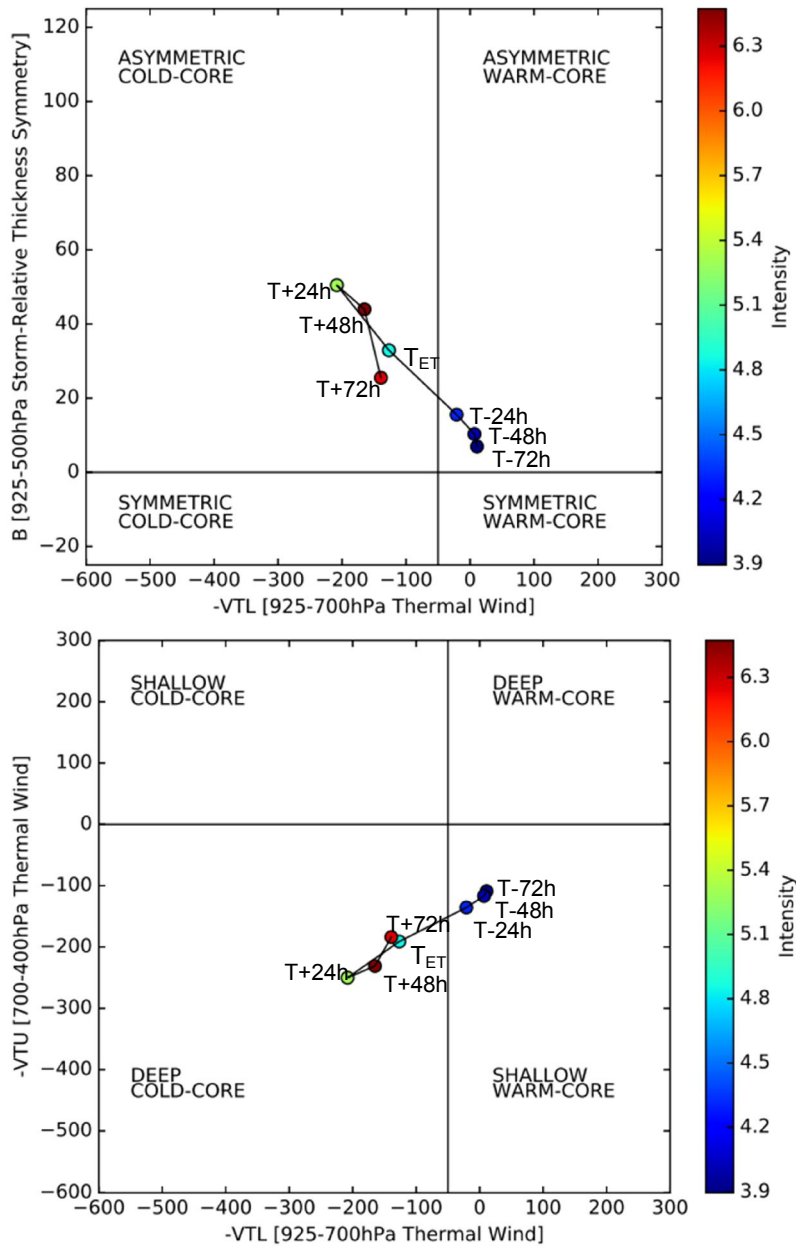


Source: Author's production.

It is worth mentioning that until 24 hours before the ET, the mean values of -VTL are positive as is expected for SCs (Table 4.2). Therefore, it is observed that during the period prior to ET, the cyclones show a typical hybrid structure, i. e., an upper level cold core and a low level warm core. At the transition time, the cyclones show a typical extratropical cyclone structure and 24 later they reach their strongest cold asymmetric structure. The cyclonic vorticity increases from 72 hours prior to ET and continues its intensification until $t = +48$ h, when the cyclones achieve their maximum cyclonic vorticity. After this the systems start to decay. A very similar behavior was observed for the extratropical transition of North Atlantic tropical cyclones (HART et al., 2006), where the tropical cyclones showed the strongest cold core structure and storm-motion relative temperature gradient after 24 hours from the ET occurrence. Moreover,

48 hours after that, these systems begin the occlusion process, due to the removal of baroclinic instability, characterized by the decrease of thermal asymmetry (Table 4.2).

Figure 4.4 – Composite mean SCET for the 1985-2015 period. (a) -VTL vs B and (b) -VTL vs -VTU.



T_{ET} represents the time of the extratropical transition occurrence. The shaded circles indicate the intensity of the relative vorticity at 925 hPa.

Source: Author's production.

The mean features of the thermal wind parameter at high and low levels, -VTU, -VTL, B and relative vorticity at 925 hPa for the ET time and also for times prior and post ET are shown in Table 4.2 and also in the life cycle compositing of SCET (Figure 4.5). During the subtropical phase, the magnitudes of mean -VTL are not high and are typically positive. Although at $t = -24$ h, mean -VTL is negative, indicating the start of the transition process. On the other hand, the mean thermal wind values in the upper troposphere are negative through the life cycle of SCET, presenting even more negative values after the occurrence of the ET, indicating the deepening of the cold core at upper levels.

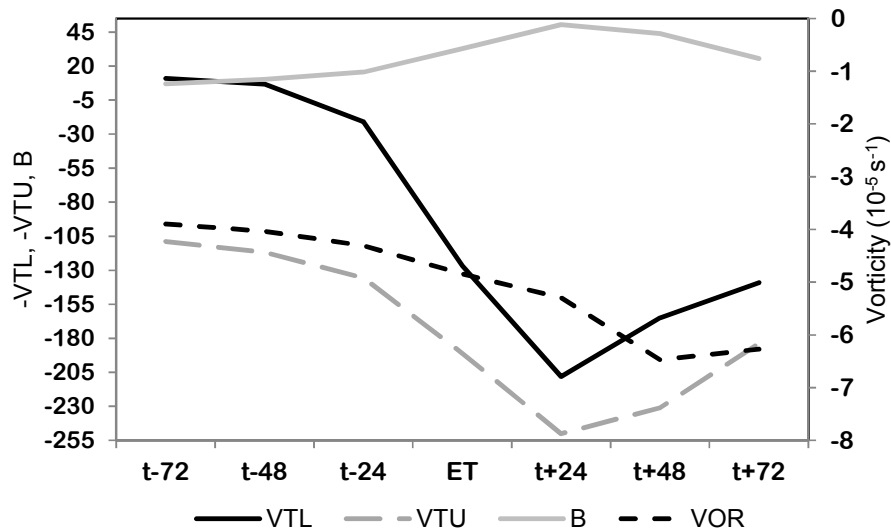
Table 4.2 – Mean features for the selected periods for SCET evolution. Values in parentheses are standard deviation.

Time	Vorticity	-VTL	-VTU	B
<i>T = -72h</i>	3.90 (2.07)	10.91 (56.21)	-108.96 (69.18)	6.96 (13.89)
<i>T = -48h</i>	4.03 (1.9)	6.85 (41.48)	-116.79 (66.29)	10.31 (14.31)
<i>T = -24h</i>	4.31 (1.72)	-20.94 (59.74)	-135.57 (61.79)	15.54 (14.93)
<i>T_{ET}</i>	4.84 (1.72)	-126.67 (67.78)	-191.10 (53.77)	32.90 (6.59)
<i>T = 24h</i>	5.30 (2.32)	-208.10 (100.03)	-250.10 (93.06)	50.46 (26.2)
<i>T = 48h</i>	6.47 (2.94)	-164.95 (165.72)	-231.99 (129.91)	43.96 (41.98)
<i>T = 72h</i>	6.27 (1.62)	-139.25 (96.35)	-183.82 (83.35)	25.49 (23.86)

Cold core extratropical cyclones have negative values of -VTU and -VTL, with -VTU having greater magnitudes while warm core tropical cyclones have positive values of both parameters. On the other hand, hybrid systems, such as SC, typically have opposite signs of -VTU and -VTL (HART, 2003). This feature is

illustrated in Table 4.2, -VTL has positive values at $t = -72$ h and at $t = -48$ h of the subtropical phase but -VTU is negative. After the transition time, both parameters have negative values, although the magnitude of -VTU is larger. Figure 4.5 emphasizes the life cycle of the SCET, the moderate range between -VTL and -VTU during the subtropical phase is obvious. This range is smaller between the ET and 24 hours after it, due the abrupt decrease of -VTL since $t = -24$ h. All CPS parameters present peak intensity 24 hours after the ET. On the other hand, relative vorticity reaches its maximum cyclonic intensity at $t = +48$ h.

Figure 4.5 – Life cycle composites of SCET for the 1985-2015 period.



Parameters shown are -VTL (solid black line), -VTU (dashed gray line), B (solid gray line) and Vorticity at 925 hPa (dashed black line).

Source: Author's production.

To give insight into the variability of the cyclone evolution, the frequency of the thermal wind at low levels and the thermal asymmetry are examined. The frequency of the warm -VTL shows that in the subtropical phase the values are concentrated between -40 and 60 (Figure 4.6a). After the transition the values

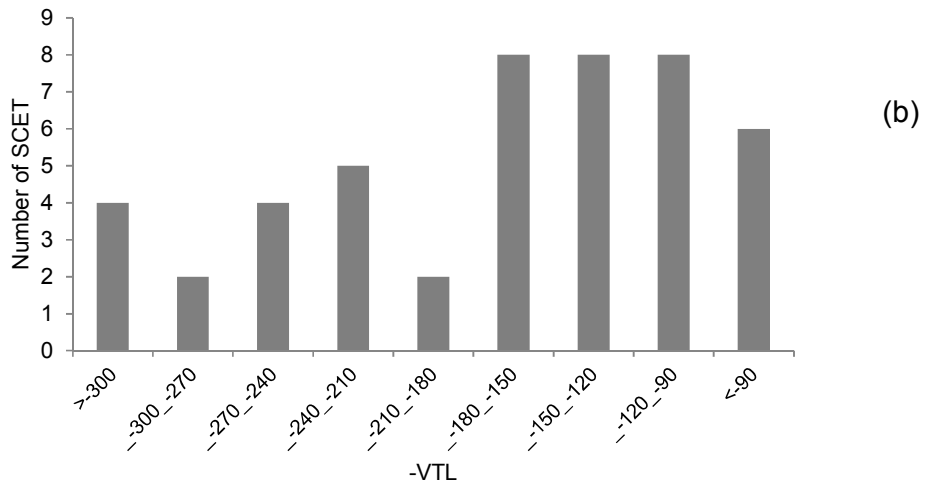
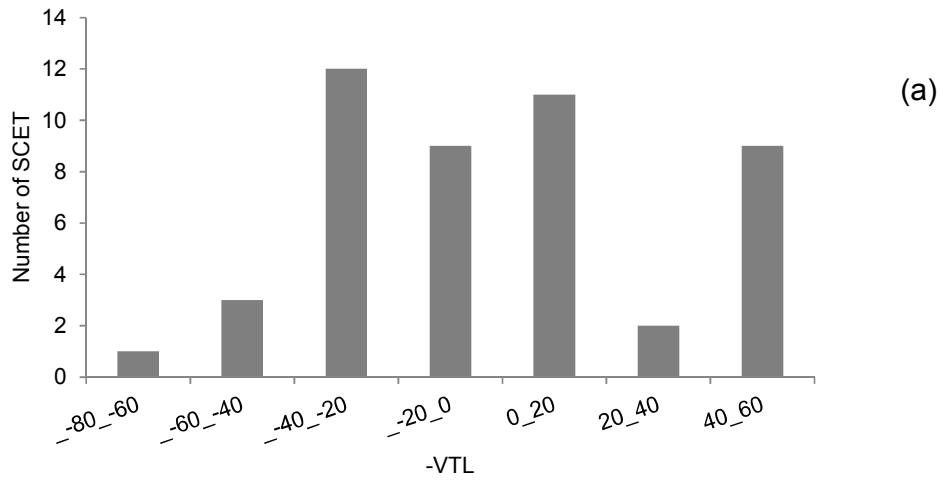
decrease with most of the cyclones showing -VTL between -90 and -180, though there are cases where the magnitude of this parameter is as low as -300 (Figure 4.6b). The increase in the magnitude of -VTL after the transition indicates the deepening of the cold core cyclone at low levels.

Analyzing the mean features associated with the thermal symmetry, one can see that all the calculated means are positive, with larger values in the post transition period. The mean magnitude of this parameter for the first 24h after the transition is 43. These values are coherent with the threshold used to identify the subtropical cyclones that undergo extratropical transition, $B > 25$ for at least 24 hours. Similarly, the means for the period prior to transition are also consistent, being less than 10. Although the above mentioned threshold is higher, generally the value of the thermal symmetry for hybrid systems is near 10 (GUISHARD et al., 2009).

During the period prior to extratropical transition, the majority of the SCET show values of B between 5 and 20 (Figure 4.7a). This characterizes the non-frontal nature of these systems during their subtropical phase (HART, 2003). After the transition time, the mean values of B increase considerably, reaching values as high as 90. However, most of SCET are in the 30 and 50 range (Figure 4.7b)

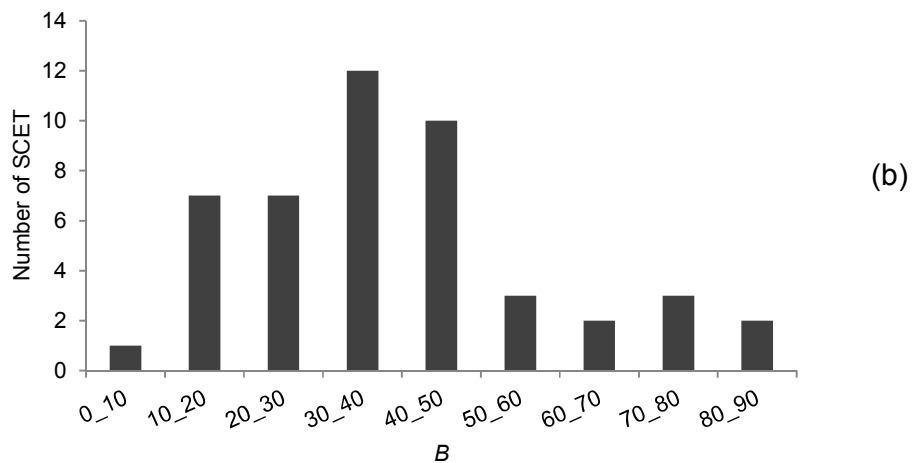
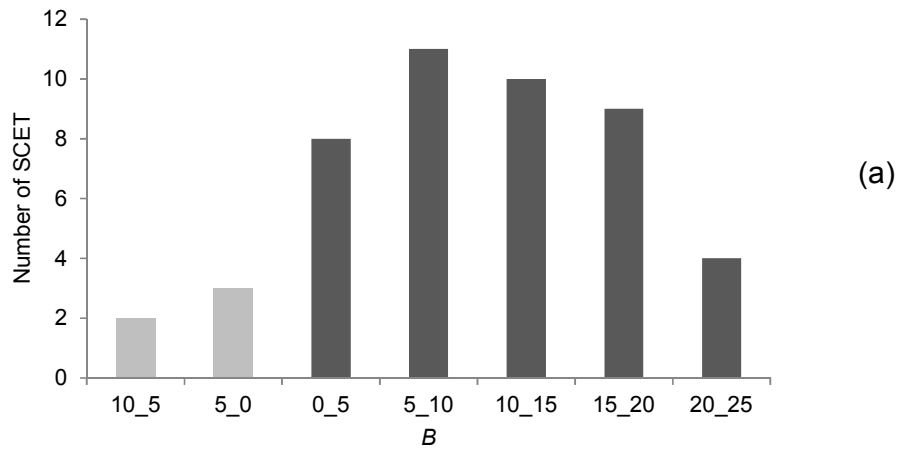
The high positive values of B represent frontal systems and also indicate the presence of warm air at the right side of the cyclones in the Southern Hemisphere. Furthermore, considering that this pattern of warm advection is overlaid on ascending air downstream of cyclones, it can be inferred that positive values of thermal asymmetry are associated with a direct thermal circulation (HART, 2003).

Figure 4.6 – Mean frequency of thermal wind parameter in the lower troposphere (-VTL) for the period (a) Prior and (b) Post extratropical transition of the SCET for the 1985-2015 period.



Source: Author's production.

Figure 4.7 – Mean frequency of thermal symmetry (B) for the period (a) Prior and (b) Post extratropical transition of the SCET for the 1985-2015 period.



Dark gray bars indicate negative values and light gray bars indicate positive values of B .

Source: Author's production.

During the austral summer of the 1985-2015 period, the annual mean and standard deviation of SC was 11.23 and 2.81 per year, respectively. This frequency is higher than the 1SC/year found by Evans and Braun (2012). The inclusion of shallow and less intense subtropical cyclones to provide a more

complete view of SC in the current study explains the significant difference in the number of identified systems. Gozzo et al. (2014) observed 7.2 CS per year in the same region. This difference could be due the different identification methods for tracking SC. Although the criteria used in the current study largely follow Gozzo et al. (2014), the inspection to eliminate cyclones with cold and westward tilting core and associated with frontal zones were not applied at this stage. The criteria used to identify SC in the above mentioned studies are shown in Table 4.3.

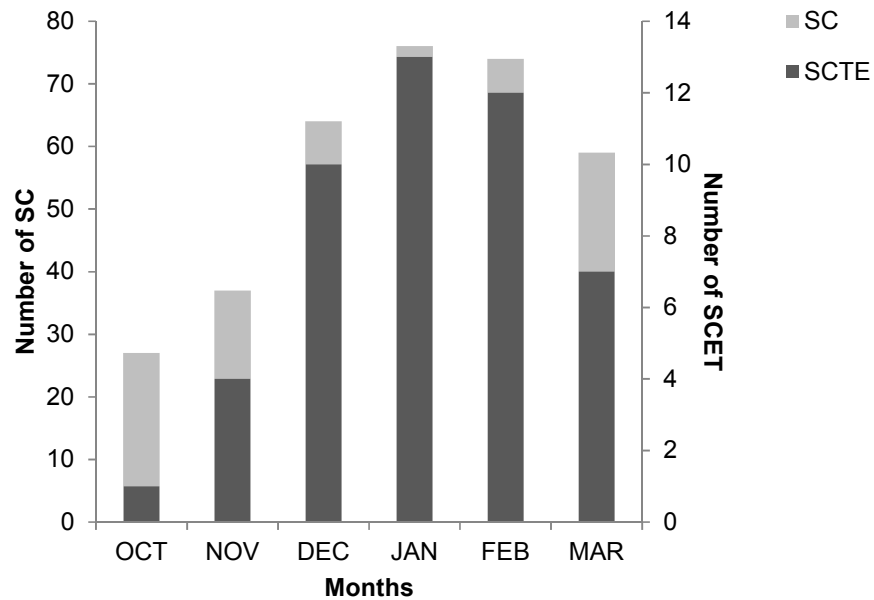
Table 4.3 – Criteria for SC identification used in previous studies.

	<i>Evans and Braun (2012)</i>	<i>Gozzo et al. (2014)</i>
<i>Data</i>	ECMWF reanalysis	ERA-Interim and NCEP-NCAR reanalysis
<i>Region</i>	20°S – 40°S	20°S – 40°S
<i>CPS parameters</i>	-VTU<-10 -VTL>-10	-VTU<-10 -VTL>-50 B<25
<i>Winds</i>	At least 17 ms ⁻¹	None
<i>Prior structure</i>	- Attains required values of -VTU, -VTL and B within 24 h after genesis. - Not present prior tropical structure or be embedded in the midlatitude flow.	Attains required values of -VTU, -VTL and B within 24 h after genesis.
<i>Synoptic feature</i>	Closed low at 500 hPa required.	Absence of frontal zones and cold and west ward tilting core.

Our analysis found 47 SCET in the whole period, therefore an annual mean of 1.6 SC/season with standard deviation of 1.3. The monthly distribution of these systems showed that the months of higher frequency was January, February and December, respectively (Figure 4.8). Gozzo et al. (2014), also observed the pure SC, i.e., cyclones that develop with subtropical features, are also more

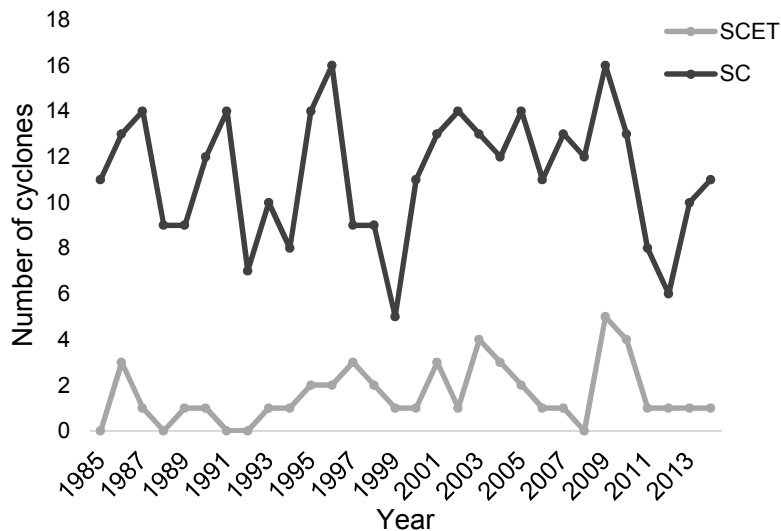
frequent during the summer (defined as DJF months) in the SAO, corresponding to approximately 8% of the total number of cyclones that occur in this region. The interannual variability of the SC and SCET are very irregular (Figure 4.9), although an increase in the number of SCET can be seen from the second decade onwards (Figure 4.10). When analyzing the number of SCET just in the months of higher frequency (DJF), it is observed that the frequency of these systems tripled in the second and third decades (Figure 4.10).

Figure 4.8- Monthly frequency of SCET (dark gray) and SC (light gray) in the SAO during the 1985-2015 period, based on CFSR reanalysis.



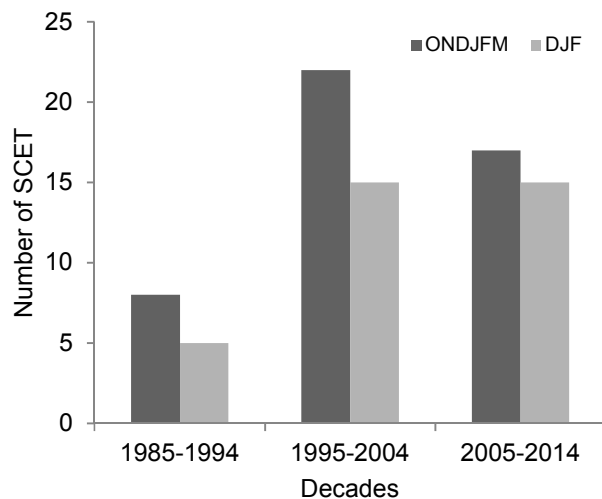
Source: Author's production.

Figure 4.9 - Annual frequency of subtropical cyclones (dark gray line) and SCET (light gray line) in the SAO during the 1985-2015 period, based on CFSR reanalysis.



Source: Author's production.

Figure 4.10 – Decadal frequency of SCET in the SAO during 1985-2015 period.



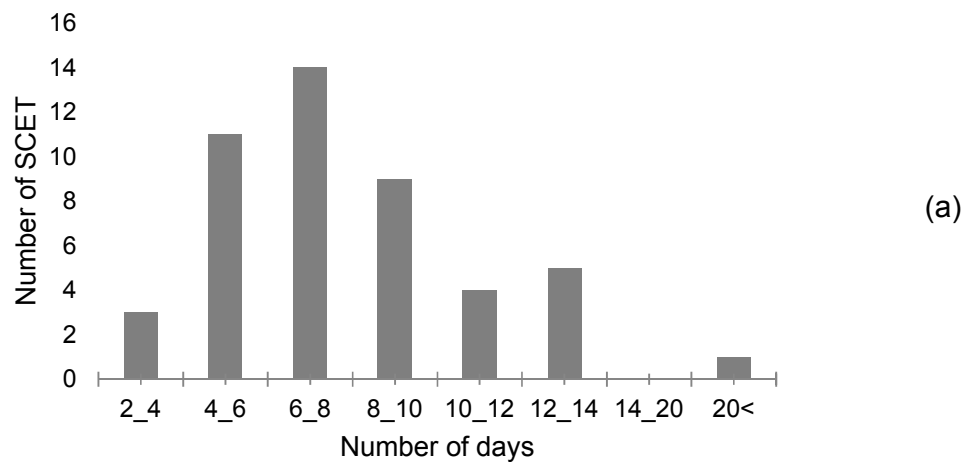
Light gray bars represent the ONDJFM months and dark gray bars represent the DJF.

Source: Author's production.

Subtropical cyclones in the SAO region can be grouped according to their lifetimes. The first is the group of approximately 4 days and the second group around 6-7 days (Figure not shown). The second group corresponds to cyclones that develop as subtropical and persists for at least 36 hours and then undergo extratropical transition (GOZZO et al., 2014). The mean lifetime of SCET observed in the present study is 7.3 days. More than half of these cyclones present life times between 4 and 8 days and greater than one third had a longer life cycle (8-14 days) (Figure 4.11). There was one SCET that lasted around 20 days.

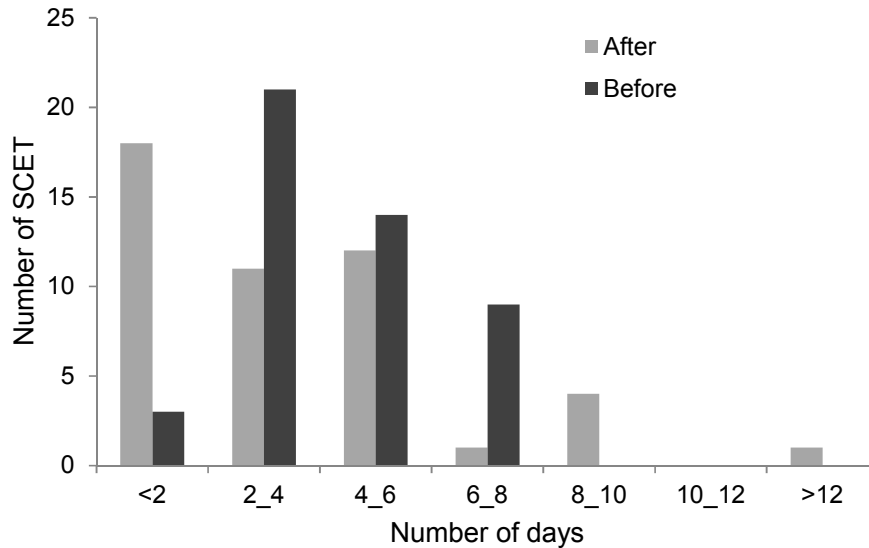
The mean lifetime of the SCET before the extratropical transition is 3.25 days and around 4.08 days after that, such that most of these systems present a lifetime of at least 2 days, before the ET. On the other hand, the majority of the cyclones last up to 6 days after the extratropical transition (Figure 4.11b). The extent of the extratropical phase of the studied systems is similar to most of the extratropical cyclones that occur in the South America region (MENDES et al., 2010).

Figure 4.11 – Lifetime of SCET (a) total and (b) before (dark gray) and after (light gray) extratropical transition during the 1985-2015 period.



(continue)

Figure 4.11- Conclusion.



(b)

Source: Author's production.

4.2 Composite analysis

In order to characterize the synoptic environment and mean features of subtropical cyclones undergoing extratropical transition in the Southwest Atlantic Ocean, composites of meteorological variables centered on the cyclones centers were calculated (section 3.2). Considering that in general composites tend to smooth meteorological fields, we defined the composites centered on the vorticity center used by the tracking method. The composite analysis area covers a 20° radius from the tracked cyclone center. These composites were based on the 47 cases of SCET which took place in ONDJFM of the 1985-2015 period. Each composite is produced at 24h intervals, starting 72 hours before extratropical transition ($t = -72h$) and ending 72 hours after that ($t = +72h$). The exact period of the transition occurrence is referenced as $t = 0h$. To simplify the SCET analysis during the studied period, the composites were divided into four categories according to their vertical structure and physical processes.

I. Dynamical features

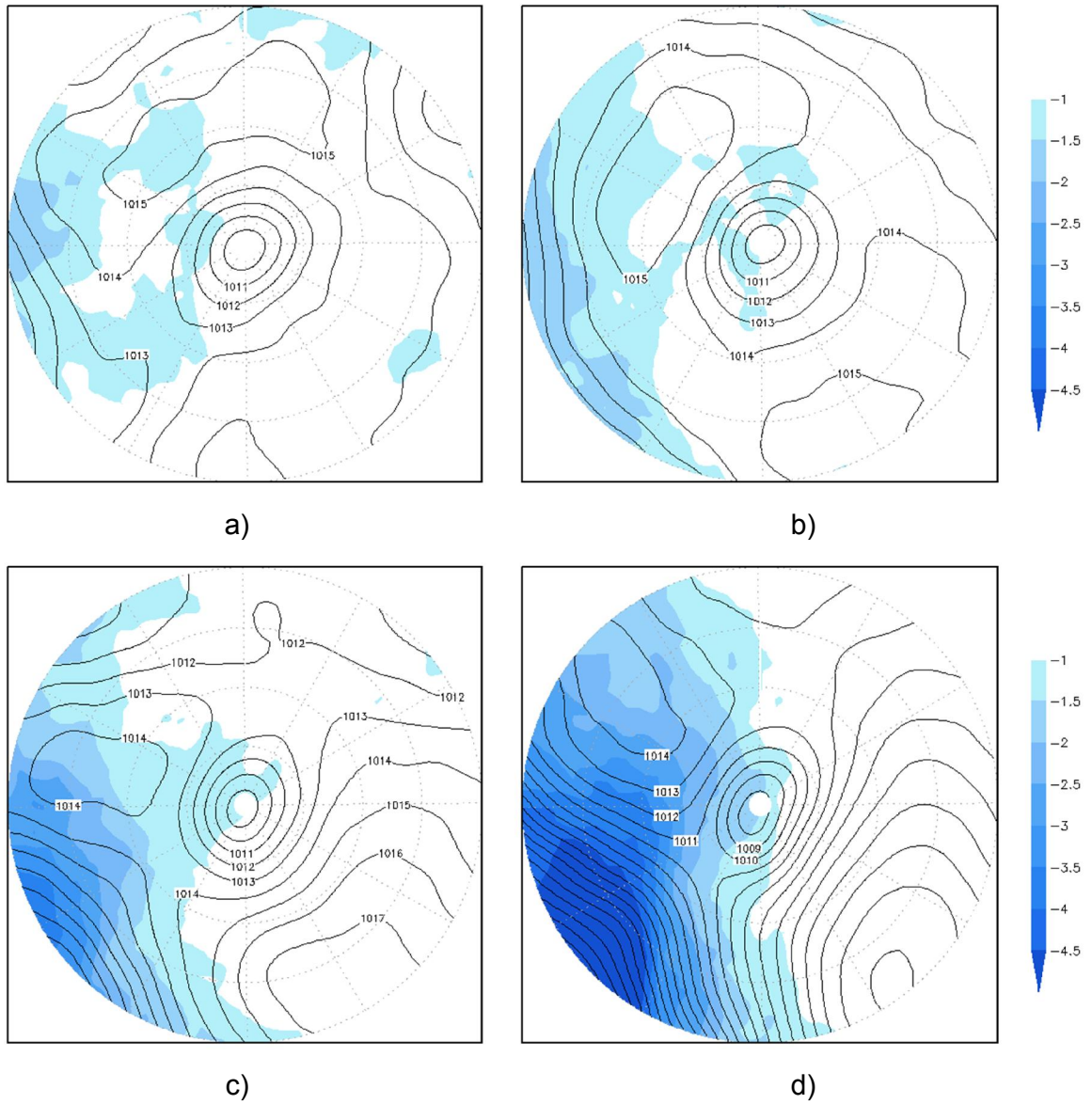
Low and upper levels composites are presented here to describe the typical vertical dynamical structure of the SCET. First, sea level pressure (SLP) and potential vorticity at 250 hPa are analyzed. These meteorological fields are crucial to understand the cyclones development and evolution. The SLP fields (Figure 4.12) show the pattern of the low level pressure center evolution associated with the subtropical cyclone, starting (ending) 72 hours before (after) the extratropical transition. During the 72 hour preceding the transition process (Figure 3.10abc) the low level center is surrounded by two high pressure centers. These surface high pressure centers are associated with the South Atlantic Subtropical High which is deformed by the surface subtropical cyclone. This period is also marked by the intrusion of negative potential vorticity anomalies at 250 hPa, upstream of the surface cyclone. As the PV anomaly approaches the left (right) quadrant at $t = -24h$, the high pressure center on that side decreases (increases) its magnitude. From this instant the negative PV intrusion is enhanced over the entire region behind the cyclone.

Following the cyclone evolution, one day after the transition ($t = +24h$) the PV anomalies reach the SCET core (Figure 4.12e). At this time an intensification of the surface low is observed and the SLP center reaches 1004 hPa. As larger PV (~ -5 PVU) overlays the cyclones ($t = +48h$) these systems continue to intensify such that the pressure decreases 11 hPa at the center in 24 hours (Figure 4.12f). It is worth noting that a closed cyclonic circulation approaches the center of the SC at that instant. The magnitude of this new cyclonic circulation is 993 hPa. Subsequently the PV anomalies continue to amplify until they reach values around -5.5 PVU over the surface cyclone core (Figure 4.12def). The configuration of the SLP field at $t = +72h$ suggests that the interaction between both cyclonic cores helps deepen the SLP center of SCET. Apparently the intrusion of PV anomalies acts as a dynamical forcing in the upper troposphere, intensifying the subtropical cyclones.

The superposition of upper level PV anomalies on the surface cyclone result in a rapid intensification of the low pressure system as also documented by

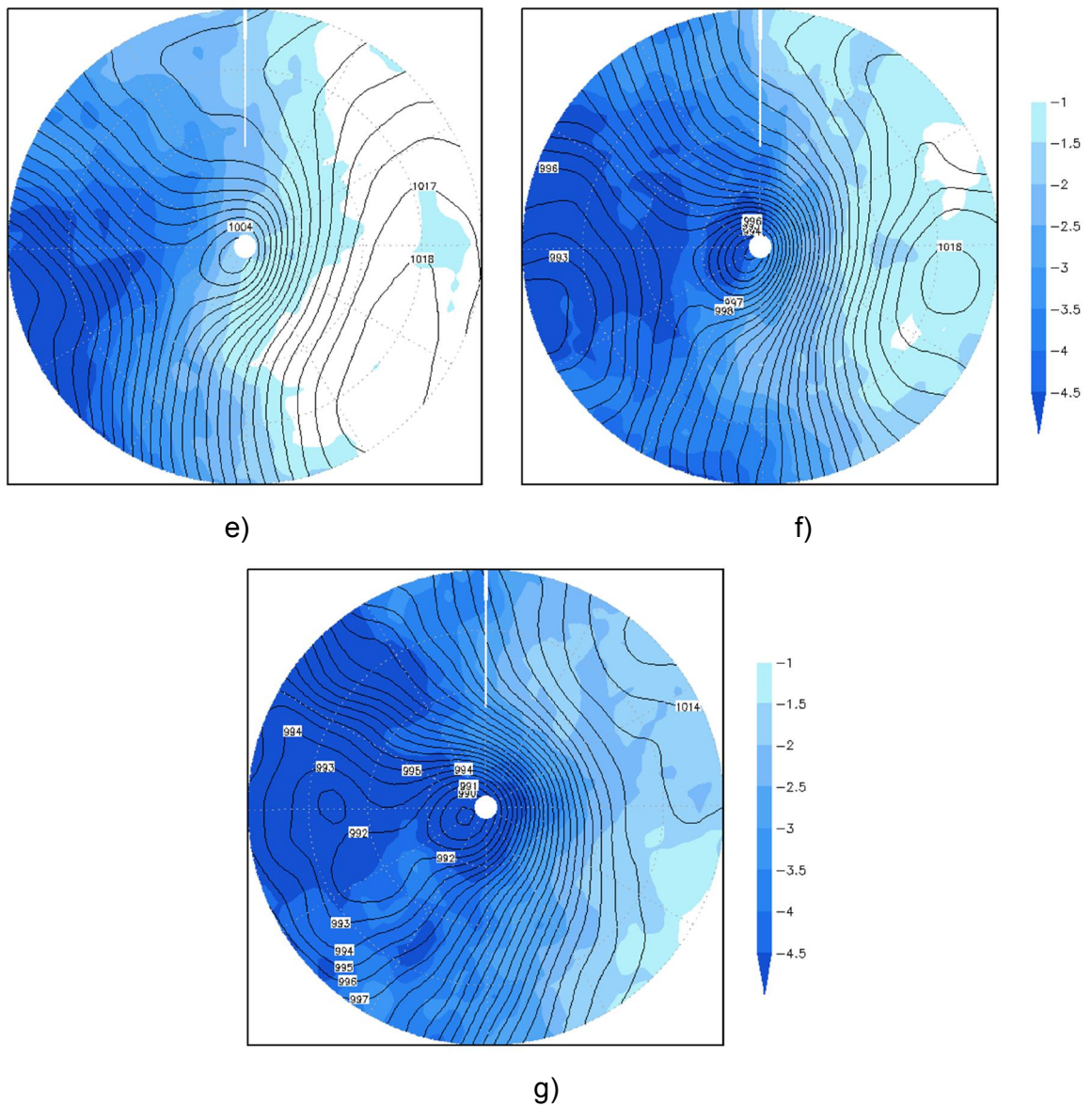
Hanley et al. (2001) when analyzing the interaction between upper level troughs and tropical cyclones in the North Atlantic Ocean. This superposition pattern acts to deepen the tropical cyclones due to the decrease of vertical wind shear. Moreover, the PV anomalies also decrease due to diabatic heating. Thus the cyclone intensification helps to weaken the PV anomalies and consequently the upper level trough does not overcome the surface cyclone center. Considering the extratropical transition of tropical cyclones, some studies indicate that stratospheric PV anomalies upstream of tropical cyclones are not essential to the transition process. However our results suggest that the extratropical transition of subtropical cyclones occur with the intrusion of upper level potential vorticity anomalies and a low level cyclonic system approaching, which afterwards interacts with the subtropical cyclone.

Figure 4.12 – Composites of SLP (contour) and Potential Vorticity at 250 hPa (shaded) of SCET in a) $t = -72h$, b) $t = -48h$, c) $t = -24h$, d) $t = 0$, e) $t = +24h$, f) $t = +48h$ e g) $t = +72h$. Units of PV and SLP are PVU and hPa, respectively.



(continue)

Figure 4.12 – Conclusion.



Source: Author's production.

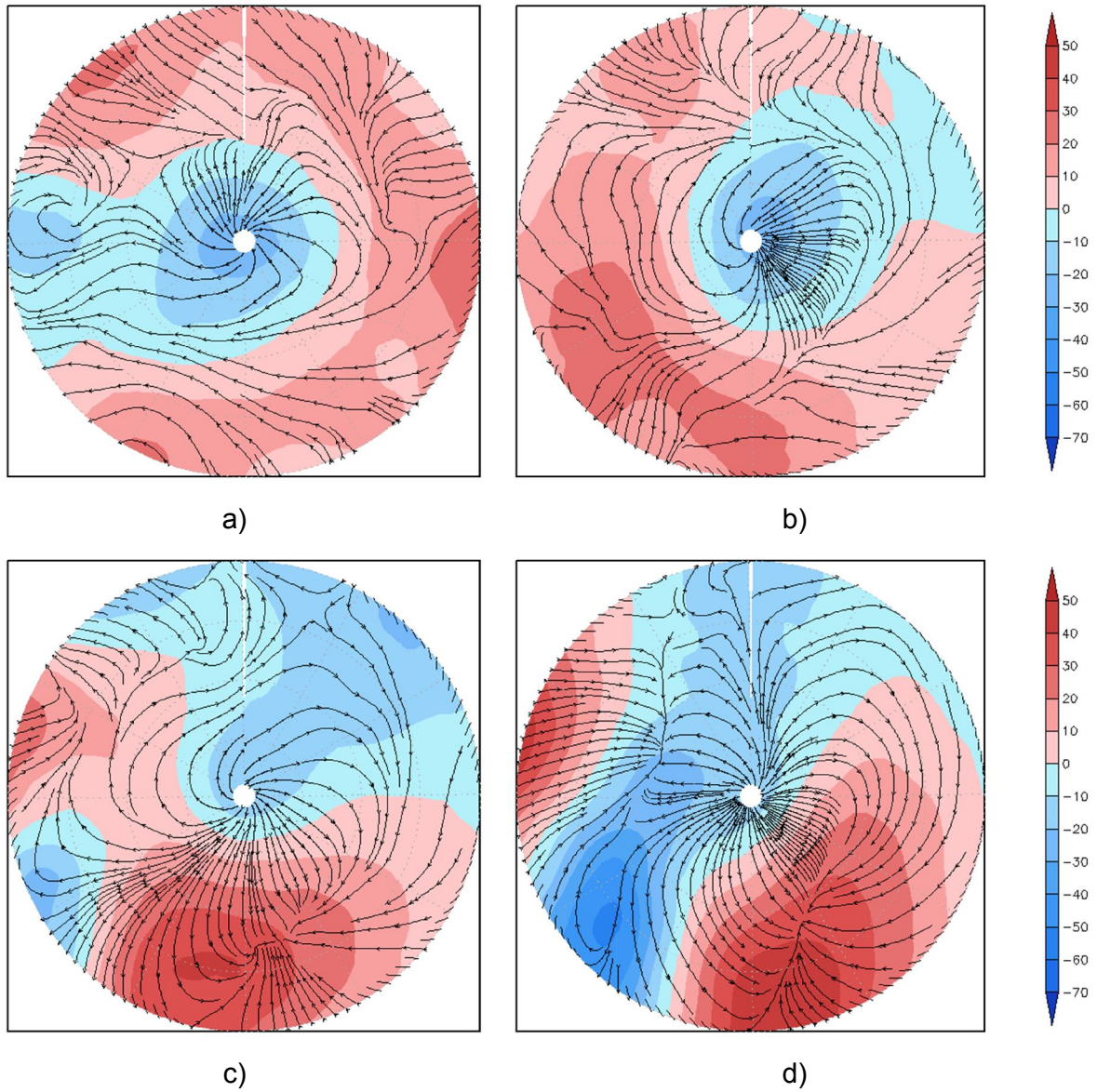
Composites of geopotential height anomalies at 500 hPa are presented in Figure 4.13. It is important to mention that geopotential anomalies play a key role to understanding cyclones dynamics, even in subtropical regions. Between 72 and 48 hours before the ET, a closed center of negative

geopotential height anomaly is observed at the middle troposphere. In this case, the negative anomaly core positioned over the center of the subtropical cyclones highlights the barotropic nature of these systems. This barotropic structure disappears in the period corresponding to 24h before to 24h after the transition. Also, positive areas of geopotential height anomalies associated with the surface anticyclone are observed throughout the analyzed period (Figure 4.13).

Following the SCET evolution, 24 hours before the transition occurrence, a new cyclonic anomaly is observed in the southwest quadrant (Figure 4.13c). This negative geopotential anomaly center is associated with the cyclonic system moving toward the SC, characterized as a low pressure center in the sea level pressure field (Figure 4.12). Subsequently, this new cyclonic system intensifies and propagates following the PV anomalies approaching the subtropical cyclone center. At the same time, an increase of the positive geopotential anomaly is observed. Also, as the PV intrusion at high levels reaches the subtropical system center, the negative anomaly of geopotential height overlays it. In particular, at $t = +48h$ and $t = +72h$ there are two coupled negative cores, one immediately over the SC and the other on the rearward of it. Finally, the later negative anomaly center is detached from the circulation (Figure 4.13fg). This is consistent with the interaction of the surface cyclonic systems mentioned earlier.

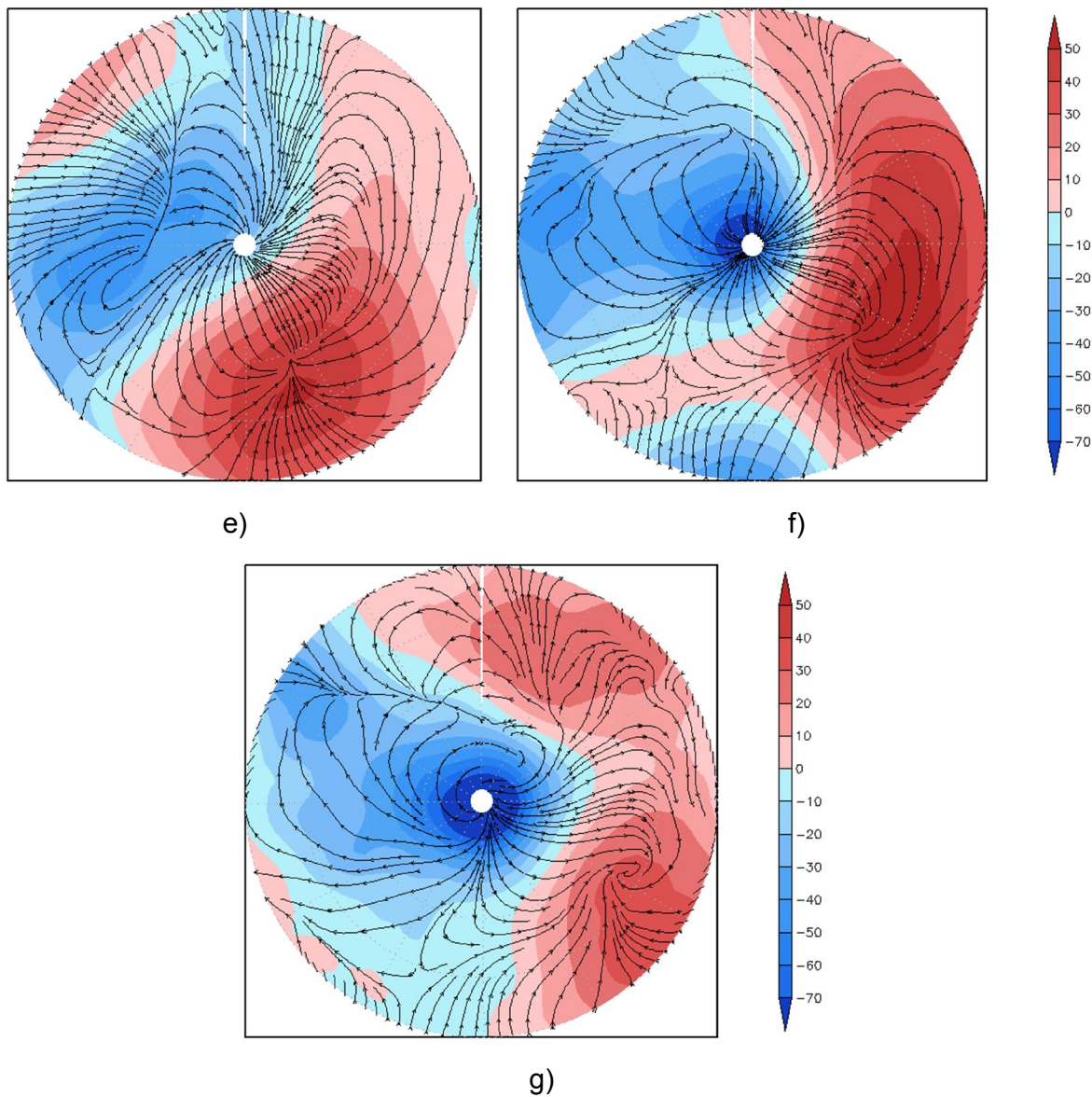
To evaluate the whole of the dynamical forcing of the SCET the wind anomaly composites at upper levels are next considered. From the horizontal wind anomalies in the upper troposphere the presence of a region of divergence over the surface cyclone through its entire lifecycle can be seen (Figure 4.13). Starting at $t = -24h$ mass convergence is observed at the right hand side of the divergence, i.e., over the surface anticyclone. At the instant of ET occurrence, and 24 hours later, convergence is observed rearward of the subtropical cyclone center (Figure 4.13de).

Figure 4.13 – Composites of geopotential height anomaly at 500 hPa (shaded) and horizontal wind at 250 hPa (streamlines) of SCET in a) $t = -72h$, b) $t = -48h$, c) $t = -24h$, d) $t = 0$, e) $t = +24h$, f) $t = +48h$ e g) $t = +72h$. Units of geopotential height are gpm.



(continue)

Figure 4.13 – Conclusion.



Source: Author's production.

The above described environment resembles the one noticed for the occurrence of the subtropical cyclone Anita. During its hybrid phase, Anita was characterized by a cut off low at the middle troposphere and vigorous cyclonic circulation at low levels, revealing a barotropic vertical structure (DIAS PINTO et al., 2013). Eventually, this subtropical system interacted with an extratropical cyclone and became an asymmetric cold core, i.e., it underwent extratropical

transition. At the transition time, the cut off low loses strength resulting in a small trough, which later merged with another propagating wave. The interaction of the subtropical cyclone Anita with the extratropical cyclone forced an eastward propagation causing motion toward colder water and increasing the vertical wind shear.

II. Thermal forcing and vertical motion response

It is well known that SST's are a key variable for the development of cyclones either in tropical as well subtropical regions. Although the occurrence of intense SC in the SAO has been observed, it is necessary to improve the understanding of the role of SST's and heat fluxes in the development of SCET in this region, in particular around the time of ET. Figure 4.14 shows composites of the total heat flux (latent heat flux + sensible heat flux) and sea surface temperature of SCET. At $t = -72\text{h}$ and $t = -48\text{h}$ the SC is located over an SST area of 24°C with moderate surface heat fluxes with values ranging from 80 to 120 Wm^2 (Figure 4.14ab). Prior to the ET, the heat fluxes decrease progressively as the cyclones propagate toward high latitudes, i.e., towards cooler SST's.

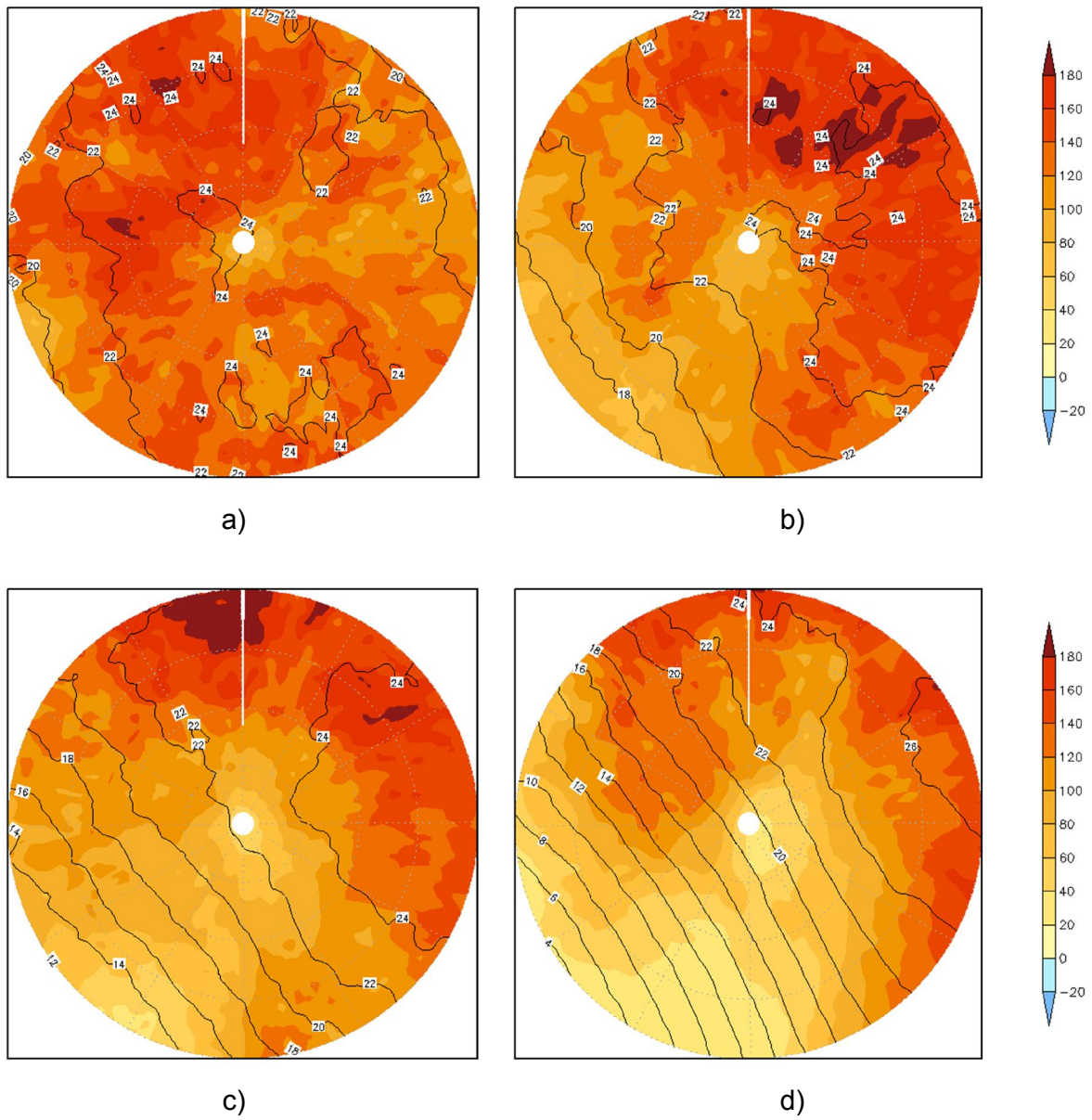
At the instant of the transition process ($t = 0\text{h}$), the SST varies between 18° - 20°C . After that the SST and heat fluxes gradually decrease in magnitude, and 72h later the SCET reaches a region as cold as 6°C (Figure 4.14cg). In fact, as described by Evans and Guishard (2009) the SC in the SAO develop above regions of relatively low SST and moderate surface fluxes. In another words, SC which occur during the austral summer over the southeastern coast of South America are associated with SST's lower than 26°C with not very intense heat fluxes. On the other hand, the heat fluxes and SST in this region are very intense during the autumn season with values of SST's around 27°C (GOZZO, 2014). The higher SSTs in autumn are associated with the high pressure systems which maintain the dry air. Also, subtropical South Atlantic SSTs are governed by the confluence of the Brazilian (warm southward-flowing) and Malvinas (colder northward-flowing) Currents. This confluence region represents large contrasts in SSTs and varies from mid latitudes in summer

(40°S – 46°S) to lower latitudes in winter (30°S – 35°S) (REBOITA et al., 2010; EVANS; BRAUN, 2012).

Throughout the period studied, the heat fluxes under the SC centers are lower than the fluxes around them. This was also observed by Dias Pinto et al. (2010) analyzing the hybrid phase and the potential for tropical transition of Anita. Dias Pinto et al. (2010) highlighted that there is a decrease in SST's and surface heat fluxes just under the cyclone center. The increase in humidity due to the organization of convective activity can contribute to the decrease of heat fluxes. Furthermore, the cloud cover affects the amount of solar energy received at the surface which can reduce the SST locally. Thus, SST cooling can reduce the thermal energy source to the turbulent heat fluxes, resulting in a weakening of the cyclones. On the other hand, cyclones can act to decrease the SST's as shown by Dare and McBride (2011) for tropical cyclones. The main mechanisms associated with this are: vertical mixing and entrainment of cooler water from the thermocline into the overlying mixed layer due to wind-driven oceanic turbulence; transient upwelling; horizontal transport of warm water away from the storm center, rain falling onto of ocean surface and other processes associated with surface heat fluxes, which often have a secondary impact on the SST cooling (DARE; MCBRIDE, 2011).

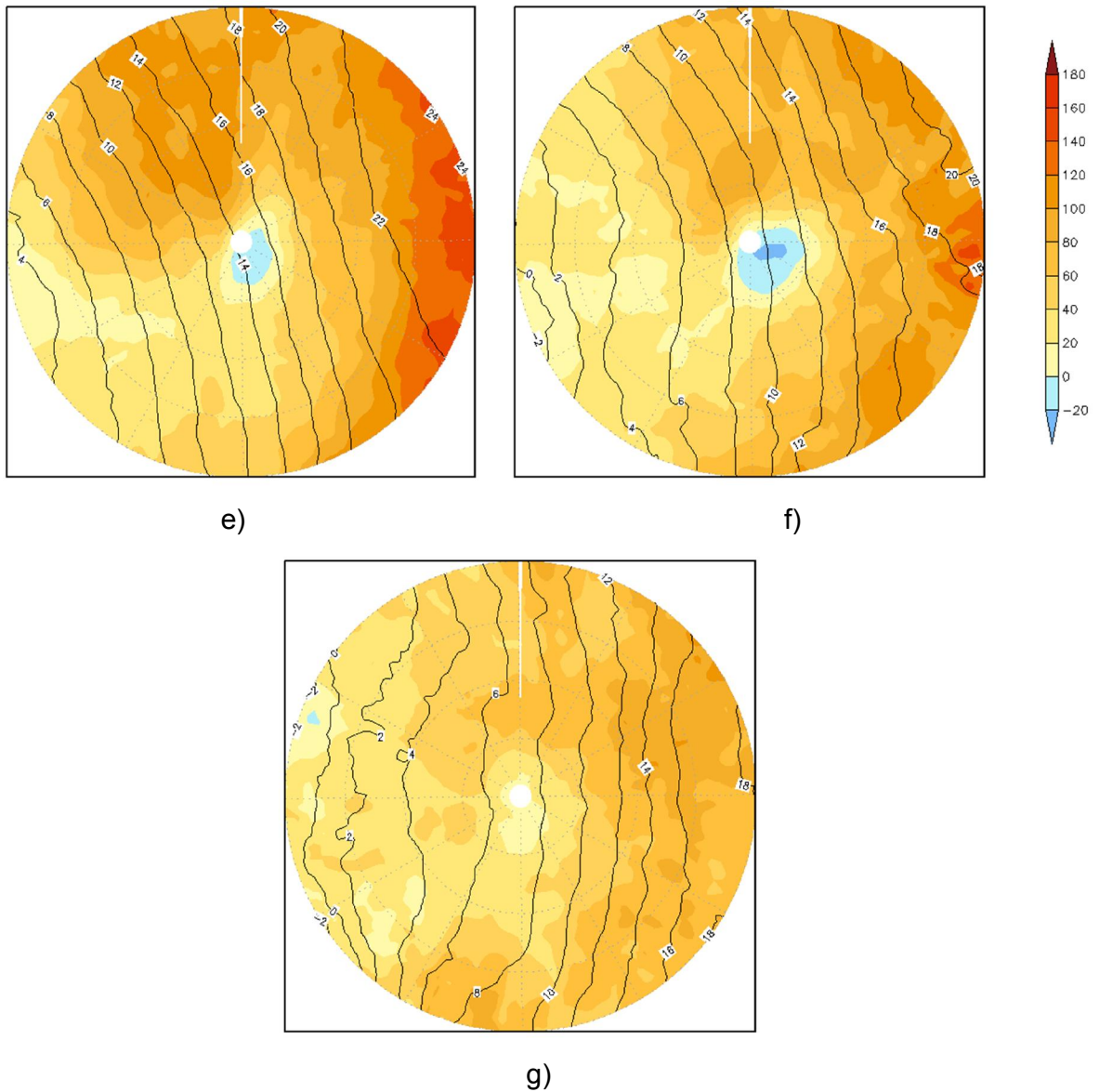
The analysis shows that the areas in the composite with the greatest heat fluxes are ahead of the SC and seem to be associated with the surface anticyclone gyre (Figure 4.12). An important aspect of extratropical cyclones that can help understanding the SCET features is that the energy transport to the atmosphere is weaker when the total heat flux is negative. This feature occurs due to higher humidity content in the atmosphere (REBOITA, 2008). On the other hand, higher energy transport is often found on the cold side of extratropical cyclones that develop over the south/southeast Brazilian coast, i.e., in the cold air advection area. The circulation associated with these cyclones transport cooler and drier air from the continent over the ocean intensifying the vertical gradients of temperature and moisture, enhancing the total heat fluxes (REBOITA, 2008).

Figure 4.14 – Composites of total heat flux (shaded – latent heat flux + sensible heat flux) and sea surface temperature (contours every 2 °C) to SCET in a) t = -72 h, b) t = -48 h, c) t = -24 h, d) t = 0, e) t = +24 h, f) t = +48 h e g) t = +72 h. Units of SST and total fluxes are °C and Wm^2 , respectively.



(continue)

Figure 4.14 – Conclusion.



Source: Author's production.

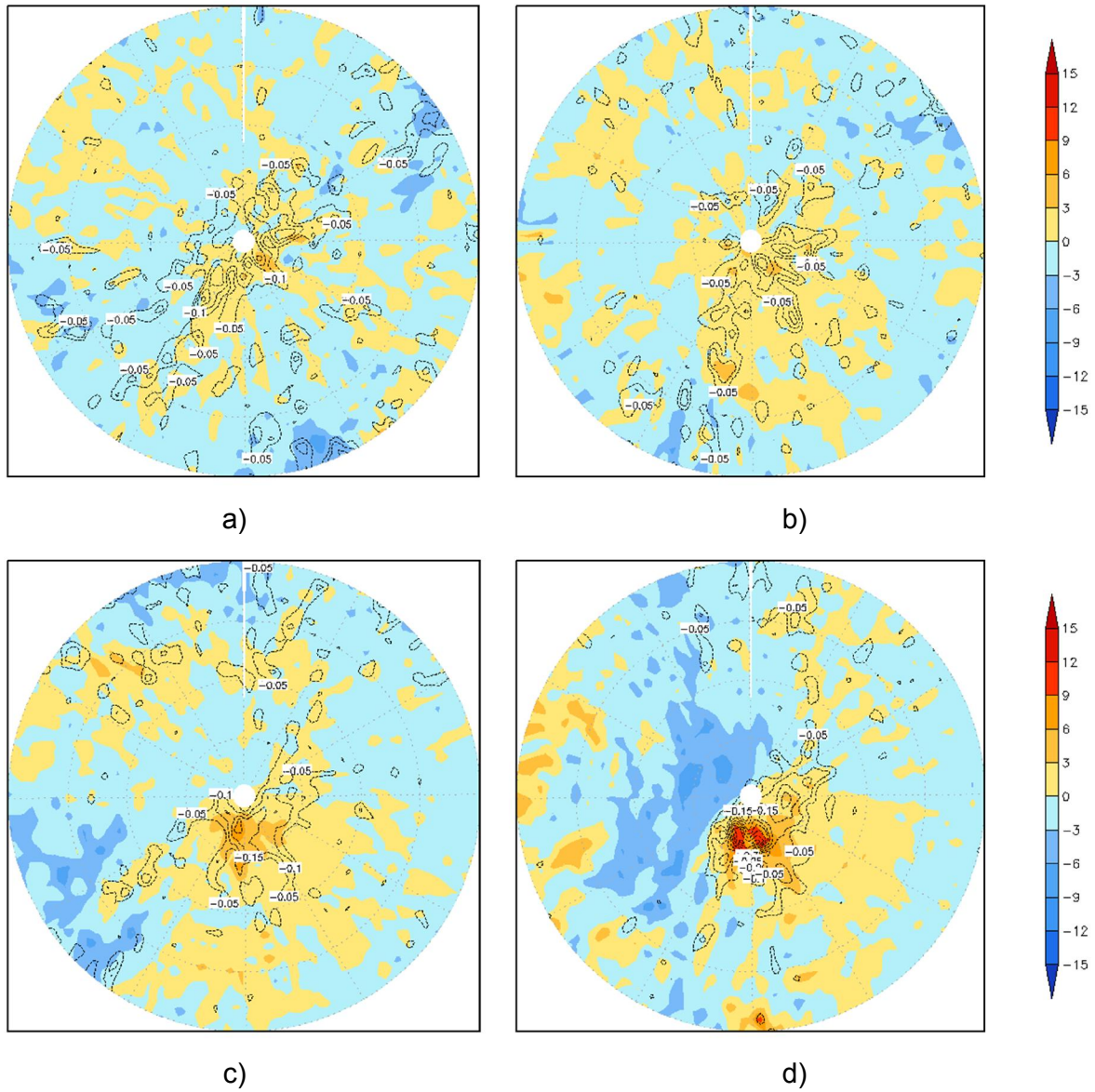
In general, the SST's and heat fluxes are moderate in the subtropical phase of the analyzed cyclones, but in their extratropical phase these variables substantially decrease. This is related to the propagation of the SCET toward higher latitudes after they have fully completed the extratropical transition. This characteristic is corroborated by the trajectories and density of extratropical

transition and lysis (Figure 4.1 and Figure 4.2, respectively). To illustrate the latitudinal propagation of the SCET, the mean latitudinal position of these systems through their entire life cycle was analyzed. The mean latitude was approximately 28°S along the period prior to the transition. On the other hand, at the instant of transition the mean position of these systems is located at 35°S. The propagation toward higher latitudes continues and at $t = 24$ h the mean cyclones center is at 39°S. At this time at least 40% of the SCET are already positioned at latitudes higher than 40°S. Finally, 72 hours after the extratropical transition, the SCET mean position is 48°S with few cyclones passing the latitude of 60°S.

III. Heat fluxes and the role of SSTs

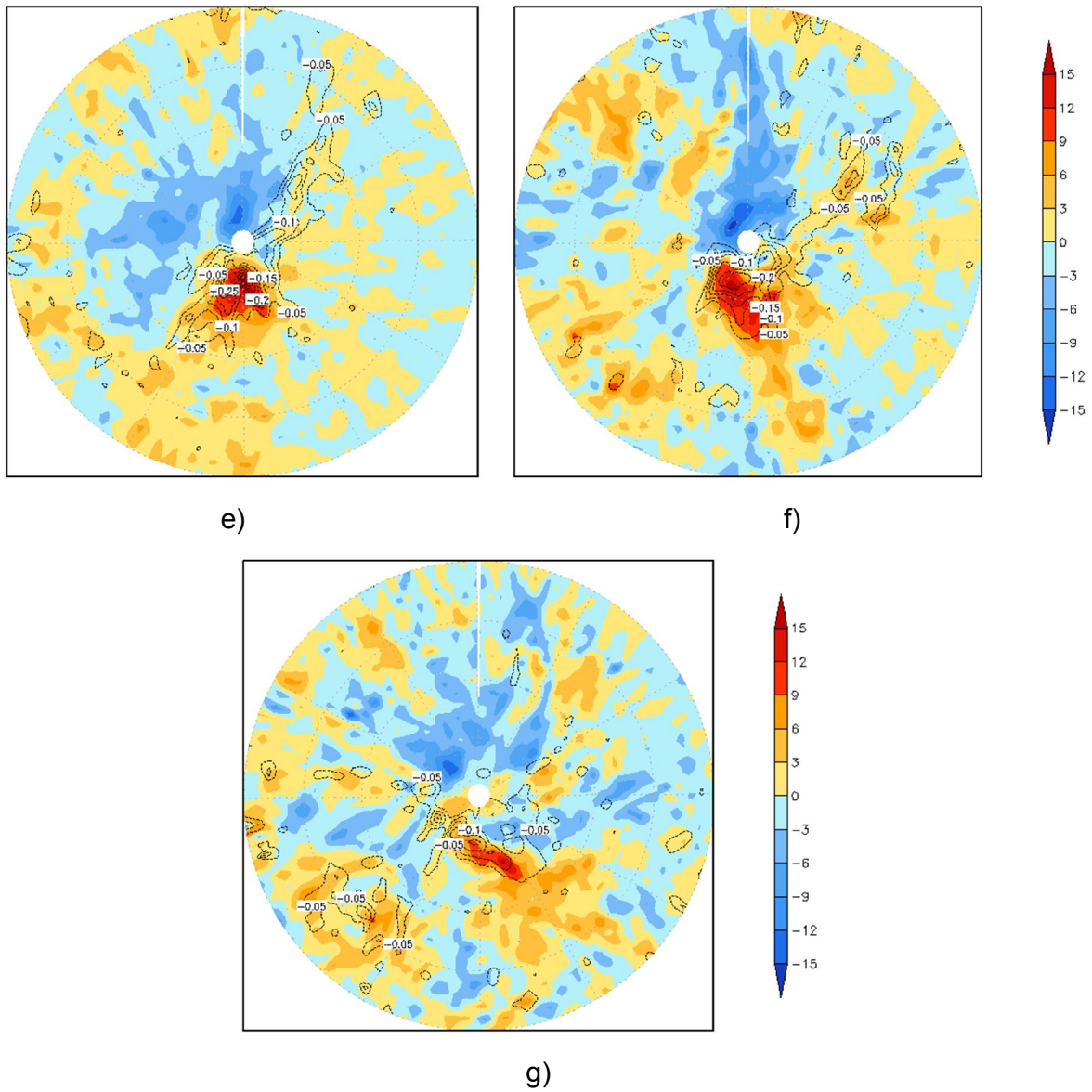
Regarding the thermodynamic features, an area of weak warm air advection and ascending motion is observed at the right side of the cyclone centers between 72 and 48 hours prior to the ET (Figure 4.15ab). Subsequently, both warm air advection and the ascending motion increases gradually. On the other hand, in the left hand sector of the cyclone cold air advection occurs. This configuration is maintained and keeps intensifying until 24 hours after the transition process, when warm advection and the ascending motion reach their maximum magnitudes (Figure 4.15def). The above mentioned pattern of warm advection to the right of the cyclone core and cold air advection at its left side is typical of extratropical cyclones and is associated with the intensification of these systems (REBOITA, 2008). Eventually, the ascending motion and the warm air advection slightly decrease while the cold air advection increases. At the final stage the warm (cold) advection area is positioned to the south (north) of the subtropical cyclones center (Figure 4.15efg). Finally the temperature advection and ascending motion become weaker and scattered.

Figure 4.15—Composites of temperature advection (shaded) and velocity potential (contour) at 850 hPa of SCET in a) $t = -72\text{h}$, b) $t = -48\text{h}$, c) $t = -24\text{h}$, d) $t = 0$, e) $t = +24\text{h}$, f) $t = +48\text{h}$ e g) $t = +72\text{h}$. Units of temperature advection is 10^{-5} K s^{-1} .



(continue)

Figure 4.15 – Conclusion.



Source: Author's production.

It is worth to mentioning that the warm air advection acts as an essential mechanism to increase the convective potential of hybrid cyclones that develops over colder SST's with weaker heat fluxes in the South Atlantic Ocean (EVANS; GUSHARD, 2009, GOZZO et al., 2014). Indeed, the SC in SAO region develops in a region of warm air advection and ascending vertical motions. As these systems deepen, the pressure gradient between them and

the South Atlantic Subtropical High increase resulting in the intensification of the warm advection due to strong northeastern winds. Simultaneously, the ascending motion intensifies due to the thermodynamic destabilization and by overlapping an area of diffluent winds at high levels (GOZZO et al., 2014).

Regarding the thermal forcing, the Sutcliffe theory of the development of cyclones found that propagation of low pressure systems is significantly influenced by the warm air advection in the atmosphere. In this context, cyclonic circulation at low levels triggers a horizontal temperature advection in the 1000 - 500 hPa layer. Hence, east of the surface cyclone warm air advection occurs, while on the western side cold air advection takes place, resulting in baroclinic intensification. The warm air ahead the surface low induces convergence and consequently cyclonic vorticity, leading the cyclone to propagate according to the maximum positive advection. This implies that the cyclone continuously reinforces itself due to the convergence at low levels, such that the later results from the divergence in the mid and upper troposphere and the warm advection. On the other hand, the cold air advection behind the cyclone contributes to the intensification of negative geopotential height anomaly at middle levels (REBOITA et al., 2017).

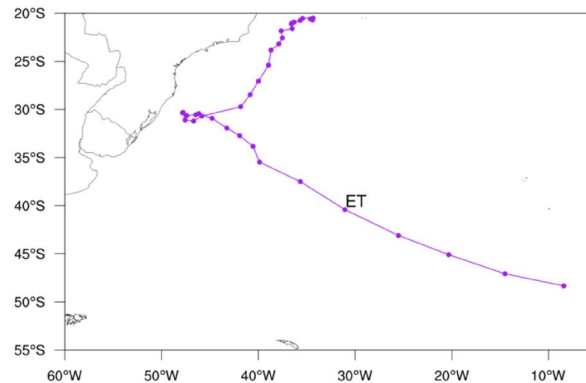
5 CASE STUDY: CYCLONE ANITA

To investigate the dynamical processes favoring extratropical transition of subtropical cyclones in the SAO region, cyclone Anita was selected. This system was chosen mainly because it presented features favoring the tropical transition. The genesis of Anita occurred in early March of 2010. It developed as a subtropical system on the Southeast coast of Brazil in an environment similar to that observed for Hurricane Catarina (DUTRA et al., 2017). After Anita's intensity decreased, it underwent extratropical transition and intensified again such that thunderstorm warning messages were issued by operational forecasters. To better understand this unusual type of weather system a synoptic analysis of the environment associated with Anita is presented next.

5.1 Synoptic analysis and control simulation of cyclone Anita.

Anita cyclogenesis occurred over the SAO, near the southeast coast of Brazil, on 5th March 2010 (Figure 5.1). The tracking shows that Anita's lifetime was of 9 days and that it displaced southwest until its mature phase. At the mature stage, where Anita positioned closest to the southern coast of Brazil, it presented a semi-stationary feature that lasts for a couple of days. These characteristics of Anita tracking were also observed by Reboita et al. (2019), but they showed that the genesis (dissipation) of Anita occurred 12 (18) hours earlier. Also, Reboita et al. (2019) found that Anita dissipated around 38°S/35°W, i.e., it did not reach extratropical latitudes. The genesis of Anita took place around 20°S/35°W in a region of a pre-existing cyclonic circulation. The development of its structure was associated with the connection between a cut-off-low and the surface subtropical cyclone (not shown). From 6th to 9th of March, a low level counterpart of Anita propagates toward the southern Brazilian coast due partially to being blocked by the zonal flow of the South Atlantic Subtropical Anticyclone (SASA). The deepening of the surface cyclone was favored by the upper level diffluence causing divergent areas which contribute to increase the ascending motion over the cyclone (not shown).

Figure 5.1 - Anita tracking based on relative vorticity at 925 hPa from CFSR reanalysis.



ET indicates the extratropical transition time.

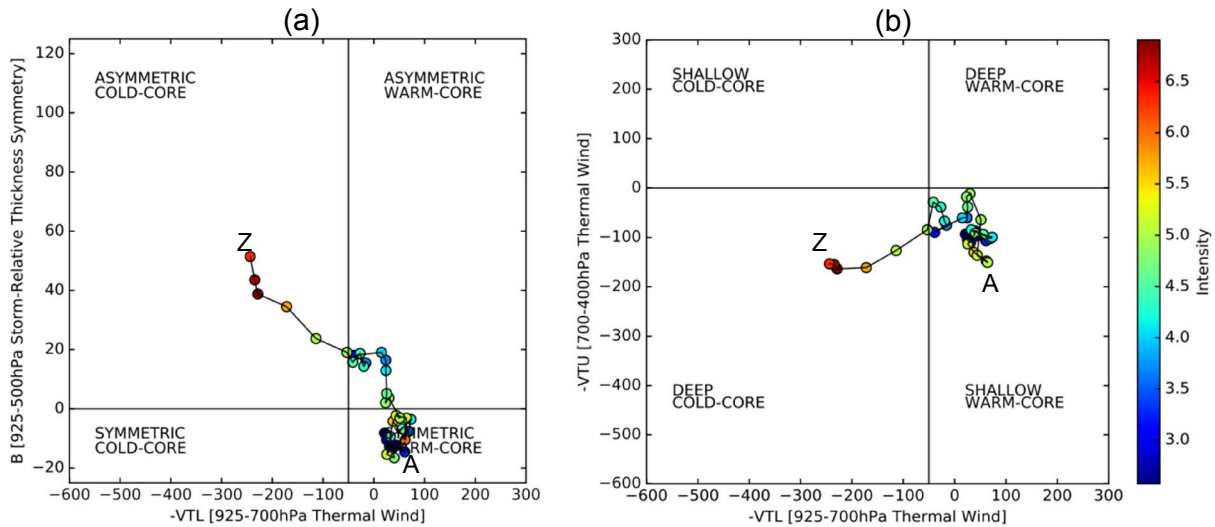
Source: Author's production.

The CPS diagrams show the evolution of cyclone Anita based on its vertical structure described by the thermal symmetry and thermal wind at low and upper levels (Figure 5.2). It is observed that Anita developed as a shallow warm-core hybrid cyclone with an upper level cold core, a low level warm core and non-frontal structure. This feature is represented by negative values of $-VTU$, positive $-VTL$ and near zero values of B , respectively. This structure was maintained until 00 UTC on 11th March when the low level warm core weakened and acquired negative values. This took place while the intensity of the cyclonic vorticity at 925 hPa was weakening. Dias Pinto et al. (2013) indicate that at this stage Anita presented potential to undergo tropical transition. Also, the peak of relative vorticity intensity during the subtropical phase occurs at 12 UTC on 8th of March.

According to the criteria used in the current study, cyclone Anita completed ET at 18 UTC on 12th of March with values of $-VTL$, $-VTU$ and B around -172, -161 and 34, respectively, indicating that the system acquired an asymmetric cold core vertical structure with frontal nature. During the extratropical phase, Anita deepened reaching its second peak intensity a few hours after the ET, at 00 UTC on 13th March. At this instant, the cold core structure also reached its

maximum magnitude (Figure 5.2). Reboita et al. (2019), Dutra et al. (2017) and Dias Pinto et al. (2013) found that Anita underwent ET between 12 UTC and 18 UTC on 11th of March. However, in those studies the ET was considered as the moment when Anita acquired cold core structure regardless of its thermal symmetry feature. Indeed, the thermal symmetry only became higher than 25 m on Dutra et al. (2017) analysis. Although, the tracking was performed using 925 hPa relative vorticity in the current and in the previously mentioned studies, there are some divergences regarding the lifetime, position and time of genesis and lysis of Anita. This could be associated with the usage of different dataset, the resolution of the data and the method applied for tracking Anita.

Figure 5.2 – Phase space diagram for cyclone Anita from 00 UTC on 5 March to 18 UTC on 13 March 2010: (left) B versus -VTL (right) -VTU versus -VTL.



Shaded circles are 925 hPa relative vorticity intensity. A indicates the beginning of Anita life cycle while Z indicates the end. Relative Vorticity units are 10^{-5} s^{-1} .

Source: Author's production.

To characterize the environment where the ET of Anita took place a synoptic analysis is presented. At 06 UTC on 9th of March, Anita had almost reached its mature stage, characterized by a barotropic structure from the surface to the

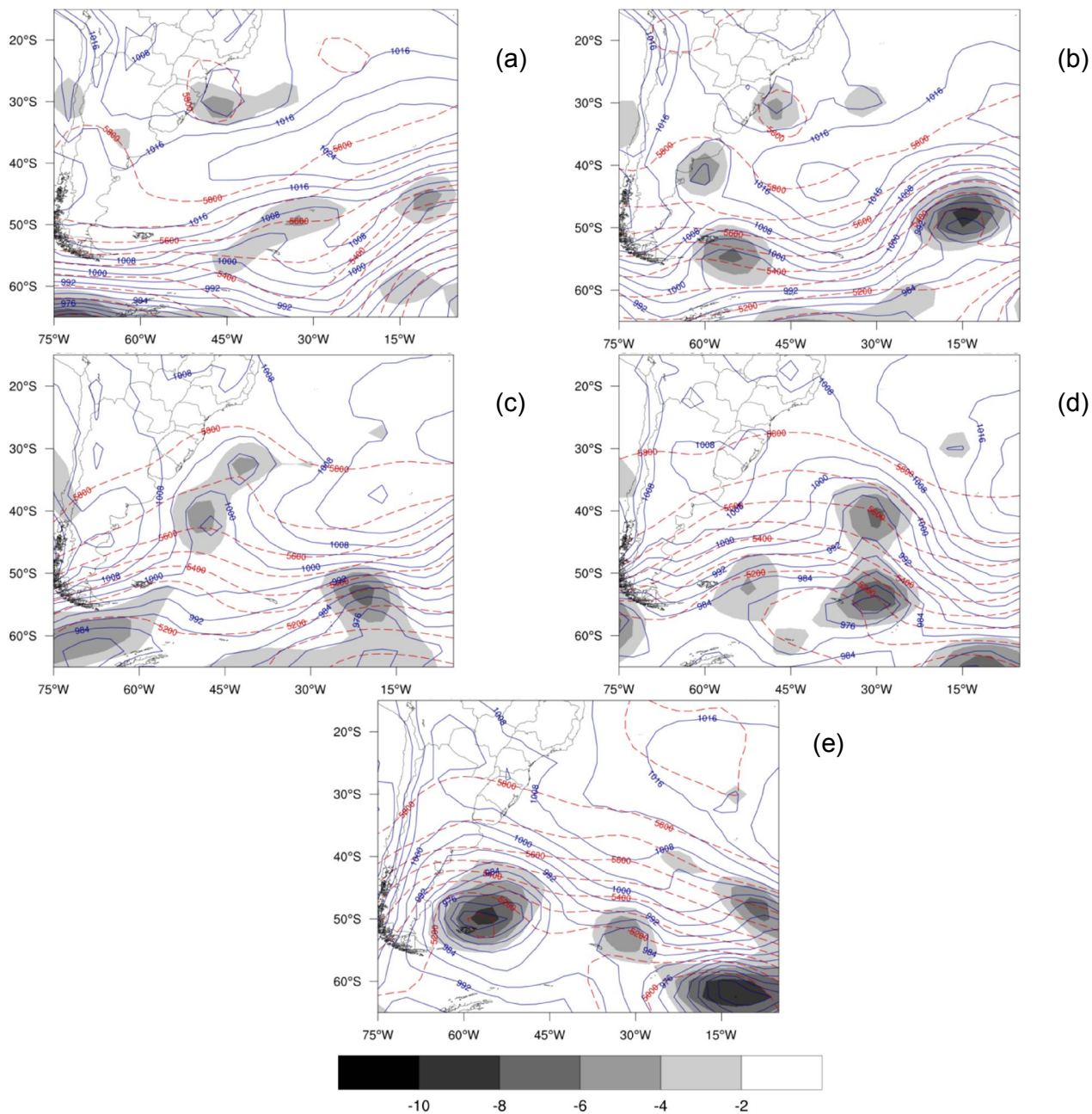
upper troposphere (Figure 5.3). At this stage, Anita was located at $30^{\circ}\text{S}/46^{\circ}\text{W}$ with an SLP core of 1008 hPa and an associated cut-off-low at middle levels. Southeast of Anita, the SASA has a peak value of 1024 hPa and continued blocking the flow. At 250 hPa, Anita's upper level counterpart was positioned over an area of negative PV and southward of it an anticyclonic circulation is observed (Figure 5.4a). This pattern is associated with a north-south dipole-blocking and remains up to 12 UTC on the 10th of March, maintaining Anita quasi-stationary. Dias Pinto et al. (2013) highlighted that this synoptic configuration is an indicative of the potential for tropical transition of cyclone Anita since it resembles the conditions observed for Hurricane Catarina. Furthermore, a cyclonic vortex which extends to the mid troposphere is observed over the east-central Argentina (Figure 5.2a, Figure 5.3a, Figure 5.4).

In the following hours, the upper troposphere cyclonic vortex and the dipole pattern weakened (Figure 5.4b). At 12 UTC on the 10th of March Anita decreased its intensity, the upper part of its vortex no longer presented a closed circulation and the associated potential vorticity weakened. According to Dutra et al. (2017) the eastward propagation of the upper cyclonic vortex located over Argentina towards the rear of Anita contributed to the weak associated dipole pattern. Although, the blocking pattern was weakened, Anita remained stationary because the anticyclonic circulation associated with SASA still prevented its propagation (Figure 5.3). Moreover, both SLP and 925 hPa relative vorticity lost intensity and the cut-off-low at middle level dissipated and was incorporated into the atmospheric flow.

It is worth noting that at 12 UTC on the 10th of March, a cyclone with a pressure center of 1006 hPa developed on the Argentine coast around $41^{\circ}\text{S}/59^{\circ}\text{W}$, hereafter it is named as ECY (Figure 5.3). Later, at 18 UTC on the 11th of March, the upper tropospheric vortex of Anita reached its final stage and turned into an extended trough centered at $30^{\circ}\text{S}/45^{\circ}\text{W}$ (Figure 5.3c). At this moment, the SASA moved eastward and was located around $35^{\circ}\text{S}/20^{\circ}\text{W}$. The surface low of Anita propagated southeastward with a 1000 hPa SLP center (Figure 5.3c). Also, the surface cyclone and the mid level trough associated with ECY,

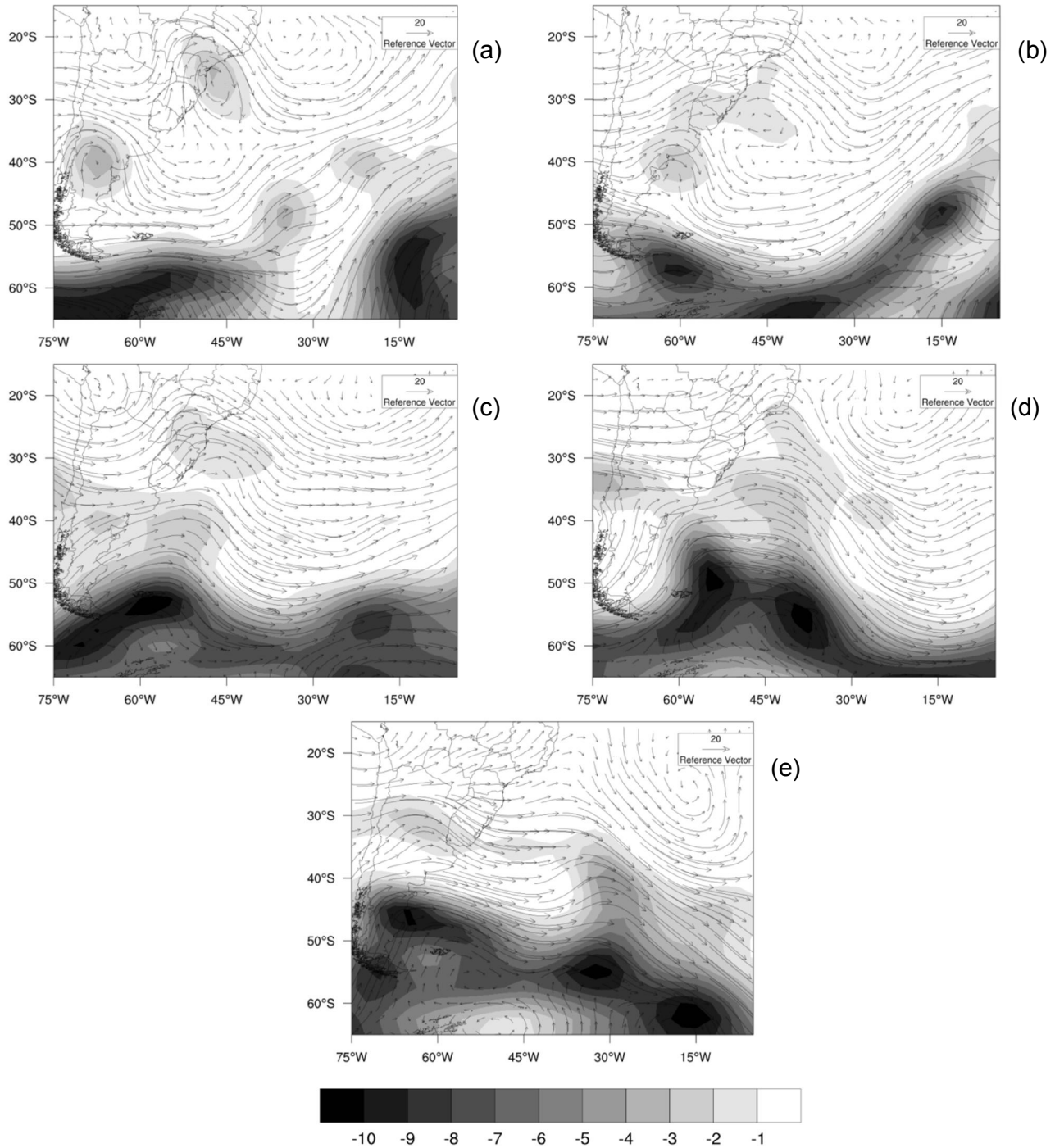
which moved faster, propagated eastward, such that cyclone Anita started merging with ECY.

Figure 5.3 – 925 hPa Relative vorticity (shaded), SLP (blue contour each 4 hPa) and 500 hPa geopotential height (red dashed contour each 100 gpm) for cyclone Anita from CFSR reanalysis for the 09-13 March 2010 period: (a) 09 – 18 UTC, (b) 10 – 12 UTC, (c) 11 – 18 UTC, (d) 12 – 18 UTC and (e) 13 – 18 UTC.



Source: Author's production.

Figure 5.4 – Wind vectors and PV at 250 hPa (shaded) for cyclone Anita from CFSR reanalysis for the 08-13 March 2010 period: (a) 09 – 18 UTC, (b) 10 – 12 UTC, (c) 11 – 18 UTC, (d) 12 – 18 UTC and (e) 13 – 18 UTC.



PV units are PVU.

Source: Author's production.

5.2 Potential Vorticity Inversion analysis

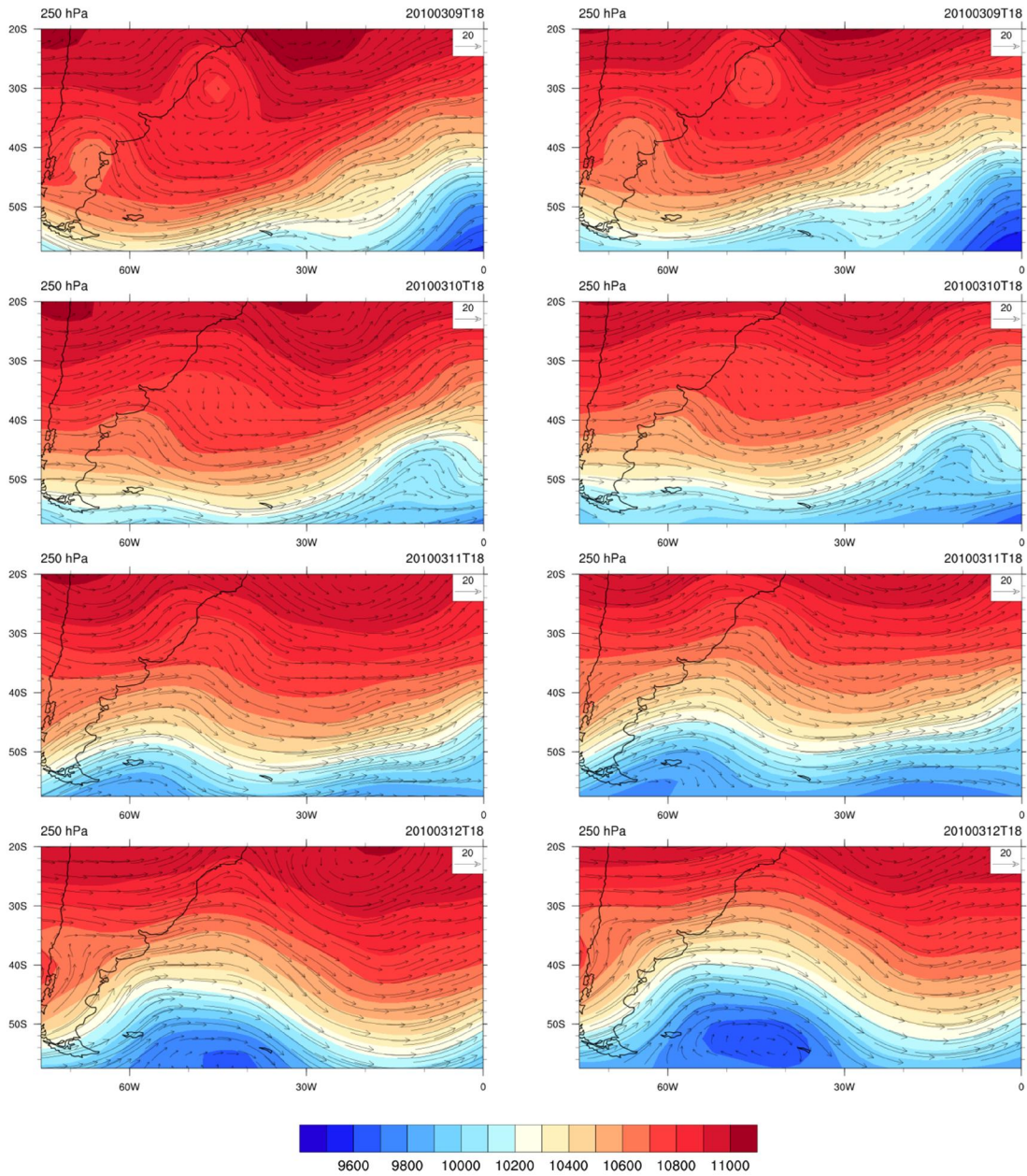
The potential vorticity inversion method, described in section 3.3.2, was applied to cyclone Anita in order to evaluate the contribution of PV anomalies for the extratropical transition. Thus, anomalies of the total PV field were inverted and the anomalies for the upper and lower troposphere were computed to give insight into the interaction of different anomalies in the evolution of Anita. The piecewise PV inversion was calculated for the 06-13 March 2010 period, at 0, 06, 12 and 18 UTC. The domain used corresponds to the region between 0° - 120° W and 15° - 65° S, with 47 points of longitude and 21 of latitude. This ensured that the boundary condition was sufficiently distant from the region of extratropical cyclone occurrence and allows the propagation to be followed in the post transition period.

From the PV inversion, the balanced fields of geopotential height and stream function were obtained. Subsequently, the temperature and non-divergent wind components were derived. In this section, the above mentioned fields are presented to verify their accuracy. The analyses are for the 9-12th March 2010 period at 18 UTC. This period encompasses the intensification of Anita until its extratropical phase. In order to attest if the method used is appropriate to recover the meteorological fields and their associated anomalies, the PVI was applied for the total PV field. Thus, the balanced fields are shown together with the CFSR reanalysis fields.

Figure 5.5 and Figure 5.6 show the balanced fields of geopotential height and non-divergent wind obtained through the inversion of total potential vorticity at 250 and 850 hPa, respectively. Also, they show the geopotential height and wind from the CFSR reanalysis at the same vertical levels and time. During the entire studied period, the balanced fields at all levels are consistent with the ones from CFSR. There is however, a small northward displacement in the balanced fields in relation to the reanalysis fields, which is associated with the boundaries computed in the PV inversion. It is observed that the magnitude of the non-divergent wind is smaller than the reanalysis wind; this occurs due the methodology used which assumes that the divergent terms of the wind can be

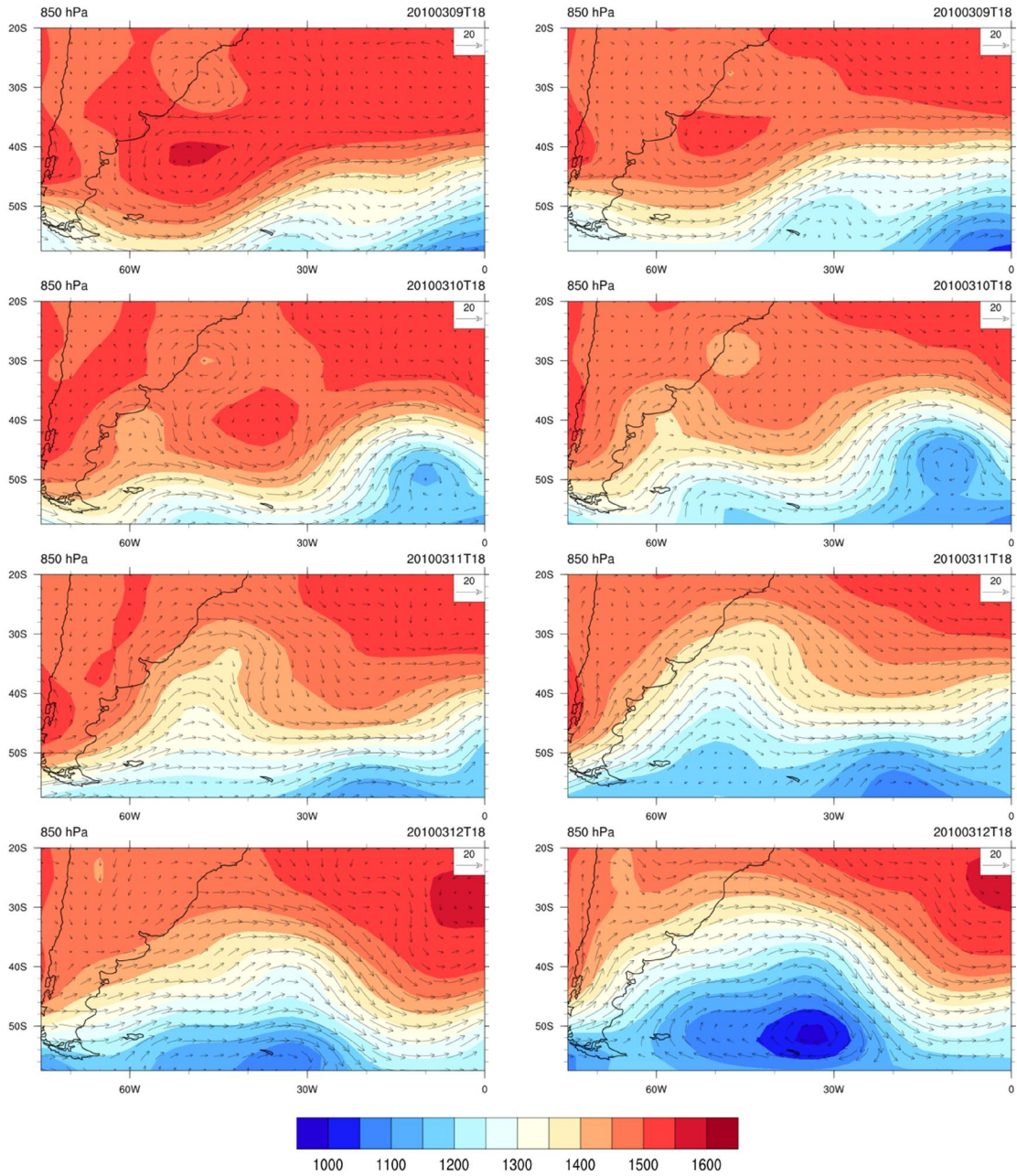
neglected compared to the rotational terms in the divergence equation. This difference is more significant in the upper troposphere, where the flux is very divergent.

Figure 5.5 – (left) Geopotential height and wind from CFSR reanalysis and (right) geopotential and non-divergent wind from PV inversion at 250 hPa on 09 - 12th of March 2010 period at 18 UTC.



Source: Author's production.

Figure 5.6 – (left) Geopotential height and wind from CFSR reanalysis and (right) geopotential and non-divergent wind from PV inversion at 850 hPa on 09- 12th March 2010 period at 18 UTC.



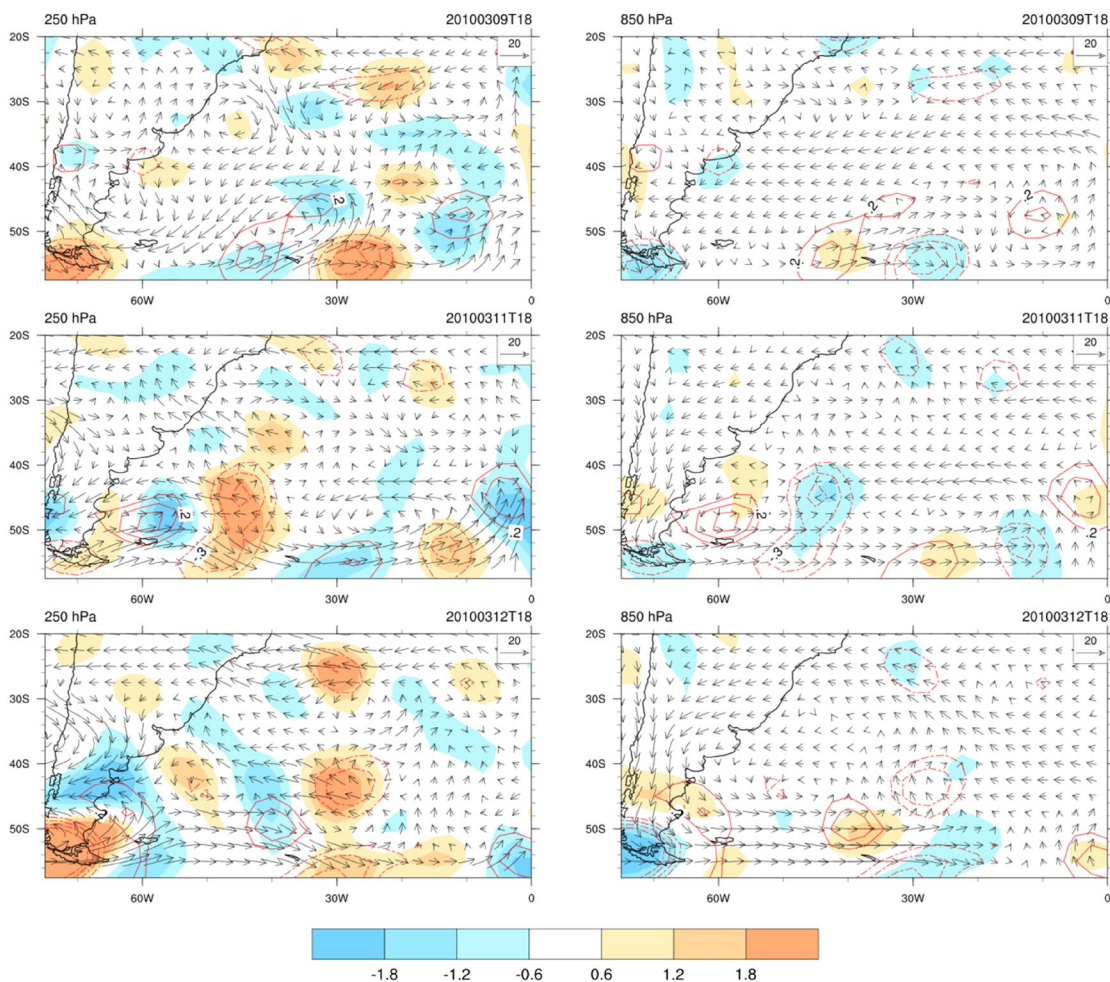
Source: Author's production.

The cyclonic vortex in the middle and upper troposphere during the mature phase (09th March) of the cyclone Anita are well represented in the balanced fields, as well as the vortex associated with the extratropical system propagating over South America, at approximately in 40°S . Furthermore, in both fields (balanced and reanalysis) the north-south dipole pattern, which takes place at high levels on the 9th of March and lasts at least 24h, is well represented.

Areas of convergence/divergence of the wind at low and high levels and the ascending and descending motion in the middle troposphere obtained from CFSR reanalysis wind field are displayed with the divergent wind over the SAO in Figure 5.7. The divergent wind was calculated as the difference between the reanalysis and the balanced wind. It is observed that the areas of mass convergence (divergence) at 250 and 850 hPa at the studied region are consistent with the ones for the divergent wind for the entire period.

In the upper (lower) troposphere, mass divergence (convergence) to the east of the subtropical and extratropical vortex, shown in Figure 5.5, agrees with the calculated divergent wind field. This feature of convergence at low levels and divergence in the upper troposphere indicates ascending motion, which is corroborated by negative values of vertical velocity at 500 hPa, as shown in Figure 5.7. It is apparent that the main areas of ascending motion near the southeast coast of South America are associated with the above mentioned divergence and convergence areas, i.e., they are associated with Anita and the extratropical cyclones interacting with it. Thus, it can be verified that the piecewise PV inversion is able to compute the dynamical non-divergent wind field adequately.

Figure 5.7 – Difference between the total CFSR wind and the non-divergent wind (vectors), divergence (shaded) at (left) 250 hPa and (right) 850 hPa and vertical velocity at 500 hPa (contour) at 18 UTC on the 09th, 11th and 12th of March.

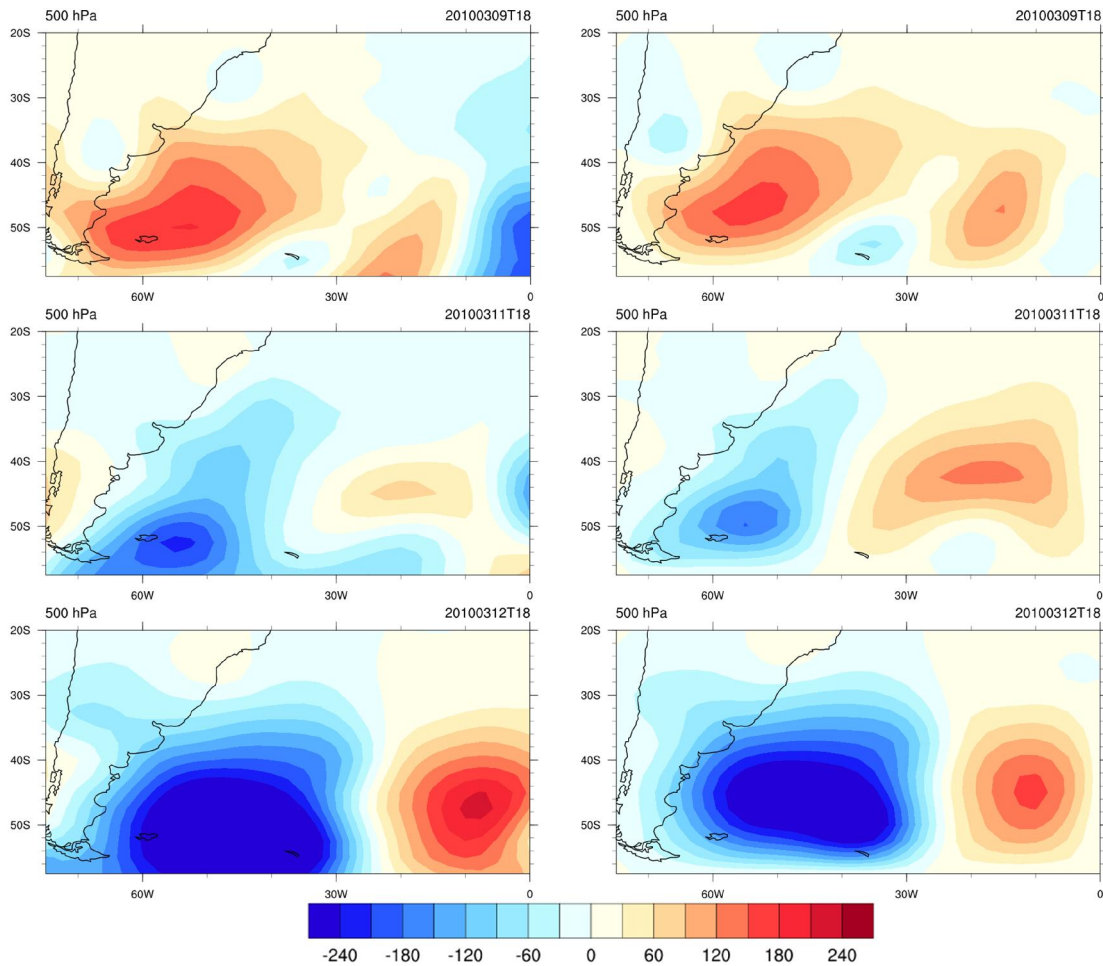


Source: Author's production.

To verify if the method represents properly the anomalous fields, the perturbed fields associated with the total PV anomaly were simultaneously obtained by considering the entire vertical column. The anomalies were calculated considering the mean from the studied period (06-14 of March). Figure 5.8 shows the geopotential height anomaly at 500 hPa, where the right column is the balanced field and the left one is from the CFSR reanalysis. The CFSR anomaly fields were computed similarly as the obtained by PVI. It is noted that

the balanced anomalies are in agreement with the reanalysis field throughout analyzed period. Specifically, the negative anomalies over the southeast coast of Brazil, associated with cyclone Anita, and the one associated with the extratropical system over Argentina, are well represented by the balanced field (Figure 5.8a-c). The main observed differences may be due to the boundary condition in the PV inversion. It can be inferred that the circulation associated with the PV anomalies is explained mainly by the dynamical balanced part of the flux.

Figure 5.8 – Geopotential height anomaly at 500 hPa from (left) CFSR reanalysis and (right) balanced field from PV inversion at 18 UTC on the 09th, 11th and 12th of March.



Source: Author's production.

Next, the contribution of different potential vorticity perturbations to the development of the Anita is analyzed. In this context, the contribution of PV anomalies at low, mid and high levels was investigated separately. Thus, the layers chosen were 400 – 100 hPa for the upper troposphere (PVu), 975 – 700 hPa for the lower troposphere (PVI) and the potential temperature anomaly at the lower boundary (TTb). The latter corresponds to the potential temperature anomalies at the surface. These anomalies were chosen due to their mutual interaction and resultant circulation which is associated with cyclogenesis (DAVIS; EMANUEL, 1991). Here, the total anomaly refers to the potential vorticity in the entire atmospheric column (PVt), as used previously for the validation of the method. Figure 5.9 and Figure 5.10 presents the vertical cross sections of relative vorticity computed from the different potential vorticity anomalies. Cross sections were taken considering the latitudinal position of Anita at 925 hPa for each evaluated time.

It is observed that the PVu contributes to the cyclonic vorticity from 100 hPa to the mid-troposphere, with a peak at 200 hPa, during the intensification (08th March, not shown) and mature (09th March) stages of Anita (Figure 5.9). Comparing the result for PVu with that from the total PV anomaly, it can be inferred that PV equivalent to PVu is essential to the upper level circulation. At these stages, the results indicate that PVI and TTb contribute to the circulation in the lower troposphere. However, PVI actually contributes to the cyclonic circulation up to 600 hPa while TTb contributes to anticyclonic circulation from 1000 to 850 hPa.

During the intensification period, the circulation associated with the total perturbation is characterized by a westward-tilted vertical structure. The individual circulations associated with the anomalies at high and low levels do not show this vertical inclination, thus, it is deduced that this structure occurs due to the superposition of the cyclonic cores in the lower and upper troposphere. On the other hand, in the mature stage of the cyclone, the circulation has an eastward inclination with height, indicating that the cyclonic vortex at high levels is overtaking the surface cyclone center. Furthermore, at this stage the surface

cyclone is propagating westward toward the southeast coast of Brazil. It is worth pointing out that between the above mentioned stages, the vertical structure is aligned, indicating a barotropic structure (not shown).

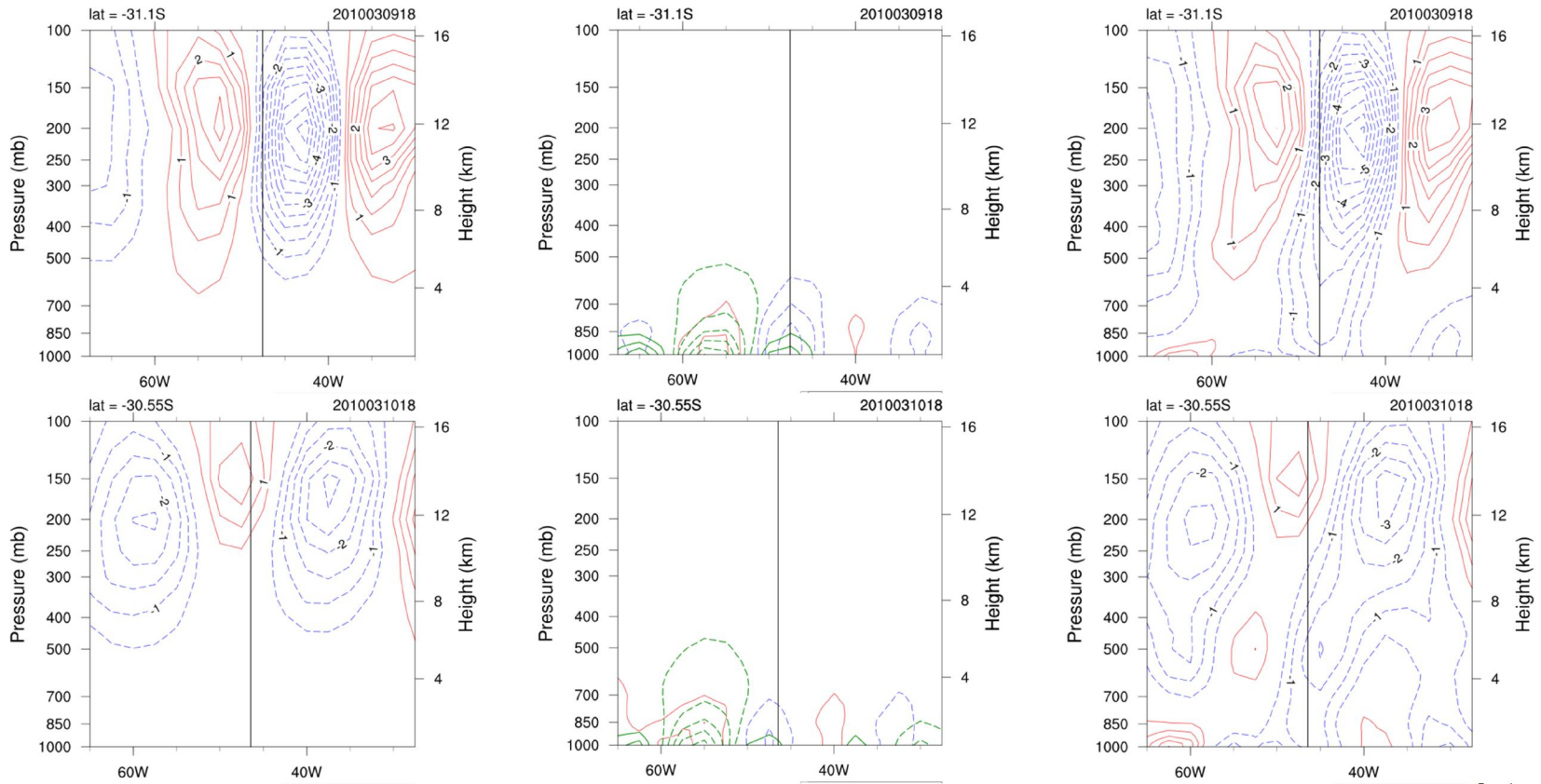
24 hours later, the surface cyclone weakens. This period is characterized by the decrease of relative vorticity, mainly at upper layers where the cyclonic vortex is less intense and more detached from the circulation. PVI anomalies continue contributing to the relative vorticity at lower levels, but at this time the peak of vorticity is between 700 and 500 hPa. Although the cyclone is weakening, the cyclonic core in the mid-troposphere actually increases its magnitude as can be seen in Figure 5.9.

During the extratropical transition phase, characterized as the period of re-intensification of the cyclone, PVu is still the main element contributing for the upper level configuration. Although, at this stage there is no cyclonic vortex associated with the surface system. On the other hand, the contribution of lower levels and lower theta boundary seems to play a key role in the strengthening of negative relative vorticity over the surface cyclone. When the transition is completed and the cyclone acquires extratropical characteristics, the PV anomalies at low levels have a bigger impact on the atmospheric circulation from the surface up to 300 hPa. At this point, the cyclonic relative vorticity presents a westward vertical tilt, indicating the coupling of the surface cyclone with the cyclonic vorticity anomalies in the upper troposphere.

In general, the upper level PV anomalies are revealed to be an important component of the circulation in the upper troposphere throughout the studied period, contributing to the development of the cyclonic vortex associated with the surface cyclone. Although, at the transition instant it was observed that there was no significant cyclonic vorticity at upper levels. Also, the contribution of low level PV anomalies extends to the mid-troposphere and seems to be the main element to the negative vorticity at low levels in the prior transition phase. After that, the PV anomalies of the lower theta boundary present a significant contribution to the re-intensification of the cyclonic circulation. It is worth mentioning that the PV anomaly at mid levels influences the vorticity anomalies

mostly between 600-300 hPa layers (not shown). Actually, its contribution seems more relevant at the point of weakening (10th of March). At the transition period, the combined contributions of the theta boundary, low and mid level PV anomalies act to intensify the deepening of the surface cyclone. Comparing the circulation associated to the potential vorticity anomalies at low and high levels, Huo et al. (1998) verified that there is a mutual interaction between these anomalies. Specifically, they observed that the circulation associated with the upper PV anomaly enhances the lower anomaly, which consequently reinforces the upper level anomalies.

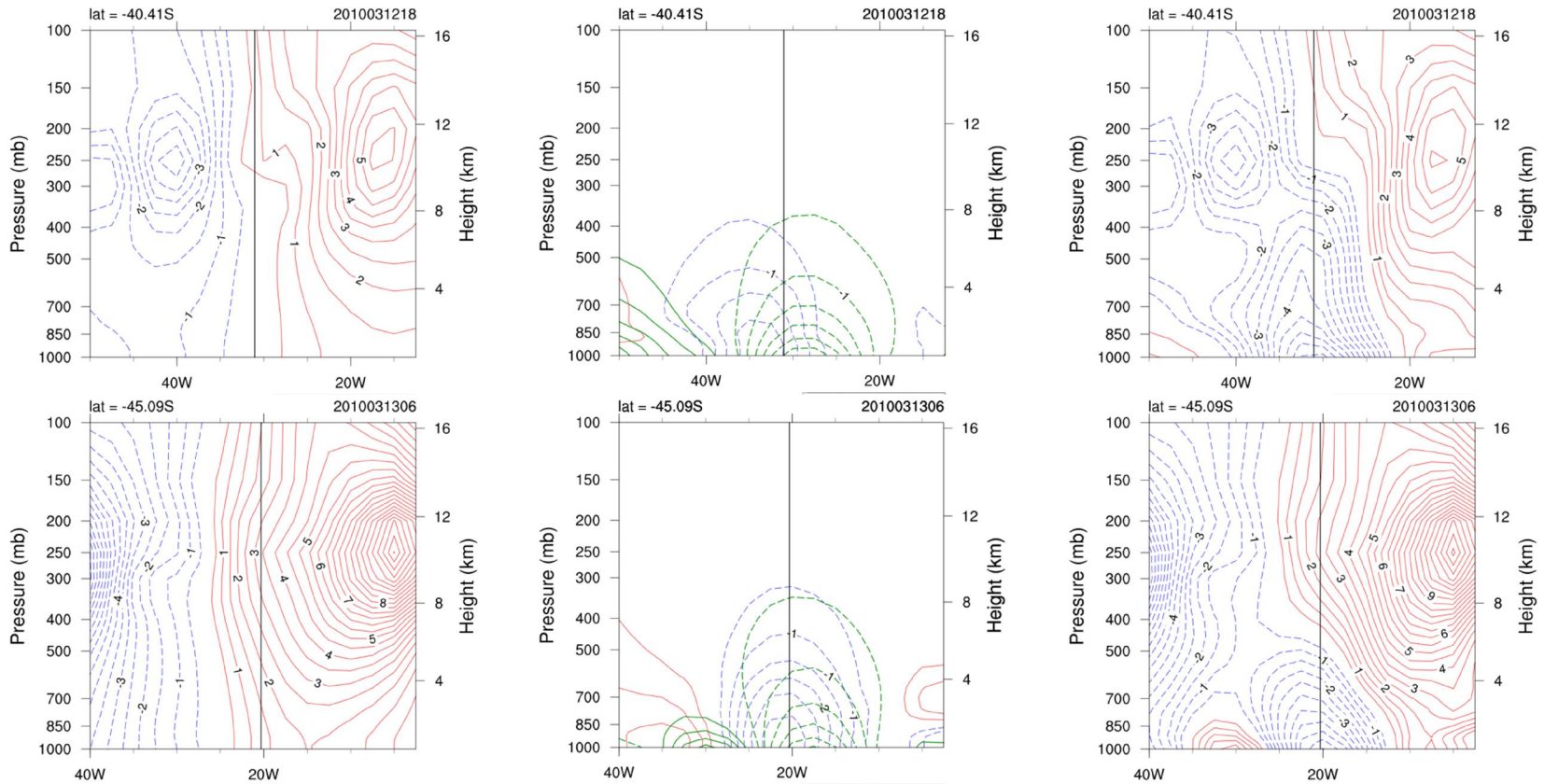
Figure 5.9– Vertical cross section of relative vorticity associated with PV anomalies at (left) high levels: 400 – 100 hPa, (center) low levels: 975 – 700 hPa (blue/red lines) and potential temperature at inferior boundary (1000 hPa – green lines) and (right) total (1000 – 100 hPa), for 18 UTC on 09th of March (top) and on 10th of March (bottom).



Blue dashed (red lines) lines represent the cyclonic (anticyclonic) vorticity. Black line represents cyclonic core at 925 hPa. Unit of relative vorticity is 10^{-5} s^{-1} .

Source: Author's production.

Figure 5.10– Vertical cross section of relative vorticity associated with PV anomalies at (left) high levels: 400 – 100 hPa, (center) low levels: 975 – 700 hPa (orange lines) and potential temperature at inferior boundary (1000 hPa – green lines) and (right) total (1000 – 100 hPa), for 18 UTC on 12 of March (top) and 06 UTC on 13 of March (bottom).



Blue dashed (red lines) lines represent cyclonic (anticyclonic) vorticity. Black line represents the cyclonic core at 925 hPa. Unit of relative vorticity is 10^{-5} s^{-1} .

Source: Author's production.

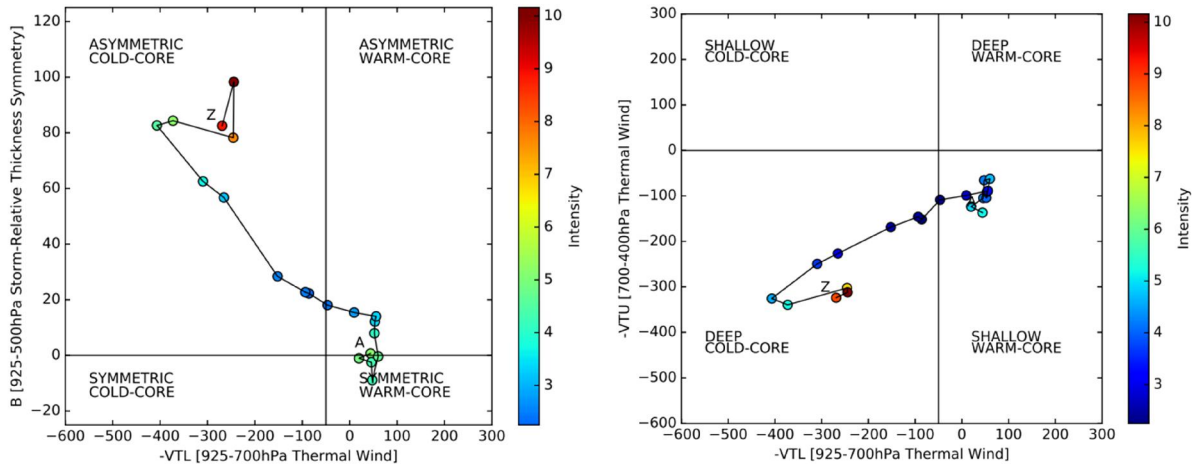
5.3 Numerical experiments: Cyclone Anita

In this section, a case study is presented to illustrate the ET of subtropical cyclones in the SAO. Cyclone Anita was selected to demonstrate the evolution and structure of a SCET. The individual contribution of different PV anomalies to the evolution of Anita was conducted through PVI method. A validation of the method is also presented in this section. The results of this investigation and the environment associated with Anita motivated three sensitivity experiments to investigate the influence of PV anomalies on the ET of Anita. These experiments are presented in the following subsection.

5.3.1 Control simulation

In the current study the control experiment (CTL) of cyclone Anita initiates at 00 UTC on 9 March and ends at 00 UTC on 14 March. The associated cyclone phase space diagram is presented to show the evolution of the Anita structure. Since the simulations started on 09 March, the life cycle of Anita in the CPS diagram also initiates later, at its mature stage (**Erro! Fonte de referência não encontrada.**). At this time, Anita presented a hybrid structure in the CTL experiment (upper level cold core and low level warm core). This structure was maintained until 00 UTC on day 12, when Anita completed its ET, with values of $-VTL$, $-VTU$ and B around -152 , -168 and 28 , respectively. Although, Anita underwent ET earlier in the CTL than in CFSR, the evolution of the structure until the ET time was very similar, with the magnitude of all three parameters presented being similar. After the ET, the CPS parameters presented higher values in the CTL. The re-intensification of Anita in the extratropical phase is also seen in the CTL, with higher magnitude of relative vorticity.

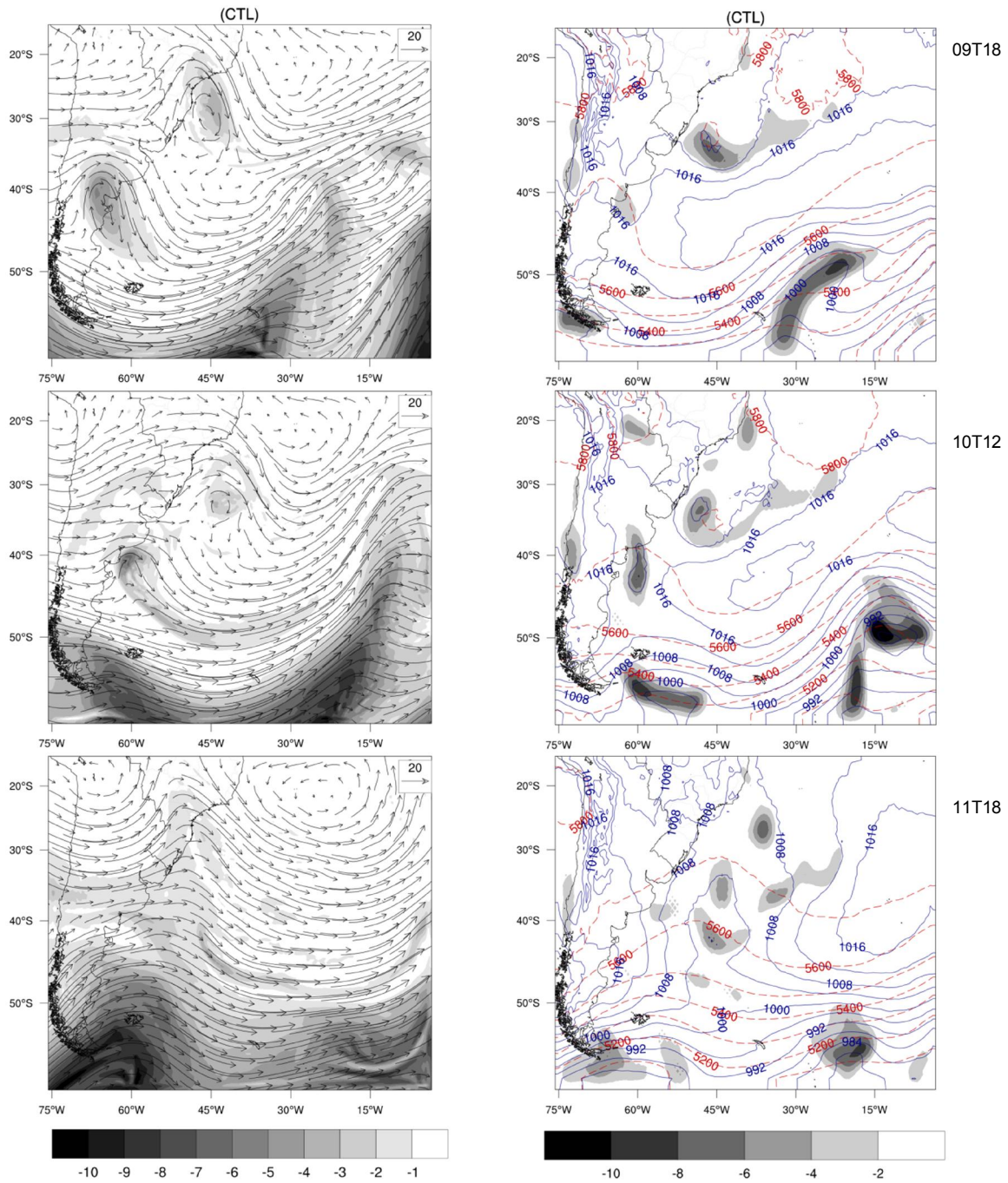
Figure 5.11 – Phase space diagram for cyclone Anita from CTL on 06 UTC on 9 March to 00 UTC on 14 March 2010: (left) B versus -VTL (right) -VTU versus -VTL. Shaded circles are 925 hPa relative vorticity intensity. A indicates the beginning of Anita life cycle while Z indicates the end. Relative Vorticity units are 10^{-5} s^{-1} .



Source: Author's production.

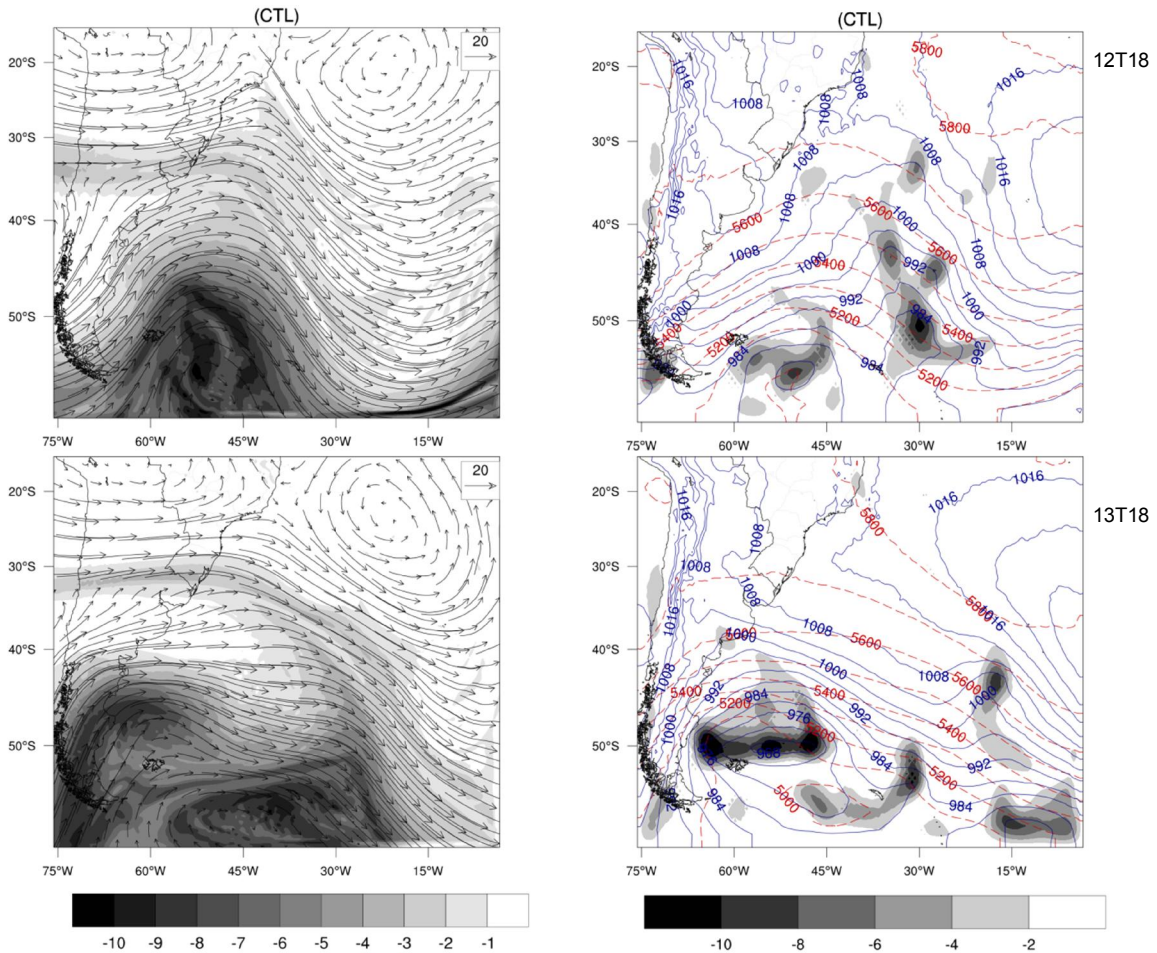
The CTL experiment was able to simulate Anita over the SAO, near the Brazilian southern coast, as well as its stationary feature and extratropical transition (Figure 5.12). At 18 UTC on the 9th of March, the CTL SLP field shows a closed surface low with a central pressure of 1004 hPa and a mid level cut-off low in the geopotential field around $30^{\circ}\text{S}/47^{\circ}\text{W}$. The associated low level cyclonic vorticity core is positioned over the SLP low with higher magnitude ($-6 \times 10^{-5} \text{ s}^{-1}$) than the observed one in the CFSR field (Figure 5.5). The mid level trough of ECY is positioned around 40°S and the SASA circulation is well represented extending westward up to 50°W with a main center of 1024 hPa. The circulation associated with the transient systems of the mid latitudes is consistent with CFSR, although the cyclonic vorticity is higher for these systems. The upper level fields show that the intensity and position of both the cyclonic vortex and PV cores are correctly reproduced, as well as the north-south dipole-pattern (Figure 5.12).

Figure 5.12–(right) 925 hPa Relative vorticity (shaded), SLP (blue contour each 4 hPa) and 500 hPa geopotential height (red dashed contour each 100 gpm) (left) wind vectors and PV at 250 hPa (shaded) for cyclone Anita from CTL for the 09-11 March 2010 period.



Source: Author's production.

Figure 5.13 - (right) 925 hPa Relative vorticity (shaded), SLP (blue contour each 4 hPa) and 500 hPa geopotential height (red dashed contour each 100 gpm) (left) wind vectors and PV at 250 hPa (shaded) for cyclone Anita from CFSR reanalysis for the 12-13 March 2010 period.



Relative Vorticity units are 10^{-5} s^{-1} and PV units are PVU.

Source: Author's production.

Major differences are observed at 18 UTC on 11/March where the surface lows dissipates and becomes part of a wide wave (Figure 5.13). In the CFSR field, the surface low fully dissipates a day later, but from 00 UTC on the 12th of March it decreased strength remaining just a narrow low. On the other hand, cyclone ECY was totally embedded in the associated flow (Figure now shown). Also, the closed surface cyclonic circulation at 55°S/29°W observed for CFSR (Figure 5.6) does not develop until the 13th March at 00 UTC (not shown). On the other hand

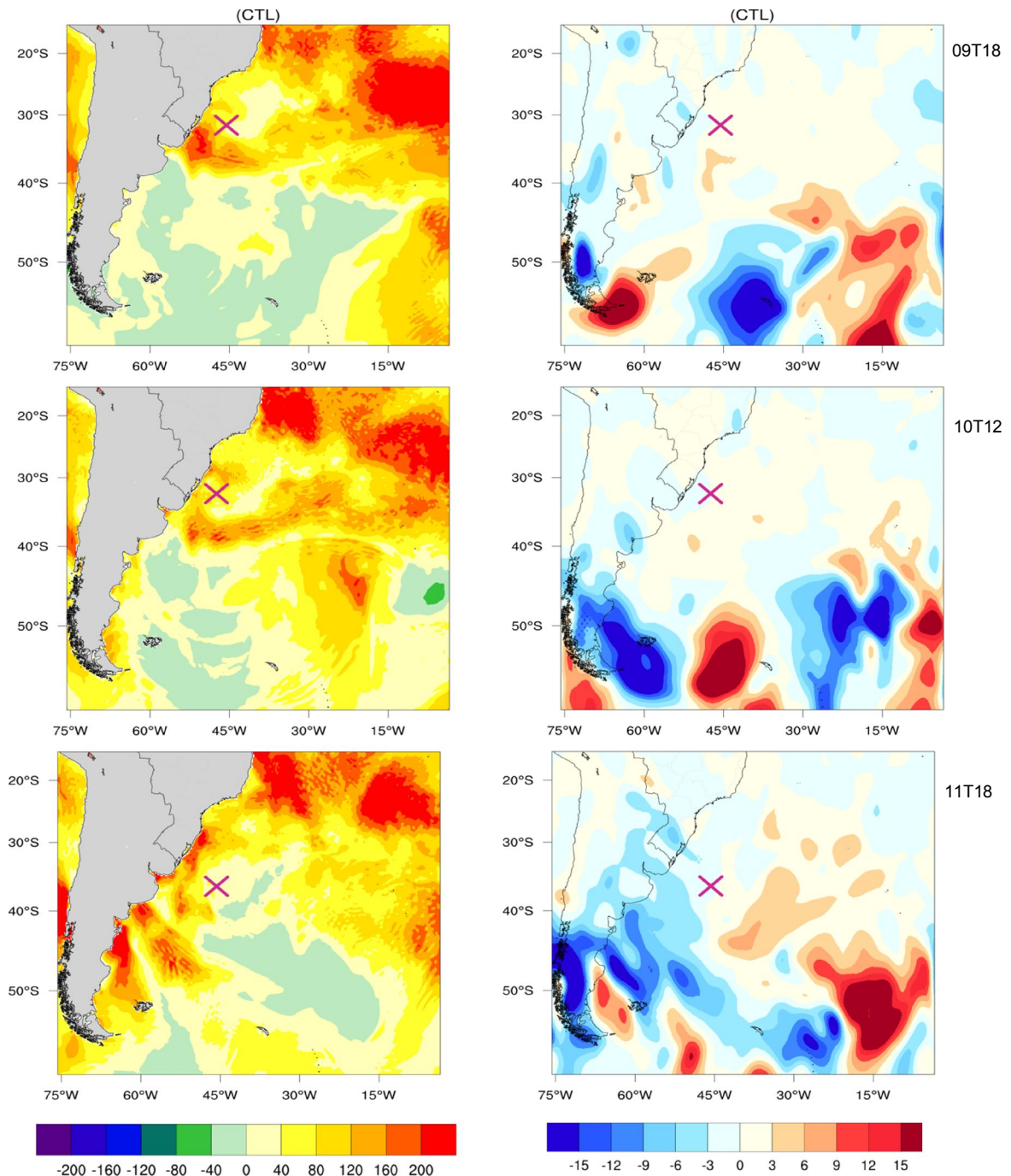
there is a low pressure system southeastward of it associated with a cyclone propagating from higher latitudes (Figure 5.13).

It is worth mentioning that several tests were made with different horizontal resolutions and parameterizations, in which the surface low/cutoff low did not develop or there was no interaction between ECY and Anita. Although the model underestimates the surface pressure centers of both Anita and ECY, the positions of the surface low and of the mid level troughs are in agreement with those observed for CFSR. Thus, despite the observed differences between the reanalysis and CTL fields, the main features of Anita and the interaction between Anita and ECY are evident.

The total surface heat flux (sensible heat + latent heat) for the 9-13th March period is shown in Figure 5.14. Total heat flux from the ocean to the atmosphere is observed in subtropical latitudes with values higher than 200 Wm^{-2} . Reboita (2008) showed that over the south/southeast coast of Brazil these fluxes are more intense in autumn and winter, with a peak around $200\text{-}240 \text{ Wm}^{-2}$. In the current analysis it is observed that in the vicinity of subtropical cyclone Anita the total heat fluxes are less intense. Dias Pinto et al. (2013) associated this feature with the organization of convective activity which enhanced the atmospheric humidity. At 18 UTC on 12 March an area of positive total heat fluxes appears over the southeast coast of South America. This area is related to the SASA which exhibits a ridge extending over the south of SA, at the rear a frontal system (Figure 5.15). Also of note is the large region of negative heat fluxes at mid latitudes. These negative fluxes intensify in the extratropical transition phase of Anita (between -80 and -40 Wm^{-2}).

Comparing the total surface heat flux derived from the CFSR reanalysis with the CTL, it is observed that the position and intensity of the positive heat fluxes are well reproduced by the model. Although the position of the negative fluxes is coincident with CFSR, the model tends to underestimate these fluxes. Specifically, the area of total heat flux associated with the transitioning cyclone is much more intense with values around -200 Wm^{-2} , i.e., twice that observed for the CTL.

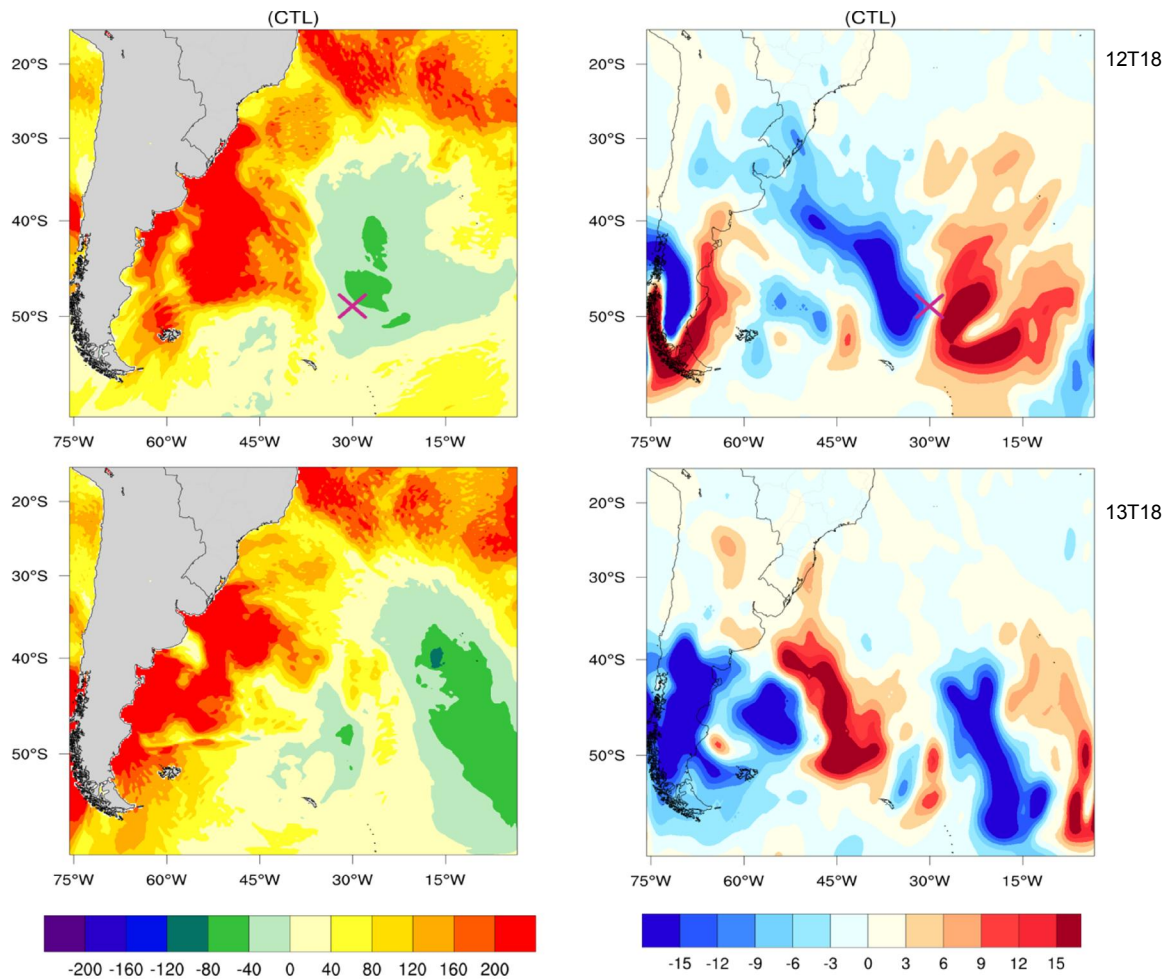
Figure 5.14- (left) Total surface heat fluxes (sensible heat + latent heat) and (right) temperature advection at 850 hPa for cyclone Anita from CTL for the 09-11 March 2010 period.



Fluxes are in Wm^{-2} . Temperature advection units are 10^{-5}Ks^{-1} . X represents the position of Anita at surface.

Source: Author's production.

Figure 5.15 - (left) Total surface heat fluxes (sensible heat + latent heat) and (right) temperature advection at 850 hPa for cyclone Anita from CTL for the 12-13 March 2010 period.



Fluxes are in Wm^{-2} . Temperature advection units are $10^{-5} Ks^{-1}$. X represents the position of Anita at 925 hPa.

Source: Author's production.

Temperature advection at 850 hPa for CTL is shown in Figure 5.14 and Figure 5.15. At 18 UTC on the 09th of March there were no areas of intense temperature advection at subtropical latitudes. However, a small area of cold advection is observed westward of Anita, over the south of Brazil. On the other hand, areas of temperature advection are observed at middle latitudes representing warm and cold fronts associated with transient cyclones. At 12 UTC on the 10th of March, an area of cold advection is observed over the continent around

40°S/55°W. This cold advection is associated with the low pressure center associated with ECY (Figure 5.12).

The intensification and eastward propagation of the transient system located over the Drake Passage helped to enhance the cold advection over southeast SA. On 11/March, when Anita was already interacting with the transient systems, the temperature advection over the SAO increased. In addition, a frontal zone is observed around 45°S/47°W, southward of Anita's center. It is worth mentioning that the re-intensification of Anita begins at this time. Also at this time, cold advection is observed over the south of Brazil. As the cyclones intensify, the cold and warm fronts also intensify over SAO. ET of Anita occurred over a frontal zone area at 18 UTC on 12 March. Colder temperature advection is observed in the south of Brazil, over Rio Grande do Sul and Santa Catarina states. Subsequently, Anita continues its southeastward propagation and the associated areas of warm and cold advection intensify (Figure 5.15). At this point, these systems are far away from the SA continent. Over the south of the continent, there is another frontal zone associated with a cyclone over the Drake Passage (Figure 5.13).

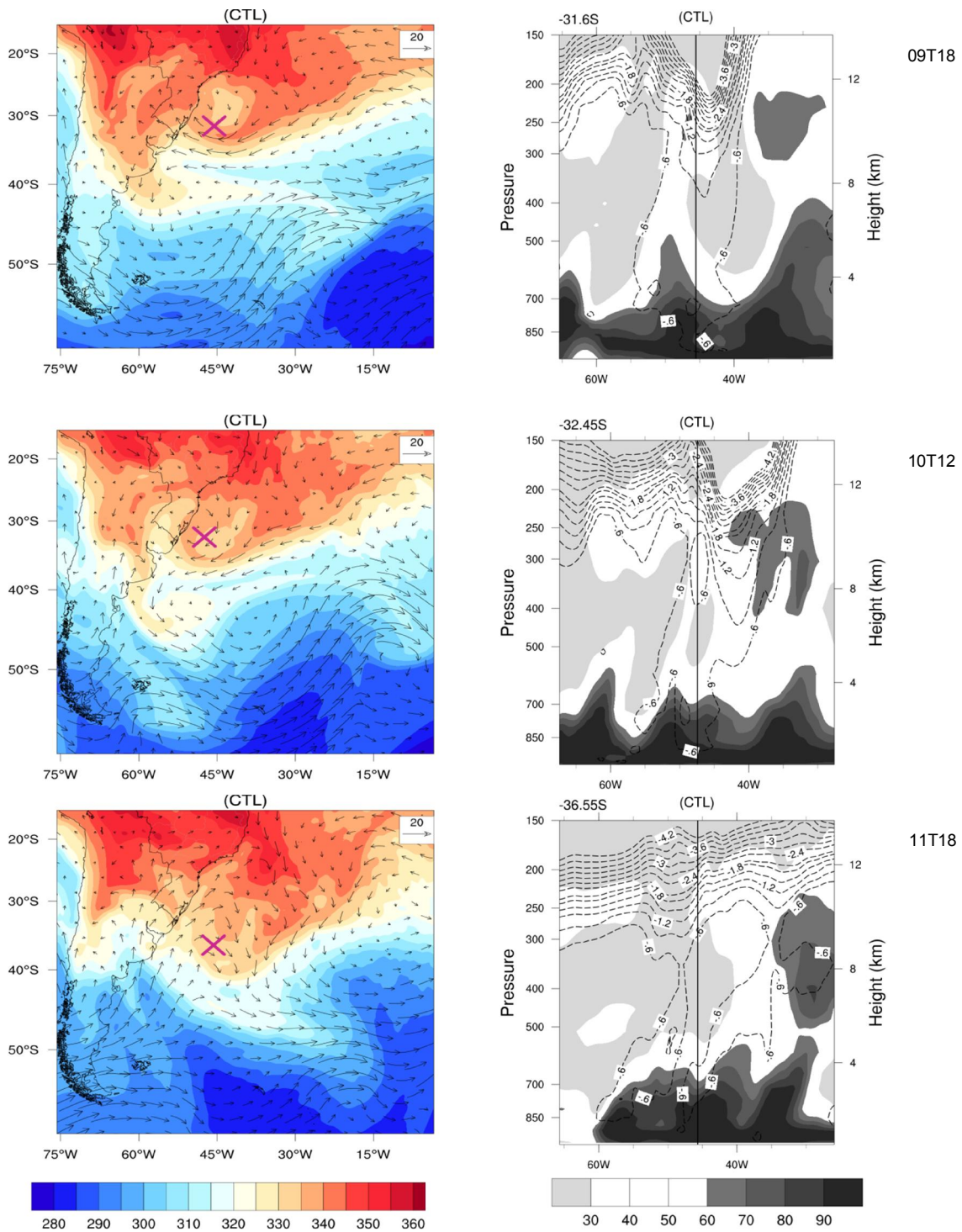
The equivalent potential temperature (ThetaE) and winds at 925 hPa show that the circulation associated with Anita and the SASA allowed the transport of colder air to the south of Brazil at day 09 (Figure 5.16). This pattern associated with the propagation of a mid latitude trough to the south of SA helped to enhance the baroclinicity around 43°S/60°W, which in turn allowed the ECY to intensify at 12 UTC on 10 March (Figure 5.16) . At this time, it is observed that over the south of the continent the winds intensified and became southerly, transporting colder and drier air to lower latitudes. Subsequently, as shown in Figure 5.12, the cyclonic circulation south of the continent propagates northeastward, causing the SASA to move eastward and allowing the southeastward propagation of Anita. This circulation advected colder air to subtropical latitudes and warmer air to higher latitudes, enhancing the baroclinicity over a large area of SAO, which helped the re-intensification of Anita. Also, the wind over the southeastern coast of SA intensified.

At 18 UTC on 12 March, the above mentioned circulation amplifies as the transient cyclone propagates northeastward. This causes an intensification of the temperature gradient over the SAO and a strengthening of the winds over this region. At this time, a cold front characterized by cold advection, convergence of winds and change in the wind direction, extends from the cyclone centered on 55°S/35°W to the coast of Rio Grande do Sul/Brazil. Also, the cold and drier air propagates northward over the continent to the south of Brazil. This area of intense temperature gradient moves away from the continent on 13 March.

The vertical cross sections of PV and relative humidity (RH) are determined at the 925 hPa position of Anita in the relative vorticity for each time step. The longitude axis was centered based on in the longitude of Anita's position. Figure 5.16 indicates the intrusion of stratospheric dry air from mid latitudes extending towards low levels at 09 of March. Dias Pinto et al. (2013) found that stratospheric intrusion of PV from latitudes higher than 45°S contributed to the development of the cut-off-low during the genesis of Anita. However, they highlighted that the incursion of PV from mid latitudes was associated with its intensification on the 06 UTC 9th of March. In the following hours, upper level PV maxima overcome the SC, but in the middle and lower troposphere PV is still over the cyclone center (Figure 5.16). The RH field presented higher values (above 90%) from surface up to 750 hPa, which is an indicative of cloudiness associated with the cyclone.

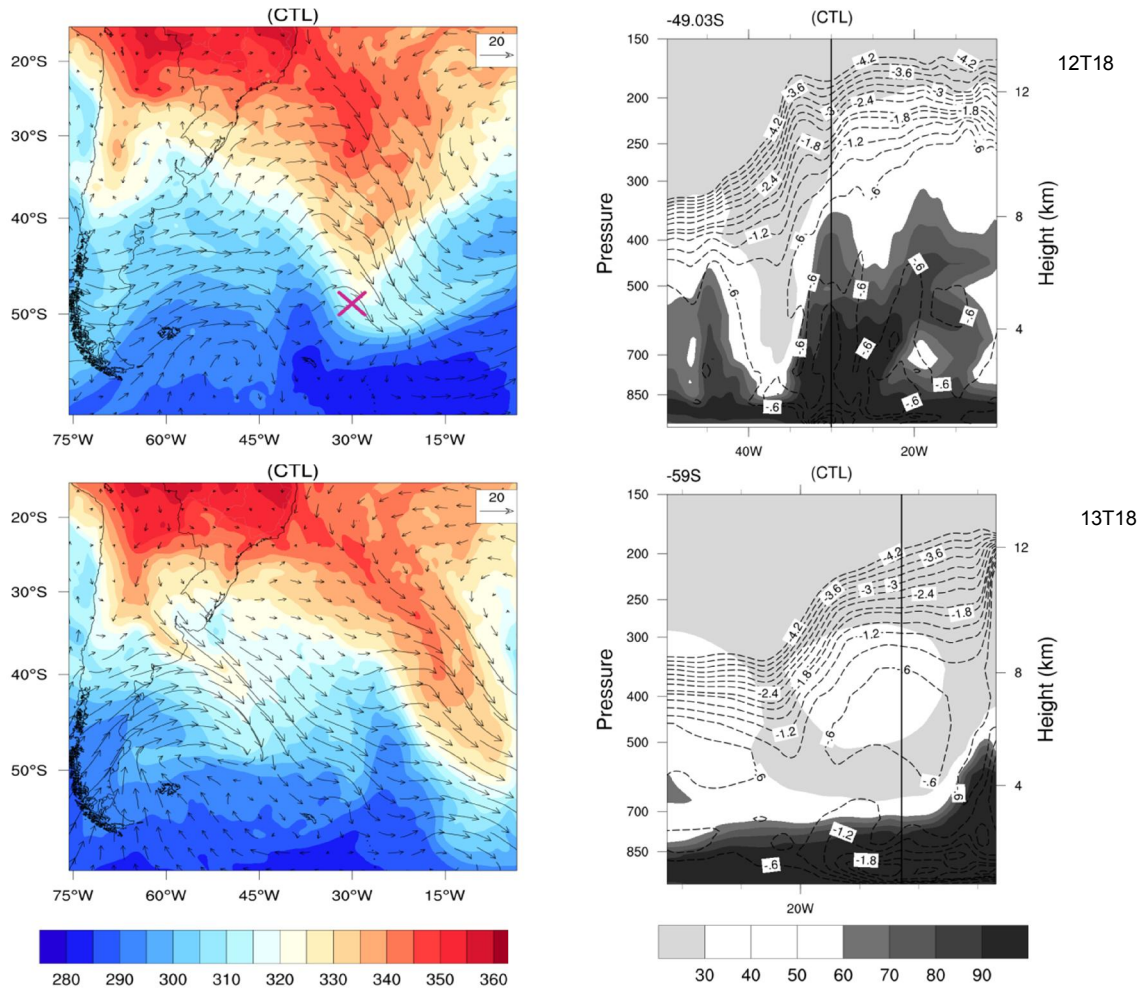
On 11th on March, there is another PV anomaly extending from the upper to lower troposphere approaching the rear of Anita. However, the upper tropospheric PV is weaker than the first observed PV anomaly. Until this day, RH presents a regular pattern with higher values at lower levels. The PV field is more perturbed on the 18 UTC 12 March, with incursion of PV from the surface up to mid levels at the center of the cyclone. Furthermore, RH extends to upper levels, with RH of 80% at 500 hPa. 24 hours later, PV is higher at the surface and there is no incursion of upper level PV anomalies in the center of the cyclone. Also, higher RH is restricted to the lower troposphere (Figure 5.17).

Figure 5.16- (left) ThetaE (K) and wind vectors at 925 hPa (right) vertical cross-section of PV (dashed lines, PVU) and relative humidity (shaded, %) for cyclone Anita from CTL for the 09-11 March 2010 period.



Source: Author's production.

Figure 5.17 - (left) ThetaE (K) and wind vectors at 925 hPa (right) vertical cross-section of PV (dashed lines, PVU) and relative humidity (shaded, %) for cyclone Anita from CTL for the 12-13 March 2010 period.



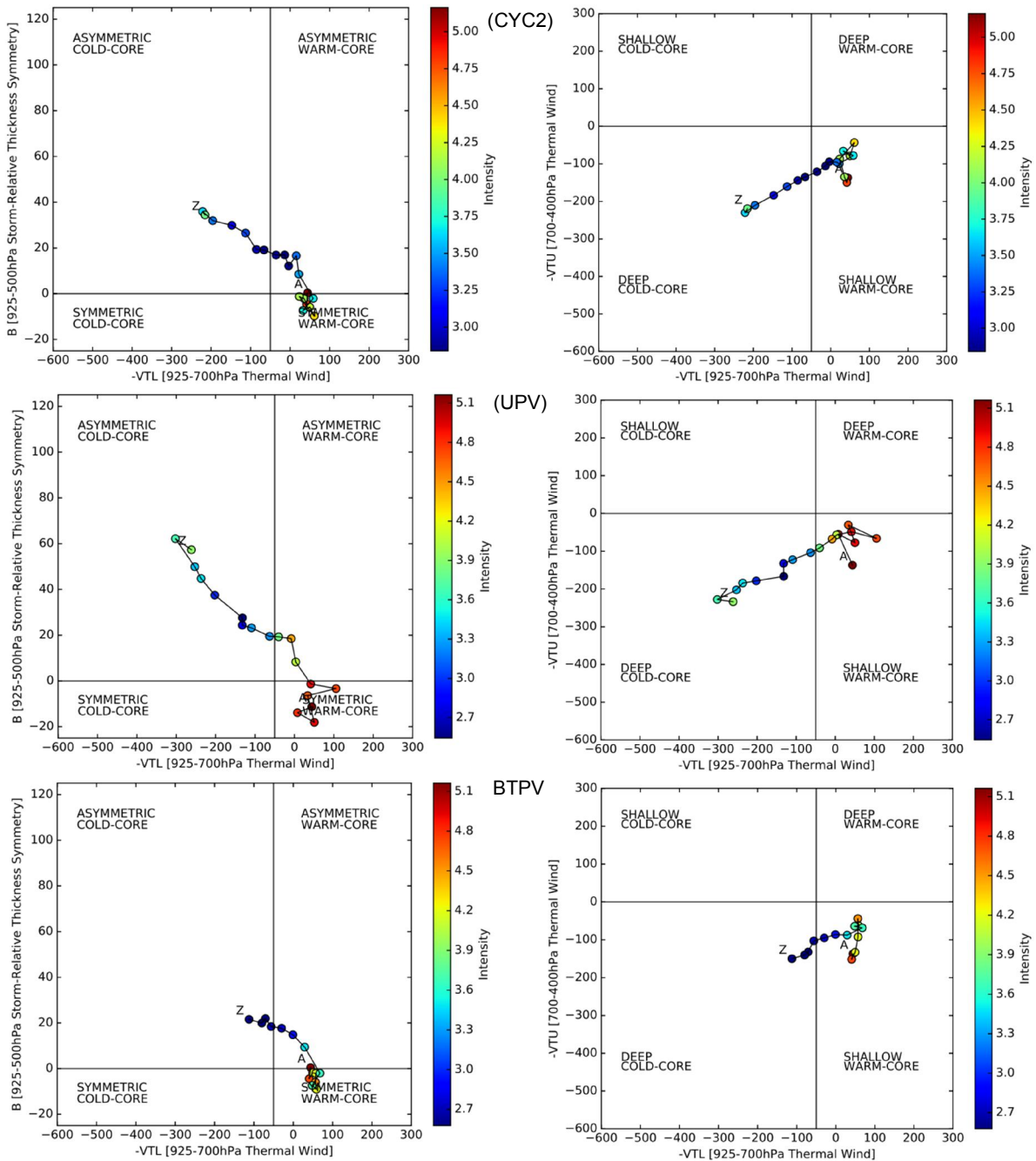
Source: Author's production.

5.3.2 Sensitivity tests

Sensitivity tests were performed to evaluate the impact of the PV anomalies on the ET of Anita. Three experiments are presented in the current study: (a) CYC2 - eliminates the PV anomalies associated with ECY, (b) UPV- eliminates the upper level PV anomalies and (c) BTPV - removes the low level PV anomalies. All experiments initialized at 00 UTC on 09 of March, i.e., during the mature subtropical phase of Anita. The balanced geopotential height, temperature and wind fields were calculated through PVI and were used to obtain the initial and boundaries conditions used in the above mentioned experiments as are described in section 3.3.

Figure 5.18 shows the evolution of the SC Anita structure for each sensitivity experiment. In all CPS diagrams the life cycle of Anita started on 09 of March at 06 UTC, during the mature subtropical stage of Anita, where it is characterized by a cold core at upper levels and warm core at lower levels. This hybrid structure remains longer in experiment CYC2, where the warm core at lower levels weakens, represented by values of $-VTL$ lower than -50 . In CYC2, this occurs at 12 UTC on 12th March, i.e., a day after what was observed for CTL. On the other hand, for UPV and BTPV this occurs at 06 UTC and 18 UTC on 11th of March, respectively.

Figure 5.18 – Phase space diagram for cyclone Anita from (top) CYC2, (middle) UPV and (bottom) BTPV. (left) B versus -VTL (right) -VTU versus -VTL.



Shaded circles are 925 hPa relative vorticity intensity. A indicates the beginning of Anita life cycle while Z indicates the end. Relative Vorticity units are 10^{-5} s^{-1} .

Source: Author's production.

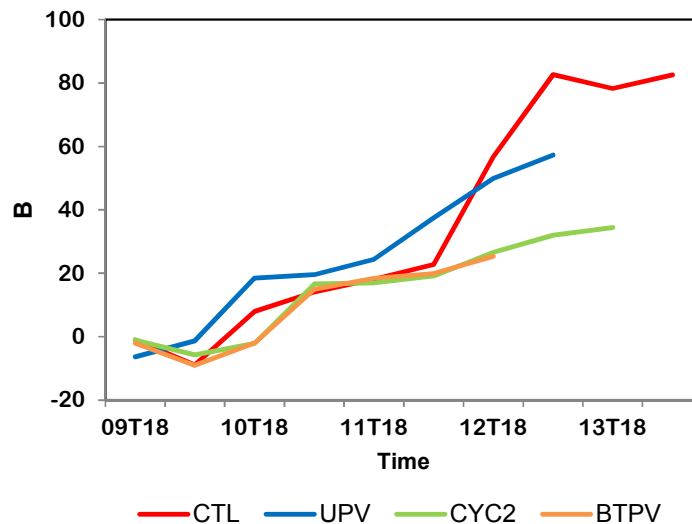
According to the adopted criteria, ET of Anita occurs in experiments CYC2 and UPV, but not in BTPV. Although, at the final day of its life cycle in BTPV, Anita presents a weak cold core structure, it does not present a frontal structure. The ET in UPV occurs at the same time as was observed in the CTL (00 UTC on 12th of March), and 18 hours later in the CYC2. The magnitude of $-VTL$, $-VTU$ and B are not very different in the experiments until the moment of ET. The low level cold core and the thermal symmetry are stronger in the absence of the upper level PV anomalies. The re-intensification of Anita is only observed in experiment UPV. However, it does not attain the magnitude as high as observed in CTL. Figure 5.19 is shown to better elucidate the evolution of the thermal symmetry of Anita in each experiment. All the experiments show a decrease in the thermal symmetry in the early hours, except the UPV experiment which shows an increase of that parameter during the entire life cycle of Anita (Figure 5.19). However, after these early hours the evolution of the thermal symmetry in UPV is similar to the CTL, with UPV presenting higher values of B until immediately after the ET. This could be due to Anita being located in a region of greater temperature gradient in UPV, compared with CTL, at the subtropical stage (Figure 5.15, Figure 5.25). On the other hand, the evolution of B for the CYC2 and BTPV experiments are more similar to CTL until 00 UTC on the 12th of March, which is the time of ET in CTL.

In all experiments, Anita presents a cold core structure at least 12 hours before it becomes asymmetric. This feature, where a storm does not penetrate into the asymmetric warm core, becoming cold core faster than it becomes asymmetric, was found as being the most frequent type of ET of tropical cyclones in NH (STUDHOLME et al., 2015). Although ET was observed in both CYC2 and UPV experiments, only in UPV the values of B are representative of a classic baroclinic cyclone as was noted in CTL. A reference value of B to indicate a classic baroclinic cyclone is around 50 m (VEREN et al., 2009).

The trajectories of Anita in the experiments compared with CTL are displaced southward, mainly in the final stages of its life cycle, after the ET (Figure 5.20),

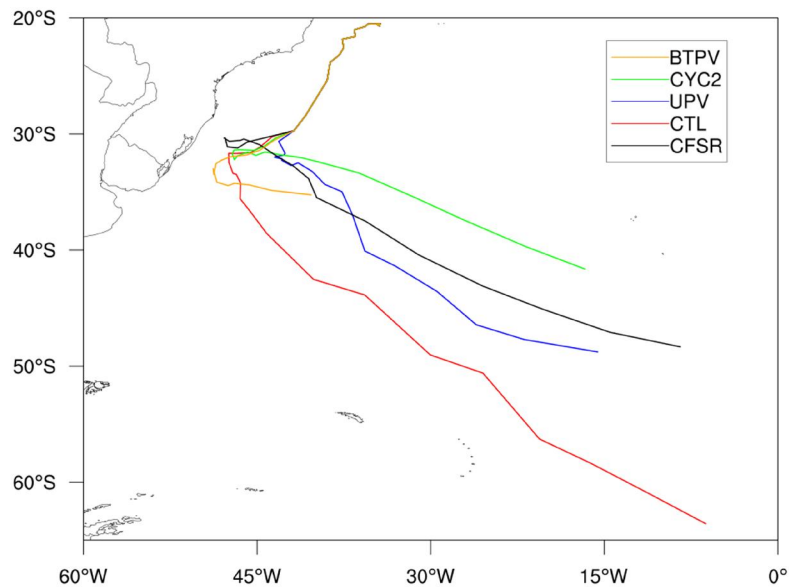
except for the CYC2 experiment. The removal of the ECY (CYC2) displaces Anita northward and decreases its propagation, but did not change its lifetime. Indeed, in this experiment Anita presents the most northward trajectory in comparison with the other ones. The trajectory of Anita in the UPV experiment, is similar to the one observed from CTL. However, in UPV the westward propagation of Anita towards the southern Brazil, during its subtropical phase, is not observed. The absence of the lower tropospheric PV decreases Anita's lifetime and its southeastward propagation. Thus, Anita does not travel far away from the south Brazilian coast during its entire life cycle. The faster (slower) southeastward propagation of Anita in UPV (BTPV) is associated with the absence (stronger) dipole-blocking pattern in the upper troposphere (Figure 5.21).

Figure 5.19 – Time evolution of thermal symmetry (B) of cyclone Anita from CFSR (black), CTL (red), CYC2 (green), UPV (blue) and BTPV (orange).



Source: Author's production.

Figure 5.20 – Trajectory of Anita cyclonic core from CFSR (black), CTL (red), CYC2 (green), UPV (blue) and BTPV (orange).



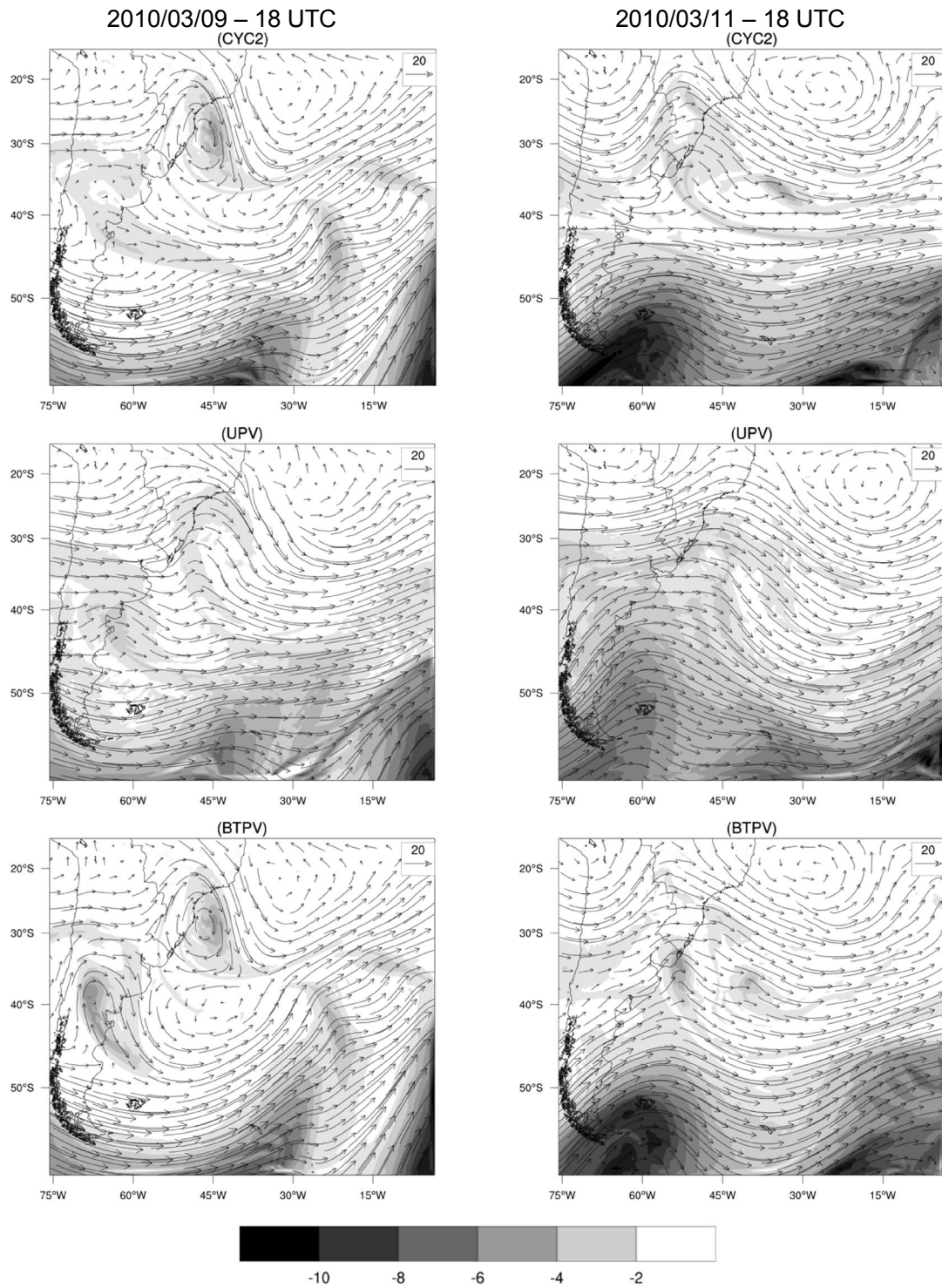
Source: Author's production.

The sensitivity test in the experiment CYC2 shows that the cyclonic vortex over east-central Argentina does not develop. However, a small trough is observed over that region, associated with weaker PV (Figure 5.21). The position of the Anita cyclonic vortex remains centered over the southeastern coast of Brazil on the 18 UTC on 09 March. The dipole blocking pattern lasts until 06 UTC on 10/03 (not shown) and dissipates only a few hours earlier than what was observed in the CTL. Thus, it is inferred that the removal of the ECY cyclonic vortex does not cause great impact on the dipole pattern, differently from what was indicated by Dutra et al. (2017). At 12 UTC on 10th of March, the upper level vortex is positioned around 33°S/47°W and after that propagates eastward and dissipates in both simulations (CYC2/CTL) (not shown). The transient systems observed in that region have the same position and strength as observed in the CTL, which is expected since in this experiment the PV anomaly was locally removed, i.e., the PV anomalies were subtracted only in the area of ECY center. It should also be noted that from 11th of March when

both cyclonic vortices have dissipated in the CTL, the upper level flow pattern is very similar in the CTL and CYC2 fields (Figure 5.12, Figure 5.22).

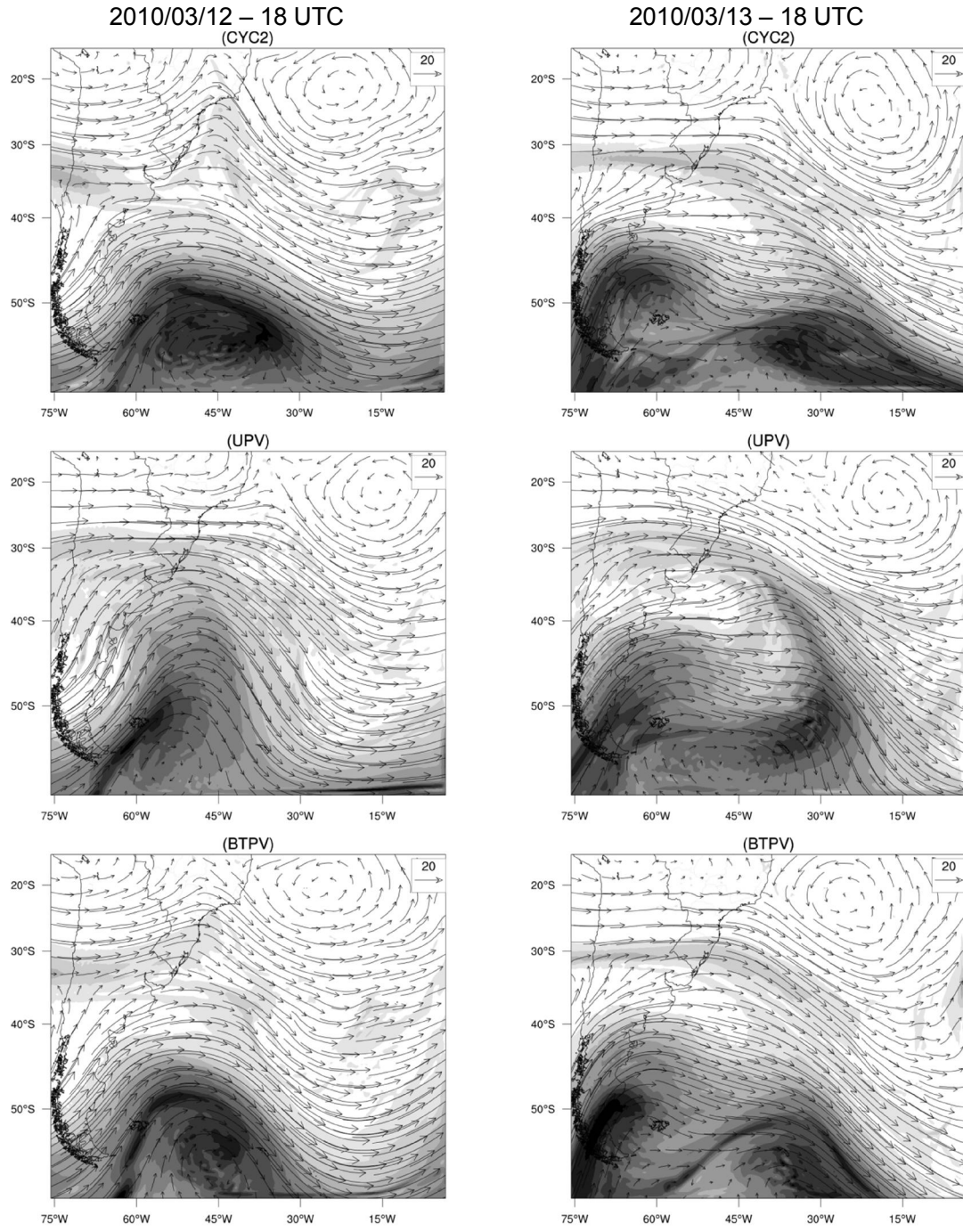
When removing PV anomalies at upper levels, the 250 hPa circulation related with cyclone Anita and ECY is weak and instead of a closed cyclonic circulation two troughs are observed positioned around $30^{\circ}\text{S}/45^{\circ}\text{W}$ (Anita) and $42^{\circ}\text{S}/60^{\circ}\text{W}$ on 9th March, respectively (Figure 5.21). The dipole-blocking pattern is not present in this experiment. This occurs because the mid latitude flow is more zonal and due to the weaker intensity of the circulation associated with Anita. Although PV in the mid latitudes is less intense than in the CTL, from 11th March onwards the upper level circulation in UPV is similar to the CTL, except regarding the trough extending up to the center of Brazil that is not observed in UPV (Figure 5.22). The removal of the low level PV anomalies intensifies the blocking pattern on 09th March (Figure 5.21), keeping the vortices closer to the continent for a longer time. On day 11, the PV anomalies associated with the ECY and Anita are observed at $35^{\circ}\text{S}/50^{\circ}\text{W}$ and $36^{\circ}\text{S}/40^{\circ}\text{W}$, respectively, i.e., while ECY vortex propagates eastward in the CTL experiment, in BTPV its propagation is northeastward.

Figure 5.21 - Wind vectors and PV at 250 hPa (shaded) for cyclone Anita from (top) CYC2, (middle) UPV and (bottom) BTPV for days 09 and 11 March 2010 at 18 UTC. PV units are PVU.



Source: Author's production.

Figure 5.22 - Wind vectors and PV at 250 hPa (shaded) for cyclone Anita from (top) CYC2, (middle) UPV and (bottom) BTPV for days 12 and 13 March 2010 at 18 UTC. PV units are PVU.

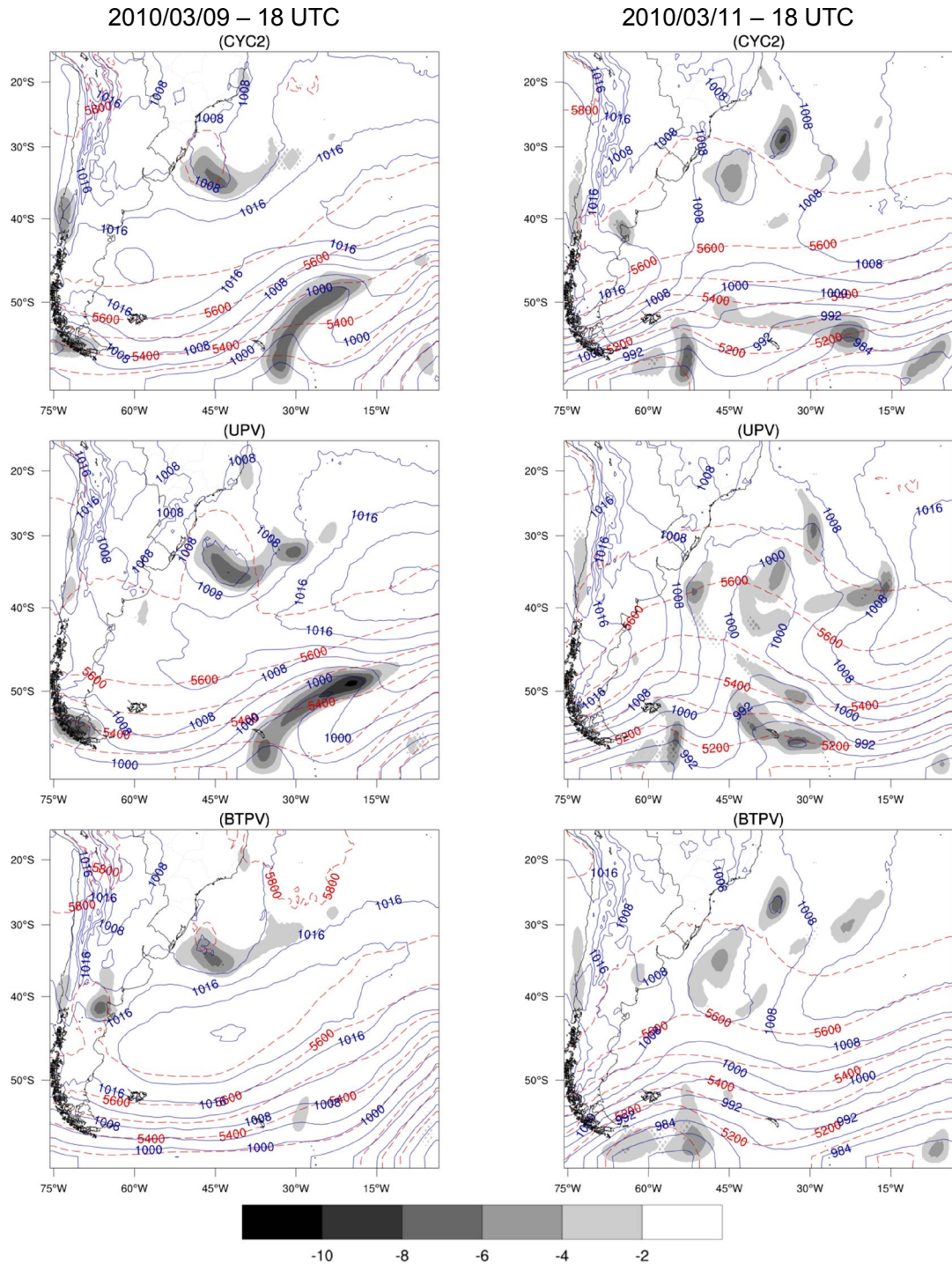


Source: Author's production.

Without the ECY PV anomaly, Anita's surface low has a 1008hPa pressure center on the 09th March, a trough at 500 hPa and a low level cyclonic vorticity core over Argentina, with ECY not developing (Figure 5.23). This pattern allowed the surface anticyclone to extend towards the continent until day 11th March. The barotropic structure of Anita is similar to that found with CTL. At 18 UTC on 11 March, Anita is not fully interacting with the transient system and its closed surface center remains longer in CTL. Furthermore, the cyclonic vorticity core south of Anita in the CTL does not develop in CYC2. On the other hand, another cyclone from subtropical latitudes is observed approaching Anita. A few hours later both cyclones intensify their interaction (Figure 5.24). This pattern prevents the southeastward propagation of Anita, keeping it in subtropical latitudes until it dissipates.

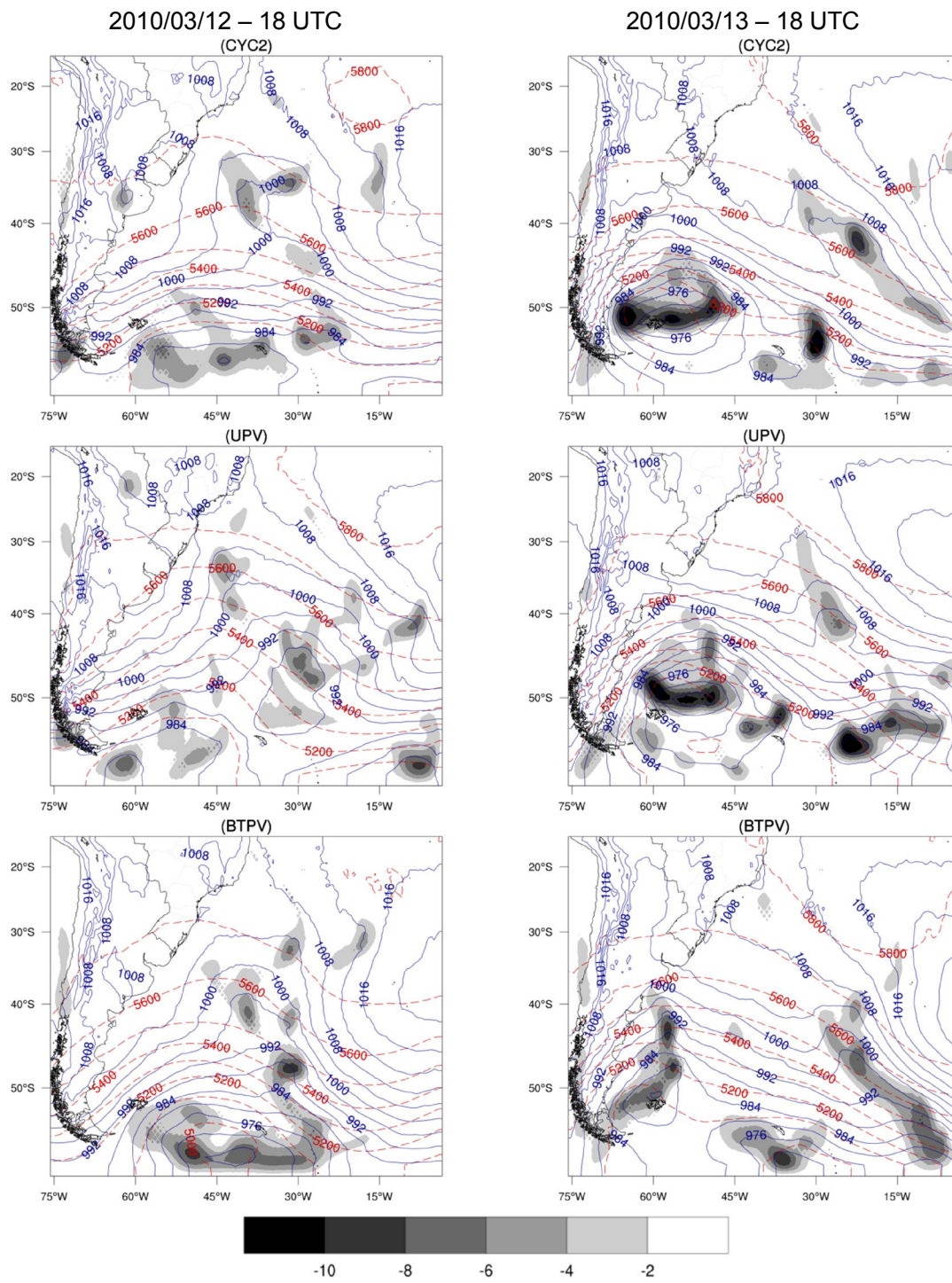
In UPV, the cut-off-low observed in geopotential height at 500 hPa for the CTL on 18 UTC on 09th March is not observed (Figure 5.23). However, the surface low is more intense with central pressure of 1004 hPa. The SASA center is also more intense in UPV than in CTL. On the 12th of March, it is observed that the trough associated with ECY was much weaker but the intensity of the surface low and cyclonic vorticity were similar to CTL. Cyclone Anita propagates southeastward faster moving away from the continent sooner than was observed for the control simulation, as was shown in Figure 5.20. This can be explained by the absence of the north-south dipole-blocking pattern at upper levels. This propagation is accompanied by the subtropical cyclone east of Anita, which presents a more intense vorticity core, and helped to deform SASA.

Figure 5.23 - 925 hPa Relative vorticity (shaded), SLP (blue contour each 4hPa) and 500 hPa geopotential height (red dashed contour each 100 gpm) for cyclone Anita from (top) CYC2, (middle) UPV and (bottom) BTPV for days 09 and 11 March 2010 at 18 UTC. Relative Vorticity units are 10^{-5} s^{-1} .



Source: Author's production.

Figure 5.24 - 925 hPa Relative vorticity (shaded), SLP (blue contour each 4hPa) and 500 hPa geopotential height (red dashed contour each 100 gpm) for cyclone Anita from (top) CYC2, (middle) UPV and (bottom) BTPV for days 12 and 13 March 2010 at 18 UTC. Relative Vorticity units are 10^{-5} s^{-1} .



Source: Author's production.

The transient cyclone in mid latitudes is displaced northward. The interaction of this system with the ECY and Anita causes its eastward propagation to be slower, displacing the SASA eastward (Figure 5.24). The extratropical surface low develops earlier but it is weaker with central pressure of 988 hPa at 18 UTC on 12 March (Figure 5.24). At this time, the cyclonic vorticity core of Anita is located over this surface low around 42°S/28°W. This feature suggests that Anita is embedded by this system. Also of note is that instead of dissipating after the interaction with Anita, ECY seems to intensify and propagates toward subtropical latitudes.

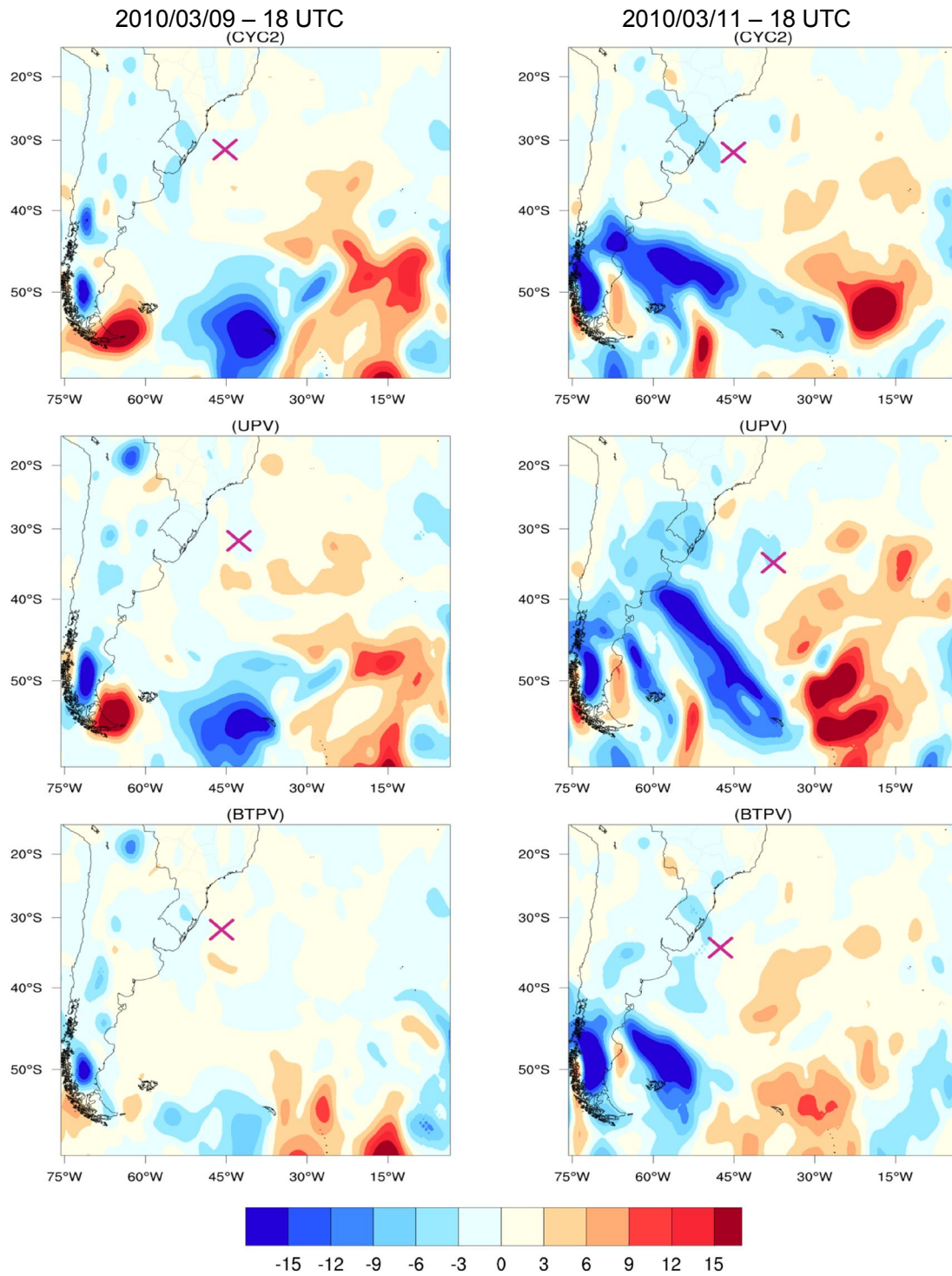
In the absence of lower PV anomalies at extratropical latitudes (BTPV), the transient systems are not observed until 18 UTC on 11th of March. Although the vorticity core and the trough associated with ECY were well reproduced, the surface does not evolve into a closed low pressure (Figure 5.23). Because the subtropical anticyclone extends westward, both ECY and Anita remain closer to the continent until their dissipation at 18 UTC on 12th of March (Figure 5.24). The low pressure center associated with the extratropical cyclone which developed around 55°S/35°W due the interaction between Anita and the transient cyclone at 00 UTC on 13th March (not shown), does not show up in the current test. In experiment BTPV, Anita presents the weakest low pressure center in comparison with UPV and CYC2. In this experiment, the transient systems are also weaker.

Until 11th March, the temperature advection field from CYC2 resembles very well the CTL one, except for the region of cold advection associated with ECY over the northeast of Argentina which is not observed in CYC2 (Figure 5.25). Although the areas of cold/warm advection are in agreement in both experiments, at 18 UTC on 11th March, these areas of temperature advection are weaker and Anita is positioned in a region of cold advection in CYC2. As opposed to that observed in CTL, in which Anita was positioned between the cold and warm advection after the ET, in CYC2 it remains closer to the cold advection until it dissipates (Figure 5.26).

Similarly to what was observed for CYC2, in experiment UPV the temperature advection field is very similar to the CTL until the 11th of March (Figure 5.25). The largest differences are the warm advection areas in the vicinity of Anita in UPV. The main area of cold advection is more intense and displaced northward in UPV, extending from the South Georgia Island up to the southeast of Argentina. Also the surface center of Anita is positioned over colder advection. This major area of cold advection continues propagating northeastward, enhancing the cold advection over the southeast of Brazil. This pattern remains for almost a day weakening the warm advection over the southern Brazil, observed in CTL. ET takes place at 00 UTC on 12th of March in a small baroclinic area, between cold advection (rear) and warm advection (forward) (not shown). Despite what occurred in CTL, in the current experiment Anita is not positioned at the center of the greater areas of advection, instead it is in the adjacencies of them (Figure 5.26).

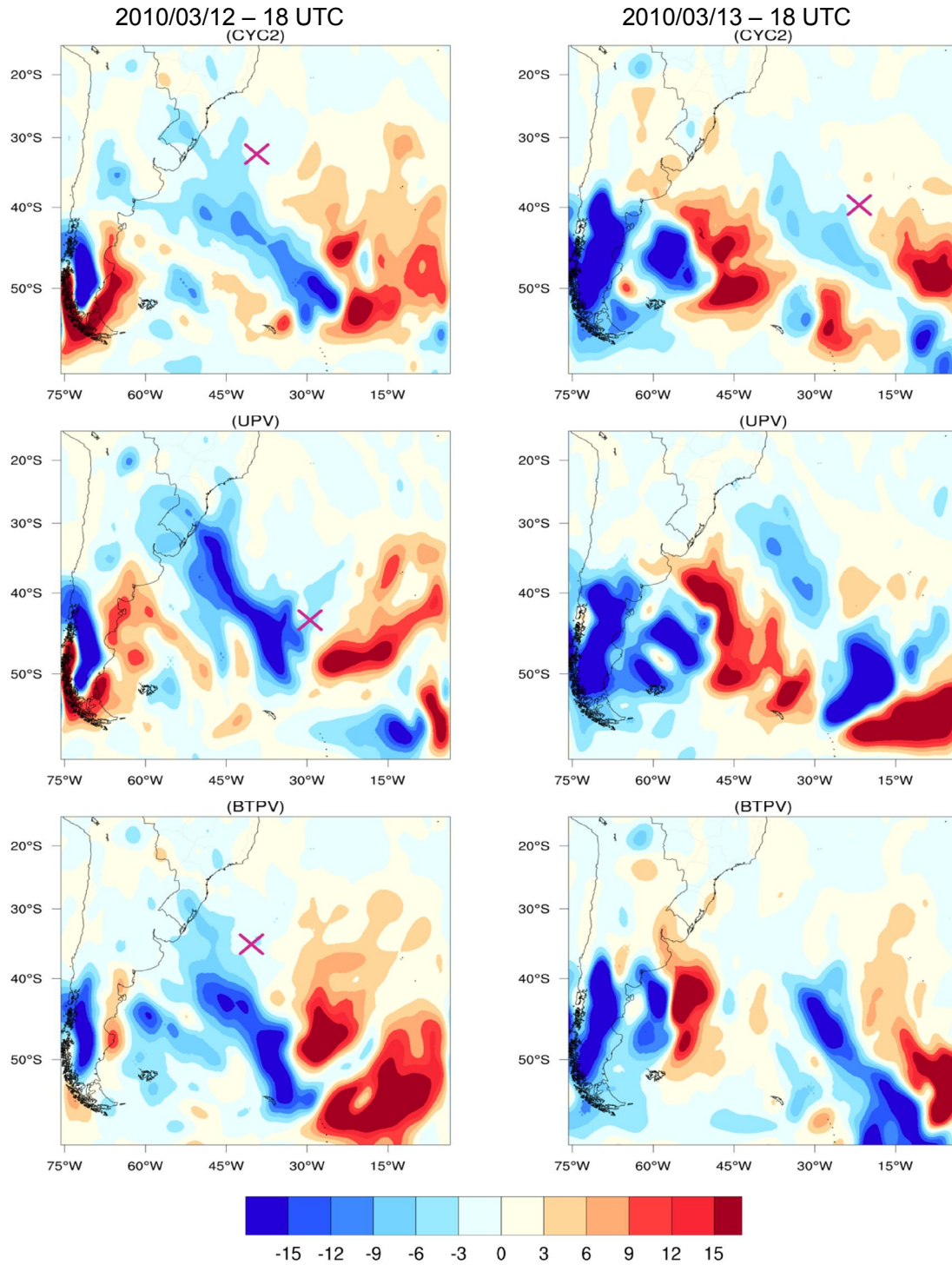
Since the transient systems are not observed in the absence of low level PV anomalies, the temperature advection field in middle latitudes is also much weaker in the BTPV experiment, mainly until 11th of March (Figure 5.25). With the propagation of a transient system over the Drake Passage (Figure 5.23), the increase in the cold advection over the south of the continent and over the SAO is observed in BTPV. At 18 UTC on the 11th March, it is positioned between the cold advection and warm advection areas centered near 37°S. Although the CTL and BTPV fields seem very similar, cyclone Anita do not propagate southward of 35°S in BTPV, as the more baroclinic areas are away from the surface cyclone. Thus, on 12th of March Anita is weaker and surrounded by cold advection (Figure 5.26). Also of note is that the extratropical cyclone over the Drake Passage and its fronts are weaker in comparison with CTL. This maintains the semi stationary pattern of Anita.

Figure 5.25 - Temperature advection at 850 hPa for cyclone Anita from (top) CYC2, (middle) UPV and (bottom) BTPV for days 9 and 11 March 2010 at 18 UTC. Temperature advection units are 10^{-5} K s^{-1} .



Source: Author's production.

Figure 5.26 - Temperature advection at 850 hPa for cyclone Anita from (top) CYC2, (middle) UPV and (bottom) BTPV for days 12 and 13 March 2010 at 18 UTC. Temperature advection units are 10^{-5} K s^{-1} .

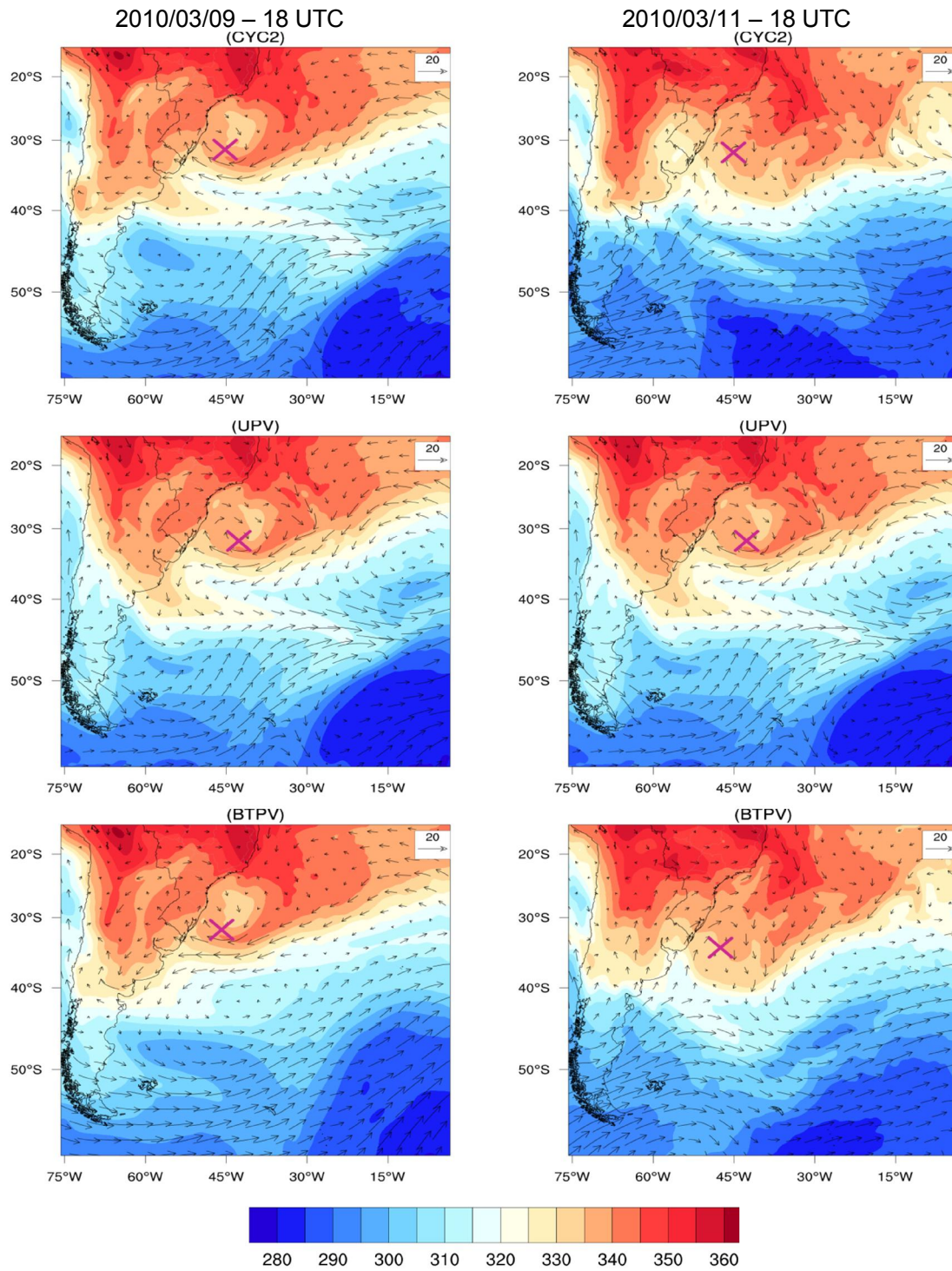


Source: Author's production.

Without ECY, the SASA extended westward, over the continent, enhancing the equivalent potential temperature (θ_E) over central Argentina in comparison with CTL (Figure 5.27). Furthermore, this circulation weakened the θ_E over the northeast coast of Argentina, reducing the temperature gradient and the magnitude of the winds in that region. At 10th March, in the absence of ECY, the wind changes direction preventing the cold air to propagate northward (not shown). Near the center of Anita, the circulation remains similar to CTL, helping the transport of colder and dry air towards Uruguay and Southern Brazil. From 11th March onwards, the propagation of the extratropical cyclone enhances the temperature gradient over the SAO. However, this temperature gradient is weaker in CYC2 at the moment of the transition (Figure 5.28).

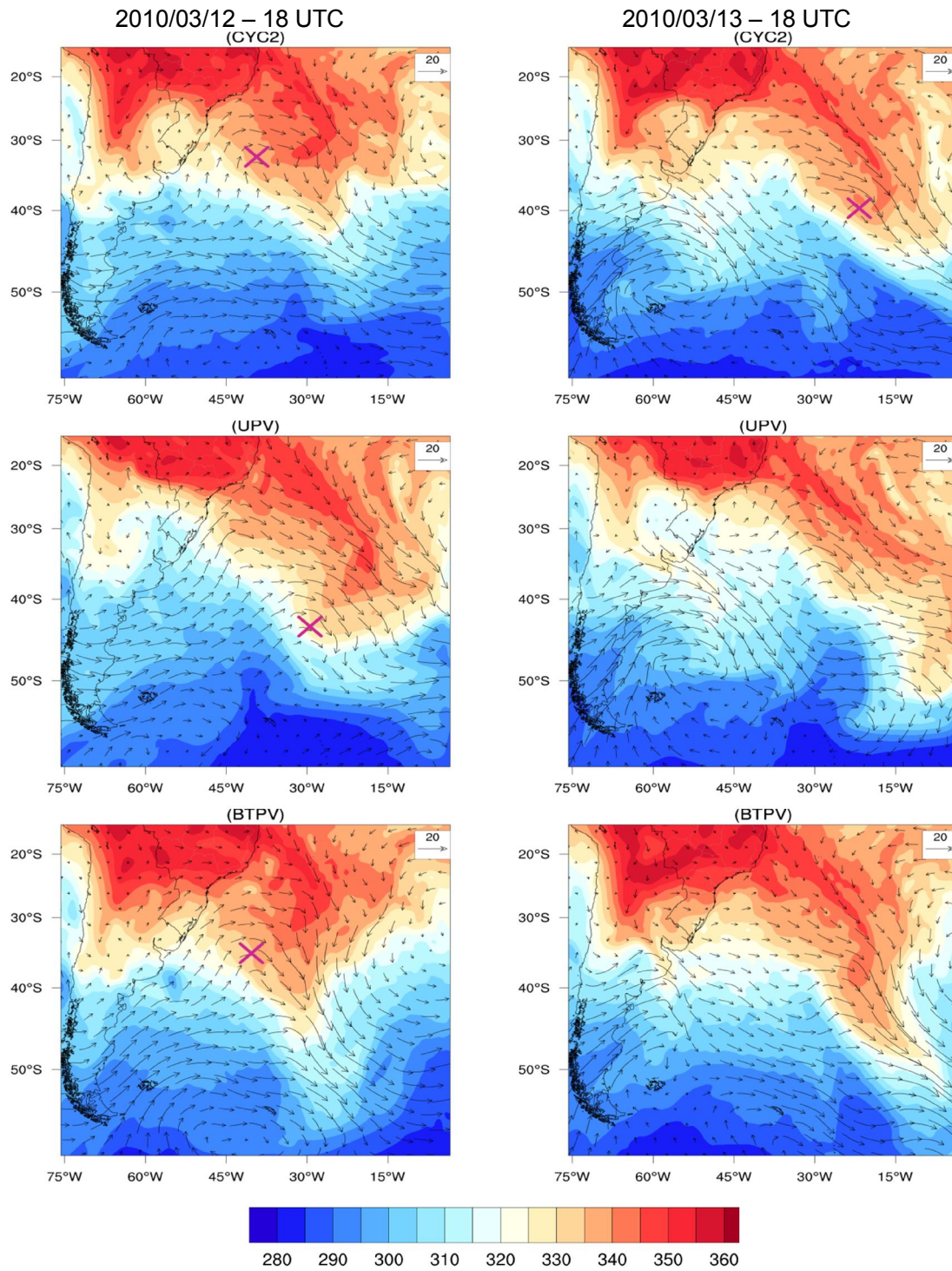
As observed for the fields analyzed previously, in experiment UPV the θ_E and wind fields present the same configuration as the CTL until day 11th of March (Figure 5.27). After that, the slow propagation of the transient cyclone and its interaction with cyclone Anita enhances the temperature gradient over the SAO. The stronger southwesterly winds over the continent advected cold and dry air over Uruguay and southern/southeastern Brazil. The main differences between the fields of CTL and BTPV, are that the mid latitude flow is more zonal during the first two days of the experiment (Figure 5.27). This is expected due to the removal of the lower PV anomalies. At this period, over subtropical latitudes, the circulation presents a pattern very consistent with CTL. As the transient cyclones propagate eastward, the flow becomes more perturbed. However, the circulation allows an area of temperature gradient to be weaker than the one observed for CTL (Figure 5.28).

Figure 5.27– Equivalent potential temperature and wind vector at 925 hPa for cyclone Anita from (top) CYC2, (middle) UPV and (bottom) BTPV for days 9 and 11 March 2010 at 18 UTC. ThetaE units are K.



Source: Author's production.

Figure 5.28– Equivalent potential temperature and wind vector at 925 hPa for cyclone Anita from (top) CYC2, (middle) UPV and (bottom) BTPV for days 12 and 13 March 2010 at 18 UTC. ThetaE units are K.

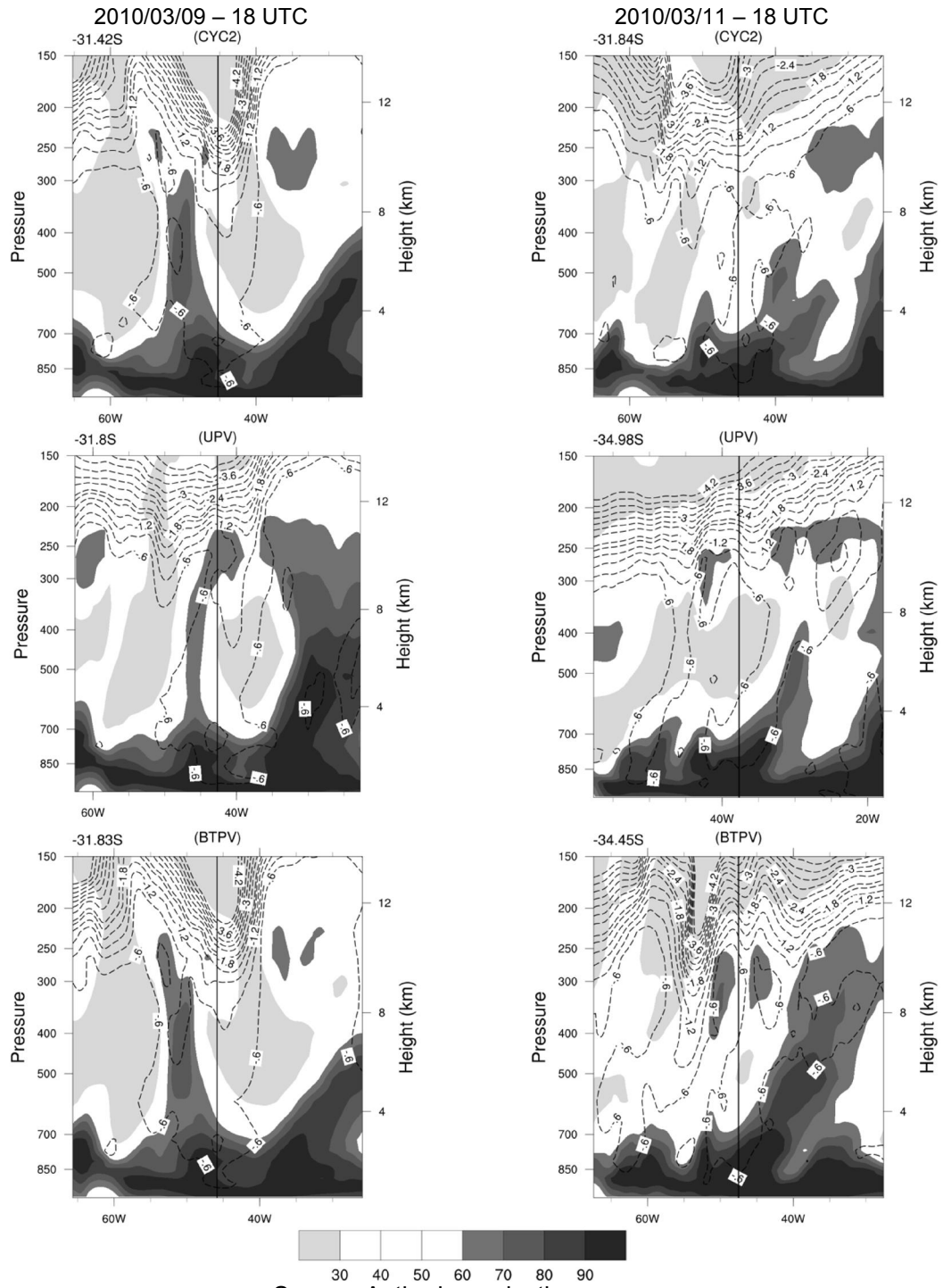


Source: Author's production.

The vertical cross section of PV and RH show a stratospheric PV intrusion extending to low levels at 18 UTC on 9th March in CYC2 (Figure 5.29). At this time, the 90% RH is observed from surface to 750 hPa. Two days later, the upper tropospheric PV over the Anita weakens, but unlike CTL it still extends to the entire atmospheric column. Higher humidity remains at low levels, but it is observed a region of 60% RH from surface up to 400 hPa in front of the cyclone center. The PV near the surface seen in CTL at 18 UTC on 12th of March is not observed in CYC2, instead there is a PV maximum from upper to low levels in this experiment. Also the RH in CYC2 does not extend to mid levels as occurred in the CTL (Figure 5.30). This is justified by the environmental differences in which Anita is embedded. As showed previously, at this time in CTL Anita was located in an area of frontal zone and instable conditions. Furthermore, this period is characterized by ET occurrence in CYC2, while in CTL the ET occurs hours before. At the final hours of its life cycle, a PV anomaly extends towards the surface at Anita's center. However, this anomaly is weaker than the one observed in CTL (Figure 5.30).

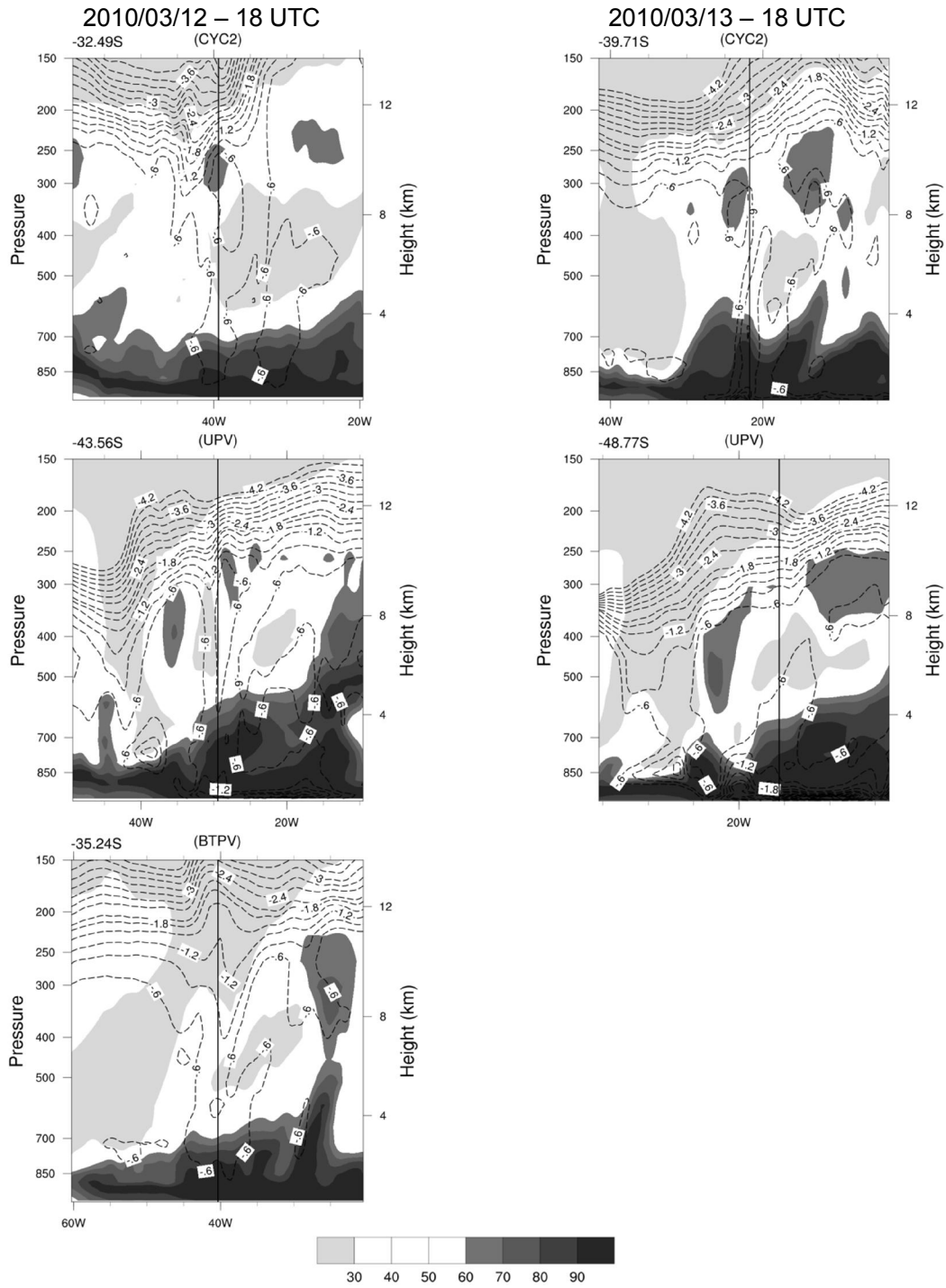
At 18 UTC on 09th March in UPV, the PV anomaly from upper to levels is weaker than in CTL and is associated with an area of 60% (90%) RH from mid to upper troposphere (at low levels) (Figure 5.29). The vertical cross-section of PV and RH on days 11 and 12 of March are similar to the ones in CTL, with PV extending to surface and higher humidity amount in levels above 700 hPa. However, the area with RH stretching above mid troposphere is displaced eastward in UPV. Similarly to CTL and CYC2, the final hours of Anita at this experiment is marked by an intensification of the lower PV anomalies and an increase in the humidity (Figure 5.30). The vertical structure of Anita in the first hours of experiment BTPV is very similar the one of CYC2 (Figure 5.29). At day 11th, the upper PV anomalies on BTPV are the strongest between all experiments. At the end of its life cycle, weaker upper levels PV anomalies are observed at the vertical cross-section of Anita. Actually, the BTPV is the only experiment in which Anita does not present surface PV anomalies in any moment of its life cycle.

Figure 5.29 - Vertical cross-section of PV (dashed lines) and relative humidity (shaded) for cyclone Anita hPa for cyclone Anita from (top) CYC2, (middle) UPV and (bottom) BTPV for days 9 and 11 March 2010 at 18 UTC. RH units are % and PV units are PVU.



Source: Author's production.

Figure 5.30-Vertical cross-section of PV (dashed lines) and relative humidity (shaded) for cyclone Anita hPa for cyclone Anita from (top) CYC2, (middle) UPV and (bottom) BTPV for days 12 and 13 March 2010 at 18 UTC. RH units are % and PV units are PVU.

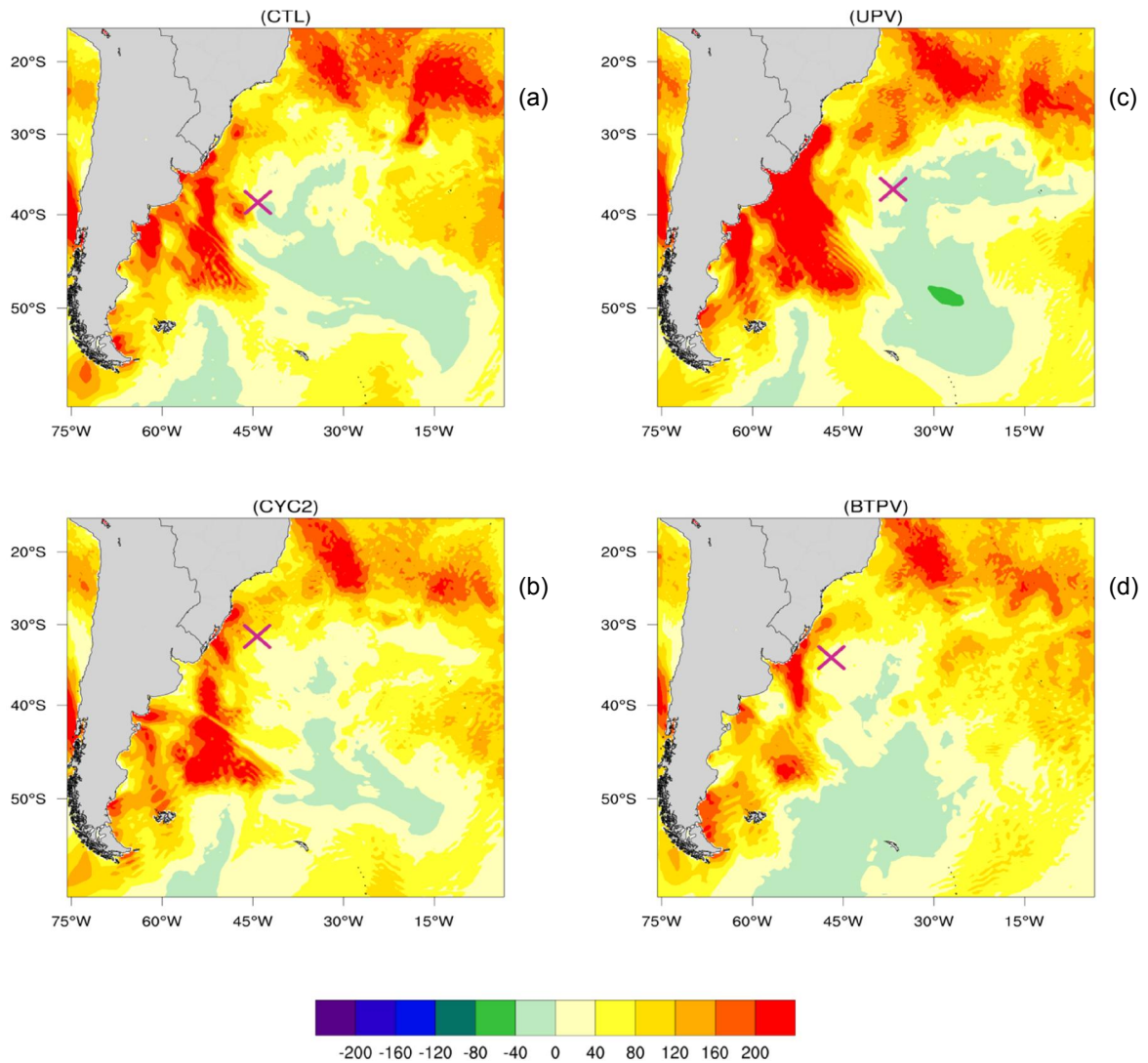


Source: Author's production.

The total surface heat fluxes do not present remarkable differences between the experiments. In fact, the fields obtained from CYC2 and BTPV are quite similar to those from CTL. Thus, only the fields for the 00 UTC on 12th of March are shown (Figure 5.31). This is the time of ET found in CTL and UPV experiments. During the subtropical phase, Anita positioned over weak total surface heat fluxes in all experiments (not shown). These fluxes remained weaker in the BTPV in relation to the other experiments. As the cold advection advances towards the southern coast of Brazil, the positive heat fluxes increase. This occurs earlier in UPV experiment, not only due to the position of the cold advection but also because it is stronger, as shown previously. Indeed, at the transition time the heat fluxes are higher in UPV (Figure 5.31). However, Anita is positioned over a region of total heat fluxes around 40 Wm^{-2} .

The ET of Anita in CYC2 occurred hours later (at 18 UTC) with increase of the total heat fluxes, due the approach of the cold advection (not shown). The pattern resembles that observed for UPV, but with the cyclone centered over total surface heat fluxes of 80 Wm^{-2} . The large area of negative total heat fluxes seen over the SAO in all experiments are associated with the warm advection, which enhance the humidity and decrease the total fluxes. The upper and lower tropospheric PV anomalies have different impact in the total surface heat fluxes. Although the patterns of total fluxes are similar, in the absence of the upper tropospheric anomalies it is strengthened while with the removal of the lower level anomalies it is weakened. This feature is more pronounced during the mature stage of Anita.

Figure 5.31 - Total surface heat fluxes (sensible heat + latent heat) for cyclone Anita from (a) CTL, (b) UPV, (c) CYC2 and (d) BTPV at 00 UTC on 12th of March.



Fluxes are in Wm^{-2} .

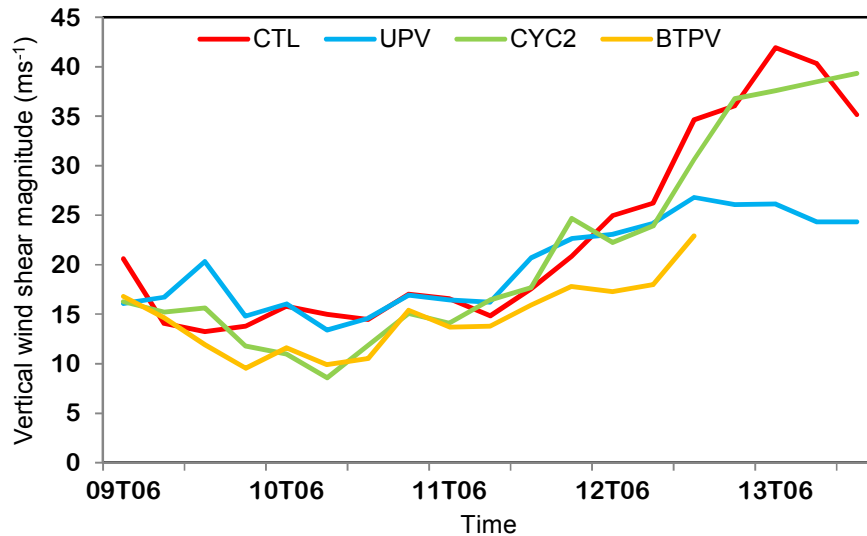
Source: Author's production.

Figure 5.32 shows the vertical wind shear magnitude over the center of Anita obtained from all experiments. The wind shear magnitude field was computed according to Guishard et al. (2009). Although the wind shear magnitude is

different between the experiments, its evolution is similar during the most part of the cyclone life cycle. During the mature subtropical phase of Anita, the wind shear from CTL, CYC2, UPV and BTPV is around 13, 15, 20 and 11 ms^{-1} , respectively. These values are between the range of 10 - 35 ms^{-1} found by Gozzo et al. (2014) for subtropical cyclogenesis. Despite this large range, they observed that most subtropical cyclones developed with vertical wind shear lower than 25 ms^{-1} . Indeed, wind shear above this value is observed only after the ET occurrence in each experiment, except for BTPV in which ET was not observed. Thus, the transitioning period is associated with the increase in the wind shear. This period is marked by the dissipation of the dipole-blocking pattern at upper troposphere and cutoff low at mid levels (Figure 5.21, Figure 5.23). Although experiment UPV does not present neither of these systems, the mid tropospheric trough associated with Anita, also weakens at this time. Reboita et al. (2017) indicated that the presence of a trough/cut-off low and blocking during the evolution of subtropical storms contributed to the low values of vertical wind shear.

It is possible to verify a slight decrease in shear between 10 and 11 of March, particularly on CYC2 and BTPV where values below 10 ms^{-1} are observed. These values are considered ideal for tropical cyclogenesis. Dias Pinto et al. (2013) showed that Anita developed over moderate wind shear but as the cyclone reached its mature phase there was a decrease in shear. This weaker shear lasts from 09 – 12 of March and characterizes the potential phase for tropical transition of cyclone Anita. The values of vertical wind shear presented in CTL are higher than what was observed by Dias Pinto et al. (2013). This could be associated with the approach used to calculate the wind shear. By analyzing six subtropical storms in the Southwestern Atlantic Ocean, Reboita et al. (2017) observed a decrease in the vertical wind shear during the mature stage of these systems.

Figure 5.32 – Time evolution of the mean of vertical wind shear magnitude (200 hPa – 925 hPa) from CTL (red), UPV (blue), CYC2 (green) and BTPV (orange).



The wind shear magnitude was calculated in an area of $10^\circ \times 10^\circ$ (latitude x longitude) centered over Anita core. Vertical wind shear magnitude unit is ms^{-1} .

Source: Author's production.

The coupling of Anita with the circulation associated with the transient cyclone, contributed to Anita becomes a deep cold core system. As mentioned previously, in all experiments the ET occurred via symmetric cold core, i.e., first become a cold core and later a deep asymmetric system. The experiments showed that ECY contributed to ET of Anita but was not the main element of this process, as ET still occurred in the absence of it. Also, although the removal of ECY decreased the vertical wind shear over Anita during its potential phase, it was not enough to allow its tropical transition as proposed by Dias Pinto et al. (2013). The removal of lower tropospheric PV prevented the southeastward propagation of Anita, allowing it to stay near to the continent and contributed to decrease the vertical wind shear during its entire life cycle. However, even though Anita did not transitioned into a deep extratropical cyclone, it still dissipated as a cold core system, inferring that this environment did not provide the necessary mechanisms to TT. Regarding the environment

associated with TT, the dipole-blocking pattern was found to be a fundamental component for the TT of Hurricane Catarina. The long lived blocking pattern sustained weak wind shear, decreased stability and increased moisture over the cyclone area for days (MCTAGGART-COWAN et al., 2006). These conditions were not observed in CYC2 or BTPV experiments, i.e., neither presented a longer-lived blocking pattern. Similarly, the cutoff low had similar lifetime in both experiments.

The removal of the upper tropospheric PV impacts directly the upper tropospheric circulation, suppressing the occurrence of the dipole-blocking and weakening the vortex associated with Anita. Also, the cut-off low did not develop at the mid troposphere and the SASA was weakened. This pattern allows the earlier southeastward propagation of Anita and subsequently displacement of SASA. Thus, Anita underwent ET after interacting with a transient cyclone. However, with the impacts on the environment caused by the removal of the upper PV, at the post-transition period Anita positioned in a region with lower gradient of temperature and weaker wind shear preventing its re-intensification.

6 SUMMARY AND CONCLUSIONS

This study analyzes the climatology and compositing analysis of subtropical cyclones undergoing extratropical transition on Southwestern Atlantic Ocean, during the austral summer (November-March) for the 1985-2015 period. To identify the SC, we adopted the methodology used by Gozzo et al (2014), which is very similar to the one proposed by Evans and Braun (2012), but with the inclusion of weaker and shallow hybrid cyclones by the removal of low level minimum wind criteria and closed low at 500 hPa requirement. This was done using NCEP-CFSR reanalysis and the TRACK code.

The SCET trajectories present a cyclogenetic concentration area near Southeast Brazilian Coast. The majority of these systems do not propagate through great distances. However, SCET do travel further distances than the other subtropical cyclones, even before the transition occurrence. The main region for SCET genesis is centered over the coast of São Paulo and Rio de Janeiro states. Actually, this preferred region for SCET genesis was also identified as a cyclogenetic activity of subtropical and extratropical cyclones of the South American continent (GOZZO et al., 2014; SINCLAIR, 1995; HOSKINS; HODGES, 2005; REBOITA et al., 2010). The extratropical transition density occurs between 20° - 50°W and 25° - 45°S over the ocean, with the highest density around 30° - 35°S and 30° - 40°W.

Regarding the dynamical features, the cyclonic vorticity at the cyclones center during the genesis and in the moment of the extratropical transition shows that they are more intense at the time of transition. The SCET mean cyclone phase space (HART, 2003) evolution, which is based on thermal wind and thermal asymmetry, shows that the cyclones have a typical hybrid structure (an upper level cold core and a low level warm core) during the period prior to ET. At the transition time, the cyclones have a typical extratropical cyclone structure. 24 hours later they reach their strongest cold asymmetric structure while the

cyclonic vorticity continues its intensification until 48 hour after ET, when the cyclones achieve their maximum vorticity.

During the austral summer of the 1985-2015 period, the annual mean and standard deviation of SC was 11.23 and 2.81 per year, respectively. This frequency is higher than the 1SC/year found by Evans and Braun (2012) and than the 7.2 CS per year showed by Gozzo et al. (2014). The inclusion of shallow and less intense subtropical cyclones and the different identification methods for tracking SC in the current study explains the difference in the frequency of the identified systems. Also, the inspection to eliminate cyclones with cold and westward tilting core and associated with frontal zones performed by Gozzo et al. (2014) were not applied at this stage.

47 SCET were identified in the studied period, therefore an annual mean of 1.6 SC/year with standard deviation of 1.3. The monthly distribution of these systems showed that the months of higher frequency was January, February and December, respectively. The interannual variability of the SC and SCET are very irregular, although an increase in the number of SCET can be seen from the second decade onwards, mainly for DJF months. The mean lifetime of SCET is 7.3 days with more than half of these cyclones present lifetimes between 4 and 8 days. Before the extratropical transition, the mean lifetime of the SCET is 3.25 days and around 4.08 days after that, such that most of these systems present a lifetime of at least 2 days, before the transition occur.

The composites analysis shows that SCET are associated with the intrusion of upper level potential vorticity and the propagation of a cyclonic system at the rear of the SCET which is characterized by a surface low and negative geopotential height anomalies in the composite fields. Also, the extratropical transition occurs over SST around 20°C with weak total surface heat fluxes (sensible heat plus latent heat). The weaker total heat fluxes and cooler SST during the extratropical phase of SCET are related with the propagation of these systems toward higher latitudes. Also of note is that warm (cold) air advection to the right (left) of the cyclones starts prior to the extratropical transition and continually intensifies until 24 hours after the ET occurrence. The above

mentioned pattern is typical of extratropical cyclones and is associated with the intensification of these systems (REBOITA, 2008).

Cyclone Anita was selected to investigate the dynamical processes favoring extratropical transition of subtropical cyclones in the SAO region. The genesis of Anita occurred in early march of 2010. It developed as a subtropical system in the Southeast coast of Brazil in an environment similar to the observed in Hurricane Catarina with a presence of a dipole-blocking pattern which keeps Anita semi-stationary for days. However, Anita's intensity decreased and it underwent extratropical transition after interacting with a transient cyclone (CYC2), intensifying again as an extratropical cyclone.

The contribution of different potential vorticity perturbation to the evolution of the cyclone Anita shows that the upper level PV anomalies are responsible for the circulation at upper troposphere along all studied period, contributing to the development of cyclonic vortex associated with the surface cyclone. On the other hand, prior to the transition phase the low level PV anomalies extends up to middle troposphere and seems to be the main key to the negative vorticity associated with the cyclone. At the transition instant, the PV anomalies of inferior theta boundary present a significant contribution to the re-intensification of the cyclonic circulation.

Sensitivity tests were realized to evaluate the contribution of three different PV anomalies for ET of cyclone Anita: PV anomaly associated with ECY (CYC2), upper tropospheric PV anomaly (UPV) and lower level PV anomaly (BTPV). The experiments show that the coupling of Anita with the circulation associated with the transient cyclone, contributed to Anita becomes a deep cold core system. In experiment UVP, the removal of the upper PV anomaly weakens the upper level circulation associated with Anita and ECY. In this experiment the dipole-blocking pattern did not develop allowing the southeastward propagation of Anita which later interacted with another transient system. Then, Anita positioned over an area of intense gradient of temperature, which helped increasing its baroclinicity. Also, there was observed an increase in the vertical

wind shear. These features led Anita to undergo ET. Despite that, the re-intensification of Anita was weak.

In CYC2, the absence of ECY shows that this system contributed to ET of Anita but was not the main element of this process, as ET still occurred in the absence of it. Actually, in this experiment the ET occurred earlier than in CTL and UPV. Although, the upper tropospheric circulation was impacted, the dipole blocking pattern still was present in this experiment, which maintained Anita semi-stationary. The approximation of another transient system was associated with weak temperature advection and vertical wind shear. The removal of lower tropospheric PV (BTPV) prevented the ET of Anita. However, even though Anita did not transitioned into a deep extratropical cyclone, it still dissipated as a cold core system. Although, in this experiment Anita stayed semi stationary near the continent and the vertical wind shear was weaker during its entire life cycle, it was not sufficient to enhance the potential for TT.

6.1 Future work

- Elaborate a sensitivity test to confirm if the intrusion of lower tropospheric PV anomaly in the environment of a SC will lead to it to undergo ET.
- Extend the numerical experiments for other SCET.
- Investigate the influence of moisture on the ET process and how it impacts the re-intensification of the SCET.
- Evaluate the impact of low frequency variability systems to SC and SCET over the SAO.
- Investigate the impact of the SST on the transition processes of SC.

REFERENCES

- AGUSTÍ-PANAREDA, A.; GRAY, S. L.; CRAIG, G. C.; THORNCROFT, C. The extratropical transition of tropical cyclone Lili (1996) and its crucial contribution to a moderate extratropical development. **Monthly Weather Review**, v. 133, p. 1562-1573, 2005.
- ARNOTT, J. M.; EVANS, J. L. Characterization of extratropical transition using cluster analysis. **Monthly Weather Review**, v. 132, p. 2916-2937, 2004.
- BENGTSSON, L.; ROECKNER, E. Storm tracks and climate change. **Journal of Climate**, v.19, p. 3518-3543, 2006.
- BENGTSSON, L.; HODGES, K. I.; ESCH, M.; KEENLYSIDE, N.; KORNBLUECH, J. L.; YAMAGATA, T. How may tropical cyclones change in a warmer climate? **Tellus A: Dynamic Meteorology and Oceanography**, v. 59, p. 539-561, 2007.
- BRAUN, A. J. **A comparison between South Atlantic and Tasman Sea subtropical storms**. 150p. Dissertação (Mestrado em Meteorologia) - The Pennsylvania State University, Old Main, State College, 2009.
- CATTO, J. L.; SHAFFREY, L. C.; HODGES, K. I. Can climate models capture the structure of extratropical cyclones? **Journal of Climate**, v. 23, p. 1621-1635, 2010.
- CATTO, J. L.; SHAFREY, L. C.; HODGES, K. I. Northern Hemisphere extratropical cyclones in a warming climate in the HiGEM high-resolution climate model. **Journal of Climate**, v. 24, p. 5336- 5352, 2011.
- CHARNEY, J. G. The use of primitive equations of motion in numerical prediction. **Tellus**, v. 7, p. 22-26, 1955.

DARE, R. A.; MCBRIDE, J. L. The threshold sea surface temperature condition for tropical cyclones. **Journal of Climate**, v. 24, p. 4570-4576, 2011.

DAVIS, C. A.; BOSART, L. F. The TT problem: forecasting the tropical transition of cyclones. **Bulletin of the American Meteorological Society**, v. 85, p. 1657–1662, 2004.

DAVIS, C. A.; EMANUEL, K. A. Potential vorticity diagnostics of cyclogenesis. **Monthly Weather Review**, v. 119, p. 1929-1953, 1991.

DIAS PINTO, J. R.; REBOITA, M. S.; ROCHA, R. P. Synoptic and dynamical analysis of subtropical cyclone Anita (2010) and its potential for tropical transition over the South Atlantic Ocean. **Journal of Geophysical Research**, v. 118, p. 10870-10883, 2013.

DUDHIA, J. Numerical study of convection observed during the winter monsoon experiment using a mesoscale two-dimensional model. **Journal of Atmospheric Sciences**, v. 46, p. 3077–3107, 1989.

DUTRA, L. M. M.; ROCHA, R. P.; LEE, R. W.; PERES, J. R. R.; CAMARGO, R. Structure and evolution of subtropical cyclone Anita as evaluated by heat and vorticity budgets. **Quarterly Journal of the Royal Meteorological Society**, v. 143, p. 1539-1553, 2017.

EVANS, J. L.; BRAUN, A. A climatology of subtropical cyclones in the South Atlantic. **Journal of Climate**, v. 25, p. 7328–7340, 2012.

EVANS, J. L.; GUISARD, M. P. Atlantic subtropical storms. Part I: diagnostic criteria and composite analysis. **Monthly Weather Review**, v. 137, p. 2065-2080, 2009.

FUNATSU, B., M. **Estudo sinótico-dinâmico de ciclogênese usando vorticidade potencial**. 145p. Dissertação (Mestrado em meteorologia) - Instituto Nacional de Pesquisas Espaciais, São José dos Campos – SP, 1999.

- FUNGAN, M. A.; RAO, V. B. Surface cyclogenesis over South America. **Monthly Weather Review**, v. 119, p. 1293–1302, 1991.
- GAN, M. A.; RAO, V. B. The influence of the Andes Cordillera on transient disturbances. **Monthly Weather Review**, v. 122, p. 1141-1157, 1994.
- GARDE, L. A.; PEZZA, A. B.; BYE, J. A. T. Tropical transition of the 2001 Australian Duck. **Monthly Weather Review**, v.138, p. 2038–2057, 2010.
- GONZÁLEZ-ALEMÁN, J. J. et al. Classification and synoptic analysis of subtropical cyclones within the northeastern Atlantic Ocean. **Journal of Climate**, v. 28, p. 3331-3352, 2015.
- GOZZO, L. F. **Ciclones subtropicais sobre o sudoeste do Atlântico Sul: climatologia e fontes de umidade**. 153p. Tese (Doutorado em Meteorologia) – Instituto de Astronomia, Geofísica e Ciências atmosféricas, Universidade de São Paulo, São Paulo, 2014.
- GOZZO, L. F.; ROCHA, R. P.; REBOITA, M. S.; SUGAHARA, S. Subtropical cyclones over the southwestern South Atlantic: climatological aspects and case study. **Journal of Climate**, v. 27, p. 8543–8562, 2014.
- GRELL, G. A. Prognostic evaluation of assumptions used by cumulus parameterization. **Monthly Weather Review**, v. 121, n. 3, p. 764–787, 1993.
- GRELL, G. A.; DÉVÉNYI, D. A generalized approach to parameterizing convection combining ensemble and data assimilation techniques. **Geophysics Research Letters**, v. 29, n. 14, p. 1693, 2002.
- GUIA, C. V. F. **Análises das características sinóticas das trajetórias dos ciclones extratropicais que atuam na América do Sul e vizinhanças**. Dissertação (Mestrado em Meteorologia) – Instituto Nacional de Pesquisas Espaciais, São José dos Campos, 2011.
- GUISHARD, M. P.; EVANS, J. L.; HART, R. E. Atlantic subtropical storms. Part II: climatology. **Journal of Climate**, v. 22, p. 3574-3594, 2009.

- HALTINER, G. J.; WILLIAMS, R. T. **Numerical prediction and dynamic meteorology**. 2.ed. New York: Wiley and Sons, 1980. 477p.
- HANLEY, D.; MOLINARI, J.; KEYSER, D. A composite study of the interaction between tropical cyclones and upper-tropospheric troughs. **Monthly Weather Review**, v. 129, p. 2570-2584, 2001.
- HART, R. E. A cyclone phase space derived from thermal wind and thermal asymmetry. **Monthly Weather Review**, v. 131, p. 585–616, 2003.
- HART, R. E.; EVANS, J. L. A climatology of the extratropical transition of Atlantic tropical cyclones. **Journal of Climate**, v. 14, p. 546-564, 2001.
- HART, R. E.; EVANS, J. L.; EVANS, C. Synoptic composites of the extratropical transition life cycle of North Atlantic tropical cyclones: factors determining posttransition evolution. **Monthly Weather Review**, v. 134, p. 553–578, 2006.
- HODGES, K. I. A general method for tracking analysis and its application to meteorological data. **American Meteorological Society**, v. 122, p. 2573-2585. 1994.
- HODGES, K. I. Feature tracking on the unit sphere. **Monthly Weather Review**, v. 123, p. 3458–3465, 1995.
- HODGES, K. I. Spherical nonparametric estimators applied to the UGAMP model integration for AMIP. **Monthly Weather Review**, v. 124, p. 2914–2932, 1996.
- HOLLAND, G. J.; LYNCH, A. H.; LESLIE, L. M. Australian east-coast cyclones. Part I: synoptic overview and case study. **Monthly Weather Review**, v. 115, p. 3024-3036, 1987.
- HOSKINS, B. J.; HODGES, K. I. New perspective on the northern hemisphere winter storm tracks. **Journal Atmospheric Sciences**, v. 59, p. 1041-1061, 2002.

- HOSKINS, B. J.; HODGES, K.I. A new perspective on southern hemisphere storm tracks. **Journal of Climate**, v. 18, p. 4108-4129, 2005.
- HUO, Z.; ZHANG, D.; GYAKUM, J. An application of potential vorticity inversion to improving the numerical prediction of the March 1993 superstorm. **Monthly Weather Review**, v. 126, p. 424-436, 1998.
- IWABE, C. M.N. **Ciclones secundários no sudoeste do Atlântico Sul: climatologia e simulação numérica**. Tese (Doutorado em Meteorologia) – Instituto de Astronomia, Geofísica e Ciências Atmosféricas, Universidade de São Paulo, São Paulo, 2012.
- KEABLE, M.; SIMMONDS, I.; KEAY, K. Distribution and temporal variability of 500 hPa cyclone characteristics in the Southern Hemisphere. **International Journal of Climatology**, v. 22, p. 131-150, 2002.
- KITABATAKE, N. Extratropical transition of tropical cyclones in the western North Pacific: their frontal evolution. **Monthly Weather Review**, v. 136, p. 2066–2090, 2008.
- KOUSKY, V. E.; GAN, M. A. Upper tropospheric cyclonic vortices in the subtropical South Atlantic. **Tellus**, v. 33, p. 538-551, 1981.
- LIN, Y. L.; FARLEY, R.; ORVILLE, H. D. Bulk parameterization of the snow field in a cloud model. **Journal of Climate Applied Meteorology**, v. 22, p. 1065–1092, 1983.
- MCTAGGART-COWAN, R.; GYAKUM, J. R.; YAU, M. K. Sensitivity testing of extratropical transitions using potential vorticity inversions to modify initial conditions: hurricane earl case study. **Monthly Weather Review**, v. 129, p. 1617-1636, 2001.
- MACTAGGART-COWAN, R.; GYAKUM, J. R.; YAU, M. K. The influence of the downstream state on extratropical transition: hurricane Earl (1998) case study. **Monthly Weather Review**, v. 131, p. 1910–1929, 2003.

- MCTAGGART-COWAN, R.; BOSART, L. F.; DAVIS, C. A.; ATALLAH, E. H.; GYAKUM, J. R.; EMANUEL, K. A. Analysis of hurricane Catarina (2004). **Monthly Weather Review**, v.134, p. 3029-3053, 2006.
- MENDES, D. E.; SOUZA, E.P.; MARENGO, J. A.; MENDES, C. D. Climatology of extratropical cyclones over the South American-southern oceans sector. **Theoretical and Applied Climatology**, v. 100, p. 239-250, 2010.
- MLAWER, E. J.; TAUBMAN, S. J.; BROWN, P. D.; IACONO, M. J.; CLOUGH, S. A. Radiative transfer for inhomogeneous atmospheres: RRTM, a validated correlated-k model for the longwave. **Journal of Geophysical Research**, v. 102, D14, p. 16663–16682, 1997.
- MORRISON, I.; BUSINGER, S. Synoptic structure and evolution of a Kona low. **Weather and Forecasting**, v. 16, p. 81 – 98, 2001.
- OTKIN, J. A.; MARTIN, J. E. A synoptic climatology of the subtropical Kona storm. **Monthly Weather Review**, v. 132, p. 1502 – 1517, 2004.
- PEZZA, A. B., SIMMONDS, I.; PEREIRA FILHO, A. J. Climate perspective on the large-scale circulation associated with the transition of the first South Atlantic hurricane. **International Journal of Climatology**, v. 29, p.1116-1130, 2009.
- PINHEIRO, H. R.; HODGES, K. I.; GAN, M. A. A new perspective of the climatological features of upper-level CUT-off lows in the Southern Hemisphere. **Climate Dynamics**, v. 48, p. 541-559, 2017.
- RAMSAY, H.; CAMARGO, S. J.; KIM, D. Cluster analysis of tropical cyclone tracks in the Southern Hemisphere. **Climate Dynamics**, v. 39, p. 897-917, 2012.
- REBOITA, M. S. **Ciclones extratropicais sobre o Atlântico Sul**: simulação climática e experimentos de sensibilidade. Tese (Doutorado em Meteorologia) – Instituto de Astronomia, Geofísica e Ciências Atmosféricas, Universidade de São Paulo, São Paulo, 2008.

REBOITA, M. S.; ROCHA, R. P.; AMBRIZZI, T.; CAETANO, E. An assessment of the latent and sensible heat flux on the simulated regional climate over Southwestern South Atlantic Ocean. **Climate Dynamics**, v.34, p. 873-889, 2010.

REBOITA, M. S.; GAN, M. A.; ROCHA, R. P.; CUSTÓDIO, I. S. Ciclones em superfície nas latitudes austrais: Parte I – revisão bibliográfica. **Revista Brasileira de Meteorologia**, v. 32, p. 171-186, 2017.

REBOITA, M. S.; ROCHA, R. P.; OLIVEIRA, D. M. Key features and adverse weather of the named subtropical cyclones over the Southwestern South Atlantic Ocean. **Atmosphere**, v. 10, 2019.

SCHENKEL, B. A.; HART, R. E. An examination of tropical cyclone position, intensity, and intensity life cycle within atmospheric reanalysis datasets. **Journal of Climate**, v. 25, p. 3453 – 3475, 2012.

SILVA DIAS, P.L.; SILVA DIAS, M. A. F.; SELUCHI, M.; DINIZ, F. A. O ciclone Catarina: análise preliminar da estrutura, dinâmica e previsibilidade. In: CONGRESSO BRASILEIRO DE METEOROLOGIA, 18., 2004, Fortaleza, CE. **Anais...** 2004. 10p.

SIMMONDS, I.; KEAY, K. Mean Southern Hemisphere extratropical cyclone behavior in the 40-Year NCEP-NCAR reanalysis. **Journal of Climate**, v. 13, p. 873-885, 2000.

SINCLAIR, M. R. An objective cyclone climatology for the Southern Hemisphere. **Monthly Weather Review**, v. 122, p. 2239-2256, 1994.

SINCLAIR, M. R. A climatology of cyclogenesis for the Southern Hemisphere. **Monthly Weather Review**, v. 123, p. 1601-1619, 1995.

SKAMAROCK, W.; KLEMP, J.B., DUDHIA, J.; GILL, D.O.; BARKER, D.; DUDA, M.G.; HUANG, X.-Y.; WANG, W. **A description of the advanced research WRF version 3**. Boulder, Colorado: National Center for Atmospheric Research, 2008. 113p. (NCAR Technical Note NCAR/TN-475+STR).

SIMPSON, R. H. Evolution of the Kona storm, asubtropical storm. **Journal of Meteorology**, v. 9, p. 24 – 35, 1952.

STUDHOLME, J.; HODGES, K. I.; BRIERLEY, C. M. Objective determination of the extratropical transition of tropical cyclones in the Northern Hemisphere. **Tellus Series A: Dynamic Meteorology and Oceanography**, v. 67, 24474, 2015.

SUGI, M. A.; NODA, A.; SATO, N. Influence of the global warming on tropical cyclone climatology: an experiment with the JMA Global Model. **Journal of the Meteorological Society of Japan**, v. 80, p. 249-272, 2002.

VEIGA, J. A.; PEZZA, A. B.; SIMMONDS, I.; SILVA DIAS, P. L. An analysis of the environmental energetics associated with the transition of the first South Atlantic hurricane. **Geophysical Research Letters**, v. 35, 2008.

VEREN, D.; EVANS, J. L.; JONES, S. C.; CHIAROMONTE, F. Novel metrics for evaluation of ensemble forecasts of tropical cyclone structure. **Monthly Weather Review**, v. 137, p. 2830-2850, 2009.

WORLD METEOROLOGICAL ORGANIZATION. **Guidelines on ensemble prediction systems and forecasting**. Geneva, Switzerland: WMO, 2012. 32p.